[Dissertations (2009 -)](#) | [Dissertations, Theses, and Professional Projects](#)

Indirect Structural Connectivity As a Biomarker for Stroke Motor Recovery

Miguel Renato Sotelo Munoz
Marquette University

INDIRECT STRUCTURAL CONNECTIVITY AS A BIOMARKER FOR STROKE
MOTOR RECOVERY

by

Miguel R. Sotelo Munoz, B.S

A Dissertation Submitted to the Faculty of the Graduate School,

Marquette University

In Partial Fulfillment of the Requirements for

the Degree of Doctor of Philosophy

Milwaukee, Wisconsin

May, 2020

<u>*ABSTRACT*</u>

INDIRECT STRUCTURAL BRAIN CONNECTIVITY AND GRAPH ANALYSIS

ACCOUNTS FOR MOTOR IMPAIRMENT IN STROKE RECOVERY

Miguel R. Sotelo Munoz, B.S.

Marquette University, 2020

In this dissertation project, we demonstrated that diffusion magnetic resonance imaging and measures of indirect structural brain connectivity are sensitive to changes in fiber integrity and connectivity to remote regions in the brain after stroke. Our results revealed new insights into the effects local lesions have on global connectivity—in particular, the cerebellum—and how these changes in connectivity and integrity relate to motor impairment. We tested this methodology on two stroke groups—subacute and chronic—and were able to show that indirect connectivity is sensitive to differences in connectivity during stroke recovery. Our work can inform clinical methods for rehabilitating motor function in stroke individuals. By introducing methodology that extends local damage to remotely connected motor related areas, we can measure Wallerian degeneration in addition to providing the framework to predict improvements in motor impairment score based on structural connectivity at the subacute stage.

We used diffusion magnetic resonance imaging (dMRI), probabilistic tractography, and novel graph theory metrics to quantify structural connectivity and integrity after stroke. In the first aim, we improved on a measure of indirect structural connectivity in order to detect remote gray matter regions with reduced connectivity after stroke. In a region-level analysis, we found that indirect connectivity was more sensitive to remote changes in connectivity after stroke than measures of direct connectivity, in particular in cortical, subcortical, and cerebellar gray matter regions that play a central role in sensorimotor function. Adding this information to the integrity of the corticospinal tract (CST) improved our ability to predict motor impairment. In the second aim, we investigated the relationship between white matter integrity, connectivity, and motor impairment by developing a unified measure of white matter structure that extends local changes in white matter integrity along remotely connected fiber tracks. Our measure uniquely identified damaged fiber tracks outside the CST, correlated with motor impairment in the CST better than the FA, and also was able to relate white matter structure in the superior cerebellar peduncle to motor impairment. Our final aim used a novel connectome similarity metric and the measure of indirect structural connectivity in order to identify cross-sectional differences in white matter structure between subacute and chronic stroke. We found more reductions in indirect connectivity in the chronic stroke cerebellar fibers than the subacute group, Additionally, the indirect connectivity of the superior cerebellar peduncle at the subacute stage correlated with the improvement in motor impairment score for the paired participants. In conclusion, indirect connectivity is an important measure of global brain damage and motor impairment after stroke, and can be a useful metric to relate to brain function and stroke recovery.

<u>TABLE OF CONTENTS</u>

LIST OF TABLES

LIST OF FIGURES

1 *CHAPTER 1: INTRODUCTION AND BACKGROUND*

1.1 **THESIS STATEMENT**

The purpose of this study is to develop imaging biomarkers that are sensitive to identifying whole brain structural networks that are damaged after subacute and chronic stroke, and to determine the influence of these remotely connected gray matter regions and white matter connections on subacute and chronic stroke impairment. The brain is highly interconnected and remote regions are vulnerable to focal lesions. We believe novel imaging techniques that measure structural connectivity via directly and indirectly connected pathways could help identify damage to remote regions of the brain and their influence on subacute and chronic stroke motor impairment.

1.2 **ISCHEMIC STROKE: MOTOR IMPAIRMENT AND RECOVERY**

1.2.1 *ETIOLOGY OF STROKE*

Stroke contributes to one out of every 20 deaths in the United States and is one of the leading causes of long-term disability (Koton et al., 2014). Hemorrhagic stroke is caused by a ruptured blood vessel that bleeds into the brain, and ischemic stroke (the most common type) is caused by a clogged artery due to plaque and atherosclerosis. In general, stroke is divided into three phases: acute (less than one week), subacute (1 week – 1 month), and chronic (greater than one month). Although locations can vary, the most common artery implicated in ischemic stroke is the middle cerebral artery (MCA) that provides oxygen and nutrients to parts of the motor cortex via the superior division, the

temporal lobe via the inferior division, and the basal ganglia and the thalamus via deeper branches. More specifically, occlusions of small arteries in the deep division of the MCA produce lacunar stroke—small but localized lesions to important motor and sensory pathways in the basal ganglia.

Stroke results in extensive local damage, with progressive degeneration outside the immediate lesion location; brain imaging allows us to assess the extent of this damage. Detrimental neurovascular events ensue immediately following occlusion. An estimated 1-2 million brain cells die every minute immediately at the core of the lesion (Lo, Moskowitz, & Jacobs, 2005). As a result, a rapid loss of local neurological function ensues in the area with reduced perfusion (Koton et al., 2014). Cellular mechanisms such as increased extracellular glutamate and intracellular sodium, calcium, and water result in further spatial spread of cellular depolarization, depletion of energy stores, and an advancement of injury outside the lesion boundary (Lee, Grabb, Zipfel, & Choi, 2000). The rapid neurodegeneration motivates acute clinical interventions that aim to resume perfusion to the brain to save potentially salvageable tissue. Perfusion-weighted magnetic resonance imaging (MRI) and diffusion-weighted MRI can be used to estimate the location and volume of potentially salvageable tissue—named the "penumbra"—and differentiate it from the lesion core—the irrevocably damaged brain tissue. The penumbra can be estimated as the perfusion-diffusion mismatch seen in MRI: the volume with reduced perfusion is larger than the area of reduced perfusion *and* abnormal diffusion, in which the volume has impaired perfusion and enhanced oxygen extraction (Chen, 2012).

1.2.2   POST-STROKE IMPAIRMENTS

Stroke deficits vary depending on the neuronal structures and the white matter bundles affected by the lesion. For example, impairments in language can include aphasia (the impairment of how you speak and write, and your understanding of language), dysarthria (the impairment of speech caused by weakened and spastic muscles), and dyspraxia (the impairment of speech due to the inability to coordinate muscles). These are caused by damage to either brain regions specialized in each of these tasks, or the damage of white matter bundles connecting to these regions (conductive, or association aphasia).

Similarly, motor impairments depend on the structures that are affected, which depends on the artery producing the occlusion; however, a common symptom post-stroke and other upper motor neuron diseases is limb spasticity (Carey, Matyas, & Baum, 2018; Gracies, 2005). Ischemia involving the middle cerebral artery (MCA) typically involves upper limb impairment, given that the tissue that the MCA perfuses includes the upper limb portion of the precentral gyrus. Lesions involving the anterior cerebral artery (ACA) damage the lower limb. Lesions of the MCA and ACA typically result in more than motor impairments, since these arteries perfuse the temporal, frontal, and parietal regions.

Impairments are also dependent on the hemisphere that is lesioned. For instance, damage to the language center in the left hemisphere produces aphasia, while lesions in the right hemisphere may result in aprosodia—the impairment in speech expressiveness. Similarly, lesions in the parietal network of the right hemisphere—and not the left— typically result in spatial neglect. This presents itself as the inability to recognize the left side of the body.

Lacunar lesions are small lesions usually in locations where large arteries divide into small-diameter arterial branches. These are typically in the basal ganglia which is fed by the MCA. These lesions generally induce pure motor impairments due to the specific damage. For example, lesions to the thalamus—a network hub specialized in relaying sensory information—produces very specific impairments depending on what nuclei is affected.

Lastly, the cerebellum is a highly interconnected brain structure involved in motor and non-motor tasks. In general, lesions to the cerebellum produce impairments in coordination of motor or non-motor tasks. Interestingly, ataxic symptoms may occur without direct damage to the cerebellum; if fibers involving the cortico-thalamic-cerebellar, or the cerebellar-cortical loop are damaged, ataxia out of proportion to weakness may be observed.

1.2.3 CLINICAL MEASURES OF MOTOR FUNCTION AND IMPAIRMENT

Clinical and research measures of motor function and impairment are used in post-stroke patients in order to assess the extent of damage to the motor system. One of the most commonly used measures is the Fugl-Meyer assessment of motor impairment (Fugl-Meyer et al., 1975). It consists of five domains measuring motor functioning, sensation, balance, pain, and joint range of motion. Higher scores indicate less motor impairment, and the assessment is measured while standing, sitting, and in the laying position. This is the primary measure of motor impairment used in this dissertation, and we focused our analysis in the upper-motor examinations. An example examination of the upper motor domain is movements of the paretic arm, measuring their ability to flex

their shoulder with little synergy. The participant is asked to keep their elbow extended at 0-degrees, forearm pronated, and flex their shoulder from 0 to 90-degrees. The highest score in this particular examination is 2, with points being deducted if synergy is present (elbow flexion, trunk movement) or if the movement cannot be completed. In our study, the upper-motor FM was assessed (only measuring motor function and range of motion), and the maximum score is 66

In addition to measures of motor impairment, measures of motor function can be administered. For instance, the Wolf-Motor Function Test (WMFT) (Woodbury et al., 2010). This exam times the patient's ability to perform tasks such as placing the forearm on the table in front or to the side of them from a neutral starting position by using shoulder abduction. Another, similar task is to further abduct the shoulder to place the forearm on top of a box that is on the table in front of them while sitting. This examination also measures the patient's ability to lift a basket, or fold a towel, thus assessing their motor function. The examination times these movements, and typically are video-recorded in order to assess the mechanisms used by the patient during the examination. The score is out of 75 (15 measurements), with two other measurements assigned to strength.

Another functional score is the Box and Blocks score (Chen, Chen, Hsueh, Huang, & Hsieh, 2009). As the name suggests, the examination requires a box and blocks. The box opens like a suitcase and when opened there is a subdivider separating the box in two. Boxes are placed on one side, and the patient is asked to move one block at a time from one side to the other as fast as possible. The time it takes to move all blocks from one side to the other is the score.

More complex measures of motor dysfunction are measurements of cerebellar injury. The Fugl-Meyer assesses dysmetria (uncoordinated movement) by measuring the time it takes for the patient to point at their nose and to the examiner's finger or pen placed in front of them three times. It is, however, difficult to measure cerebellar function in stroke participants due to the possibility that their hemiplegia and reduced weakness may either hide cerebellar dysfunction or produce false observations. The scale for the assessment and rating of ataxia (SARA) (Schmitz-Hubsh et al., 2006) is a 40-point scale (higher scores indicate more ataxia) that measures the lack of muscle control and coordination. Measures include gait, stance, sitting, speech disturbance, finger chase, and the heel-shin slide (the latter two are also measured in the Fugl-Meyer).

Other measures of motor dysfunction include measurements of gait, including the six-minute walk test ("ATS Statement: Guidelines for the Six-Minute Walk Test," 2002) which assesses the distance covered during a 6-minute time period, and the Timed Up and Go test (Podsiadlo & Richardson, 1991) which assess fall-risk.

1.3   MAGNETIC RESONANCE IMAGING

1.3.1   BASICS OF MRI

The magnetic resonance imaging (MRI) signal is based on the response a proton exhibits in the presence of an outside magnetic field, $\mathbf{B_0}$, and radiofrequency impulses. In most medical applications, the MR scanner measures the signal from the hydrogen proton, partly because this is the most common element in our body, and its nuclear magnetization is susceptible to the radiofrequency pulses (described later) the produce a signal. For Hydrogen atoms, 7 parts per million become aligned to the outside magnetic

field, and this produces a net magnetization vector, **M**. These aligned protons spin parallel to the main magnetic field. The proton's mass, its gyrometric ratio, and the **B$_0$** field all induce angular momentum on the spinning proton, causing it to precess away from the main **B$_0$** direction giving **M** a longitudinal (M_z) and a transverse (M_{xy}) component. The precession frequency is called the Larmor frequency.

In order to obtain a signal, the vectors must have a net vector in the transverse plane. This is because the longitudinal portion of **M** (M_z) is negligible in the presence of the larger **B$_0$**. By applying an external radio frequency (RF) pulse set to the precession Larmor frequency, the protons are tipped to a plane specified by the tip-angle. This is because the RF pulse frequency is tuned in resonance to the Larmour frequency, allowing the spinning proton to absorb energy from the RF coil, allowing the proton to rotate its axis away from the main magnetic field. Assuming the tip angle is 90°, this RF pulse will tip protons with the Larmour frequency equal to the RF frequency towards the transverse plane. The synchronized precession in the transverse plane produces a sinusoidal signal that can be measured, called the transverse magnetization signal, M_{xy}. According to Faraday's law of induction, this signal produces a magnetic flux through the receiving coil, inducing a small electromotive force that the receiver coil (in modern systems, typically the same coil as the pulse-generating RF coil) receives as a function of time.

After absorbing energy from the RF pulse, the precessing protons gradually emit energy and their net magnetization becomes out of phase and eventually return to the low-energy state (the **B$_0$** direction, where the largest contributor to the **M** vector is M_z). The rate at which the protons become out of phase in the transverse plane is defined by a T2 time constant, while the rate at which the protons return to point in the Z-direction is

defined by a T1 time constant. These constants influence the signal strength and are
dependent on the tissue where the protons reside. In our application, the tissues are white
matter, gray matter, and cerebral spinal fluid. Two important parameters in MR imaging
is the TR (the "repetition time" or the time between consecutive points in a repeating MR
sequence) and the TE (the "echo time", or the time between the the RF pulse and the
center of the read-out gradient, described later) These parameters are engineered in order
to discern differences in tissue imaging contrast based on either the T1 signal (a T1-
weighted MRI) or the T2 signal (T2-weighted MRI).

1.3.2 SIGNAL ACQUISITION

The following text describes a gradient echo pulse sequence (Figure 1.1). In this
dissertation, a gradient echo was used to obtain T1-weighted images. A gradient in the Z-
direction (G_z) added to $\mathbf{B_0}$ will cause protons to spin at different Larmor frequencies
based on the spatial location in the Z direction. RF pulses are then iteratively (based on
the TR and the field of view in the Z direction) applied at different resonant frequencies
based on the Larmor frequency at that particular imaging slice to selectively tip protons.
A Fourier Transformation can decompose the free induction decay (FID or received
signal) into a spectrum of frequencies. If no gradient is used, (i.e, if the RF pulse is
applied to the volume in the presence of a static magnetic field), the resulting frequency
spectrum will contain one frequency, which is the Larmor frequency. In order to obtain
spatial resolution, different frequencies are required, each mapping a frequency in the
frequency space (k-space) to the imaging space. A gradient field, $\mathbf{G_r}$, is applied in
addition to the static magnetic field. This is applied after the slice is selected (after G_z and

the RF are applied), and during the read-out time interval. $\mathbf{G_r}$ produces sinusoids oscillating at different frequencies, all dependent on the spatially varying gradient. As a result, the frequency spectrum of the FID signal contains a spread of frequencies encoding space according to the spatial gradient, therefore producing an array of summed frequency values that encode space (Figure 1.1).

In the gradient echo pulse sequence (Figure 1.1), the gradient $\mathbf{G_r}$ contains an X (G_x) and a Y (G_y) component. In a given imaging slice, the G_x encodes spatial information in the X direction in the imaging space by varying frequencies in the X direction in k-space. In order to obtain a spatial encoding in the Y-direction, G_y, is applied right before the read-out G_x. In the transverse plane, this causes protons spinning at the higher magnetic field in the Y-direction to spin faster than those in the lower magnetic field in the Y-direction. When the gradient G_y is turned off and the read-out gradient G_x is turned on, all protons in one X-slice return to the same frequency; however, protons are phase-shifted from each other in the direction of the Y-gradient due to the previously applied G_y. These sinusoids contain the same frequencies obtained before *in addition to* phase shifts. The signal obtained by the coil is a sum of frequencies encoded in the X-direction, and also phase shifts in the Y-direction. By obtaining the FID signal over time (in the read-out direction, G_x) and repeating this for a different G_y effectively samples the k-space (frequency space) of the image. An inverse Fourier Transform transforms the signal form the k-space into the image space. This is repeated for all slices by varying G_z (Figure 1.1).
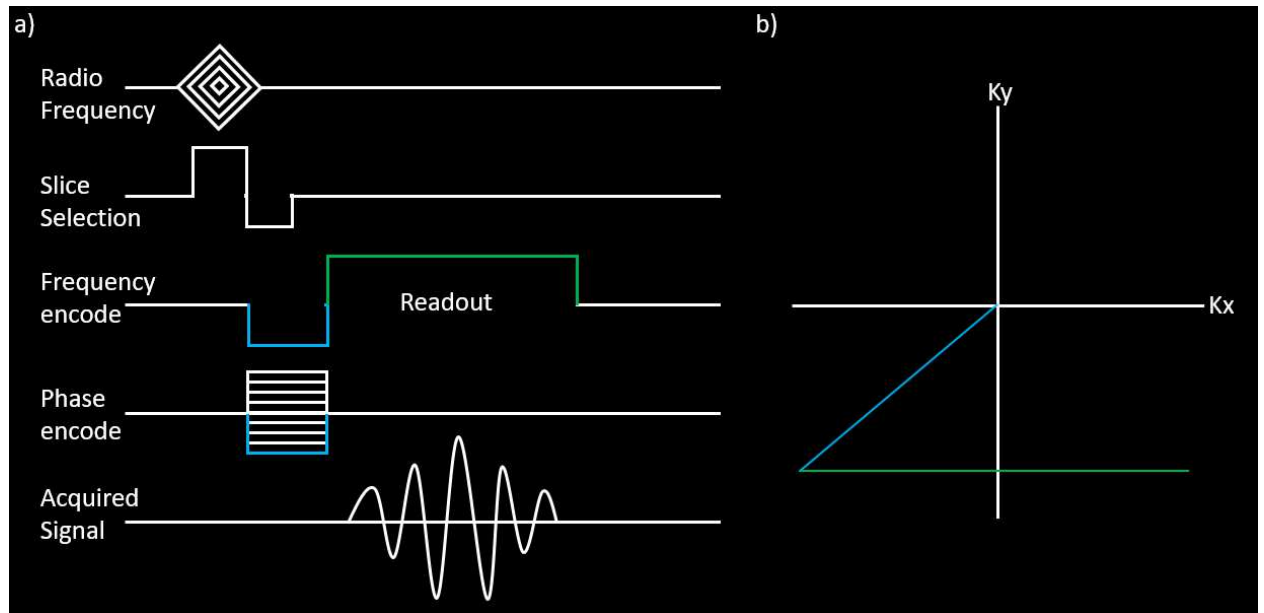
Figure 1-1: Gradient Echo Pulse Sequence Diagram

a) Pulsed sequence diagram for the typical gradient echo (GRE) pulse sequence. b) k-space illustration of the frequency and phase encoding (blue), and the read-out (green)

1.4 DIFFUSION MRI: AN INDIRECT MEASURE OF WHITE MATTER STRUCTURE

1.4.1 THE DIFFUSION MRI SIGNAL

The following describes a spin-echo sequence. In this dissertation, a modification of the spin-echo sequence was used in order to obtain diffusion weighted MRI. Diffusion Weighted Imaging (DWI) is based on Brownian motion, in which water molecules randomly diffuse in a Gaussian spatial distribution. DWI is sensitive to the diffusion rate of water, and this is linked to signal intensity in sequences that produce DW Images (Hagmann et al., 2006). The pioneering work of Hahn, (1949), where he discovered that the motion of spins lead to a decrease in signal intensity, and the fundamental equations derived by Torrey, (1956) is the foundation of DWI.

As previously introduced, a gradient magnetic field causes phase shifts on the spins in the direction of the applied gradient. The pulsed-gradient spin echo sequence introduced by Stejskal and Tanner, (1965) adds diffusion gradients to the pulse sequence diagram described before (Figure 1.2). In addition to the slice selection gradient, the frequency-encoding gradient, and the phase-encoding gradient, a diffusion gradient is applied in a specified cartesian direction (**G**), strength (g), pulse duration δ, and time between dephasing and rephasing pulses Δ (Figure 1.2). Applying the phase shift (dephasing) gradient causes spins to have varying precession frequencies based on spatial location (Figure 1.1 and 1.2). Turning off the gradient results in the spins returning to the same Larmor frequency; however, each spin has its own spatially dependent phase encoding. A second phase shift (rephasing) gradient and a 180-degree inverting pulse is then applied that is equal in strength but opposite in direction. All spins that remained static in the direction of the gradient will return to their initial state. In other words, a spin with a positive phase shift after the first gradient encoding will have its phase shift negated after the second gradient encoding. On the other hand, spins that have diffused in the direction of the gradient will retain some phase shift. Phase shifts result in less synchronous sinusoids in the FID signal, resulting in lower intensity values. Spins that have moved a larger distance in the time between the dephasing and rephasing gradients will experience a larger signal intensity loss. This procedure is repeated multiple times for multiple diffusion gradients. The MRI parameters defining the diffusion gradients (g, δ, Δ), and the gyromagnetic ratio γ are often described as the b-value, b (Equation 1.1) (Figure 1.2).

$$b = \gamma^2 \delta^2 (\Delta - \tfrac{1}{3}\delta) g^2 \qquad\qquad \text{Equation 1.1}$$

The FID signal magnitude is described as in Equation 1.2, where S_i is the FID magnitude of the ith diffusion gradient, where $i=0$ is referred to as the b0 image (no diffusion encoding), and D is the diffusion coefficient. The equation is often solved for D to obtain the diffusion coefficient given the baseline signal, the signal acquired, and the MRI parameters.

$$S_i = S_0\exp(-bD)$$ Equation 1.2

Lastly, analogous to k-space, **q-space** is sampled by repeating the pulsed-gradient spin echo sequence; each **q**-vector represents one phase shift gradient weighting direction and strength, and this represents one diffusion weighted image (Hagmann et al., 2006; Özcan, Wong, Larson-Prior, Cho, & Mun, 2012).
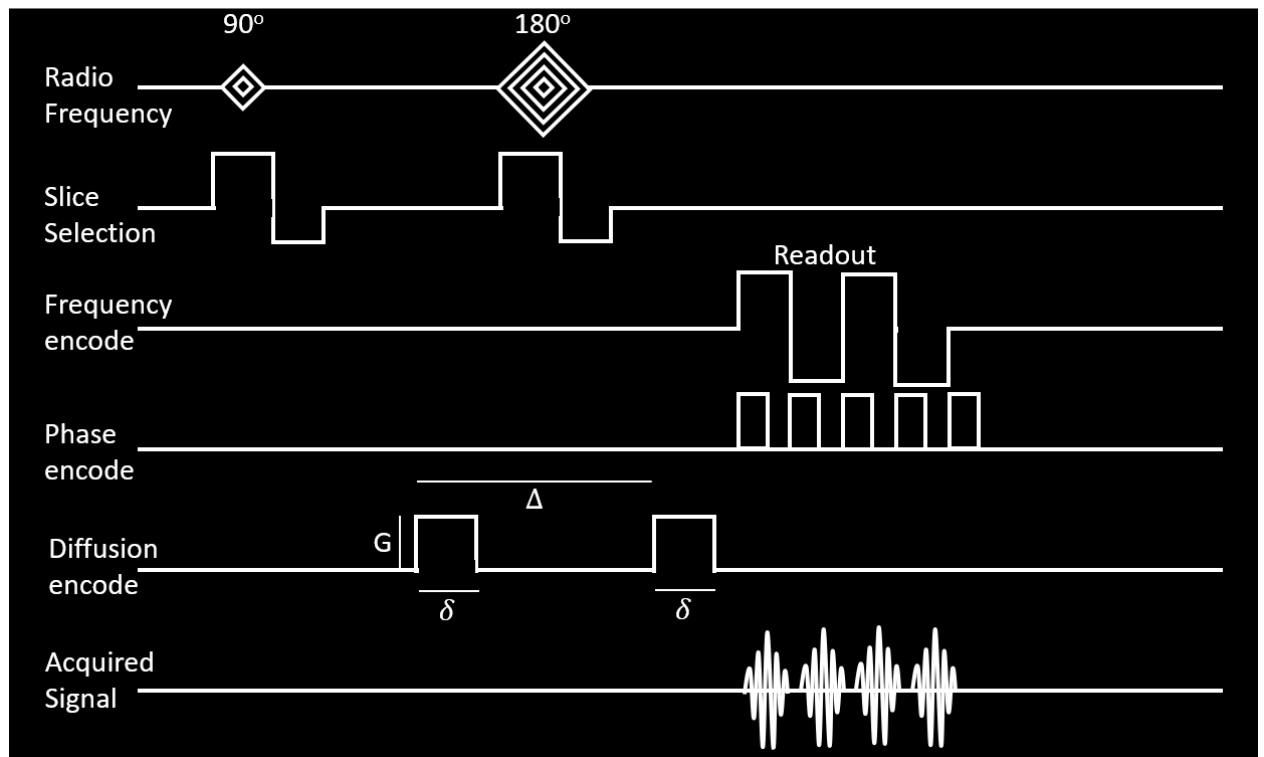
Figure 1-2: Pulsed Gradient Spin Echo Sequence Diagram

Pulsed gradient spin echo sequence diagram utilized in diffusion imaging. The Diffusion encoding parameters determine the b-value weighting. The 180-degree pulse effectively reverses the direction of the diffusion encoding, so that the second diffusion encoding gradient is equal and opposite in direction.

1.4.2   ESTIMATING FIBER ORIENTATION

1.4.2.1   *WHITE MATTER ANISOTROPY*

The diffusion signal captured by diffusion imaging depends on the tissue being imaged. The brain consists of cortical, subcortical, and cerebellar gray matter, and these regions are connected via tightly bound axonal fiber bundles called white matter. In an open medium, water molecules will randomly diffuse with a Gaussian spatial distribution; however, in the presence of impermeable barriers, the displacement distance is reduced, and the distribution would be narrower when compared to unrestricted diffusion. Axonal fibers are surrounded by glial cells, and densely packed bundles of axons create a diffusion barrier to water molecule diffusion perpendicular to the fiber bundles, whereas diffusion is unrestricted parallel to the fiber bundles (Hagmann et al., 2006). Isotropic diffusion describes water diffusion that is unrestricted during the observed time frame. Cerebral spinal fluid exhibits isotropic diffusion, and since water diffusion is unrestricted, the diffusion signal is low. Anisotropic diffusion describes water diffusion that is restricted in at least one direction. White matter exhibits anisotropic diffusion, and hence the diffusion signal would be low in the direction of white matter tracks if the b-vector is applied in that fiber bundle orientation. To capture complex fiber structures and orientations in the brain, multiple b-vectors are required. Gray matter exhibits a combination of iso- and anisotropic diffusion.

1.4.2.2 *MATHEMATICAL MODELS FOR FIBER ORIENTATION*

Diffusion models are utilized in order to reduce the high dimensionality of diffusion imaging data. The diffusion imaging sequence produces many 3D images, containing information about the diffusion profile at any given voxel in 3D space for every vector in q-space. This high-dimensionality image is reduced using diffusion models that assign a scalar to the anisotropy of the signal, and a separate image describing the main directionality of the underlying fiber orientation distribution. Other scalars can be obtained, such as the mean diffusivity (MD) which describes the mean diffusion in the diffusion signal.

The diffusion tensor model is the most commonly applied diffusion model. It results in a 3x3 matrix that applies an ellipsoidal shape to the diffusion in 3D space by assuming that the displacement distribution is Gaussian. Another assumption in the model is that the diffusion signal at every voxel originates from one fiber bundle; this assumption is complicated by the underlying complexity of the brain's fiber orientations. From the matrix, three eigenvectors describe the diffusion shape in three orthogonal directions, and the largest eigenvector describes the primary diffusion direction (Basser, Mattiello, & LeBihan, 1994). A minimum of six diffusion-weighted images (b-vectors, or samples in q-space) are needed in order to model the tensor. The most commonly reported value from the tensor model is the fractional anisotropy (FA), which compares every eigenvalue (λ_i) with the mean of the eigenvalues (λ_μ) (Equation 1.3).

$$FA = \sqrt{\frac{3}{2}} \sqrt{\frac{(\lambda_1 - \lambda_\mu)^2 + (\lambda_2 - \lambda_\mu)^2 + (\lambda_3 - \lambda_\mu)^2}{\lambda_1^2 + \lambda_2^2 + \lambda_3^2}} \qquad \text{Equation 1.3}$$

An assumption in the tensor model is that there is only one main fiber direction. Although this may be true for larger fiber bundles such as segments of the corticospinal tract and the corpus callosum, 63-90% of voxels in the brain are estimated to have complex fiber structures such as crossing or kissing fiber bundles (Jeurissen, Leemans, Tournier, Jones, & Sijbers, 2013). In the tensor model, crossing fibers of similar size would be estimated by the tensor model as a disc rather than an ellipsoid, because there would be no dominating eigenvector; there would be no preferential diffusion direction, and the tensor would be more isotropic.

To capture complex fiber structures, the q-space can be sampled more densely by acquiring many diffusion-weighted images (high angular resolution diffusion MRI, or HARDI). Every b-vector samples a point in q-space, where the distance between the origin and the sample is the b-value; measuring 150 or more diffusion-weighted images constructs a "ball" in q-space (if the b-value is kept constant). The resulting 4D diffusion image (150 diffusion-weighted images, in addition to the b0 images) can be modeled at each voxel with an orientation distribution function (ODF), which is a deformed sphere with a radius in a given direction proportional to the sum of the values of the diffusion probability density function in that direction (Hagmann et al., 2006).

One approach to estimate the distribution of fiber orientations in a voxel is using constrained spherical deconvolution (CSD) (Tournier, Calamante, & Connelly, 2007) by deconvolving the signal obtained during HARDI by the response function; the response function assumes the signal of a single fiber bundle. Another model is the simple partial volume model (the ball-and-sticks approach), which is the one we employed in this dissertation. This model assumes the diffusion signal comes from two-compartment

partial volume model: an anisotropic and an isotropic compartment. The model is then expanded to a distribution of fiber orientations by assuming that every subvoxel has only one fiber direction, and that the acquired MR signal is the sum of subvoxels. Again, the model assumes an isotropic component and an anisotropic component defined by a distribution of fiber orientations. For more information, we direct the reader to the publication where the model is developed (Behrens, Woolrich, et al., 2003). The major parameters obtained from this model include the fraction of the signal contributed by anisotropic fiber direction, f, and the dispersion of the main and secondary (in crossing-fiber voxels) fiber directions. These could in turn be used as surrogate measures of FA (Douaud et al., 2009).

1.4.3   ESTIMATING FIBER TRACTOGRAPHY

Given the local voxel-level fiber orientation, fiber tractography methods can be implemented to obtain a measure of global structural connectivity. Specific fiber bundles can be constructed by placing seed points, way points, and end points; additionally, stopping criteria are required to prevent fiber tracks from entering implausible regions. Seed points initialize a trajectory, and subvoxel steps are iterated in the direction of the fiber orientation at the voxel. Subsequently, these fiber tracks enter a new voxel and continue in the direction defined by that voxel. If the goal is to construct the corticospinal tract, the seed point may be set at the premotor cortex, way points may be defined at the posterior limb of the internal capsule, and the end point would subsequently be at the pons. Thus, only fiber tracks that touch all three regions would be accepted. Whole-brain tractography seeds the entire brain volume (either at the white matter-gray matter

interface, or all of the white matter) (Hua et al., 2008). Tractography can be constrained further to only include tracks that end in gray matter (Lemkaddem, Skioldebrand, Dal Palu, Thiran, & Daducci, 2014; R. E. Smith, Tournier, Calamante, & Connelly, 2012).

Deterministic fiber tractography projects one fiber trajectory (streamline) along the main fiber orientation. Typically, the stopping criteria is an anisotropy threshold (based on the tensor model), or the maximum curvature of the track (Mori, Crain, Chacko, & van Zijl, 1999). A common limitation to deterministic tractography is its inability to map out crossing fibers, specifically those crossing in the pons, or fanning fibers specifically those in the corona radiata (Behrens, Johansen-Berg, et al., 2003).

Probabilistic tractography utilizes complex models that can estimate multiple fiber orientations at a voxel, such as CSD or the ball-sticks model. This methodology estimates a distribution of possible connections by sampling multiple streamlines; the probability of a connection can then be estimated as a normalized sum of fibers crossing a voxel. Unlike the deterministic approach which seeds one voxel and generates one streamline via a defined fiber orientation, probabilistic tractography—in particular, the algorithm employed in FMRIB Software Library (Behrens, Berg, Jbabdi, Rushworth, & Woolrich, 2007)—randomly seeds hundreds to thousands of starting points in a sphere within the voxel and generates thousands of streamlines via perturbations around the primary and secondary fiber orientations. At every step, the streamline trajectory is perturbed slightly; however, trajectories are favored in the direction of greatest diffusion coefficient.

Using the ball-and-sticks model, probabilistic tractography utilizes the dispersion as a measure of uncertainty—how certain the algorithm is of the fiber orientation. The

greater the dispersion, the greater the standard deviation in that particular fiber orientation. If two fiber populations are estimated per voxel, two dispersion images are estimated, each with 50 perturbations along that fiber orientation. Seeding thus follows a unique direction at every iteration. As streamlines enter a new voxel, the streamline draws from *that* orientation distribution, the main fiber orientation, and the dispersion. Lastly, with the exception of the fiber curvature angle, probabilistic tractography employs other termination criteria as compared to deterministic tractography. Rather than use a fiber anisotropy threshold to terminate streamlines and prevent them from entering regions with low uncertainty, probabilistic tractography continues to propagate streamlines. However, as streamlines enter regions with high uncertainty (low anisotropy), streamlines take on a wider distribution of trajectory directions. Thus, the probability of any of those streamlines being the true underlying fiber bundle decreases.

Probabilistic tractography requires more computational power than deterministic tractography to map the whole-brain structural connectome due to the thousands of streamlines per voxel. Computer parallelization techniques can be employed by splitting up the total number of generated streamlines into multiple computer cores, and randomly selecting from the orientation distribution in every core so that no two cores produce the same results.

1.5   BIOMARKERS OF MOTOR IMPAIRMENT AND RECOVERY

1.5.1   WHITE MATTER INTEGRITY

As previously stated, measures of diffusion anisotropy and fiber connectivity can be used as biomarkers for stroke recovery and rehabilitation. Motor impairment, fine

motor control, and hand function is related to FA of the corticospinal tract (Koyama &

Domen, 2017; Mang et al., 2015; Puig et al., 2010; Schulz et al., 2012; Wen et al., 2016)

in both chronic and acute stroke (Puig et al., 2011). The FA rests on the assumption of

one major fiber bundle in the voxel, and although it has been validated in large fiber

tracks (Budde & Annese, 2013; Budde & Frank, 2012), it is only sensitive to local effects

of the lesion (Kalinosky, Schindler-Ivens, & Schmit, 2013) and is affected by complex

fiber structures (Behrens, Woolrich, et al., 2003). Not only will FA be smaller in areas of

crossing fibers. A decrease in FA might indicate axonal degeneration (Vedantam et al.,

2014). However, an increase in FA might not necessarily mean *increased* axonal

integrity; white matter degeneration in perpendicular fibers (Douaud et al., 2011;

Wheeler-Kingshott & Cercignani, 2009) can artificially increase FA.

1.5.2 WHITE MATTER CONNECTIVITY

1.5.2.1 CALCULATING THE CONNECTOME FROM TRACTOGRAPHY

A connectivity matrix can be constructed after calculating fiber tracts seeded at

every voxel. Voxels can be grouped based on anatomical information from gray matter

gyri segmentation, or using segmentation based on independent component analysis from

fMRI data. Voxels that share a fiber tract are then considered structurally connected, and

the sum of the connectivities of all voxels in a region are summed to represent that

region's connectivity. Alternatively, the connectome can be kept at the finer resolution of

the voxel level (Rubinov & Sporns, 2010; Zalesky et al., 2010). Key terms in graph

analysis are nodes (gray matter regions in our context), edges (white matter tracts), direct

connections, or level-1 connections (in which two gray matter nodes are connected by a

white matter tract), and indirect connections, or level-2 connections (in which two gray matter nodes are connected via a third node). A "step" refers to the progression from direct to indirect connections (level-1 to level-n).

1.5.2.2 *GRAPH ANALYSIS*

Graph analysis utilizes graph theory and mathematical approaches to solve these problems. These calculations are done at the matrix level. Given that a row and column in a connectivity matrix denotes two gray matter nodes (assuming the row and column are unique), and the white matter tract is represented by a vertex in the matrix, graph theoretical parameters can be computed. A direct connection is all nodes connected to a node of interest by an edge. In the matrix, a direct connection can be determined by obtaining the set of all columns with non-zero entries for every row. An indirect connection is a connection that connects two nodes via a third node without forming triangles; in other words, a node cannot be an indirect connection if it is already a direct connection. This can be calculated in the matrix by first determining all of the columns with non-zero entries at every row and looking at that set of rows to identify columns that were not present in the first set. Other advanced measures include the clustering coefficient which measures the level of connectedness between all direct connections of a node, and the shortest path length which measures the minimum number of steps connecting given regions. Lastly, the small-world metric measures the level of segregation and integration in a graph network. Read Rubinov & Sporns, (2010) for a review.

Some measures have been developed in the context of human brain connectivity. J. J. Crofts & Higham, (2009) developed the weighted communicability as a way to increase the sensitivity to disruptions in connectivity in the contralesional hemisphere. Indirect connectivity—in which two nodes are connected via an intermediary node—is particularly applicable in brain connectivity analyses because regions in the brain are either directly or indirectly connected. Typically, direct connections are assigned as "level-1" connections, while the immediate indirect connection is the "level-2" connection. Direct connections of indirect neighbors ("level-3") have been found to be sensitive to changes in brain connectivity after stroke, with higher sensitivity to global damage to connectivity and higher predictability to motor impairment after stroke (Kalinosky et al., 2013).

1.6 MOTOR-RELATED PATHWAYS AND RECOVERY

The brain is a collection of gray matter regions housing neural bodies that process information, and white matter volumes bundling axonal fiber that transfer information. Damage to the motor system can be caused by either damage to the gray matter regions initiating movement, to regions involved in the coordination of movement, or to white matter volume involved in the conduction of motor and sensory information. In other words, the motor system is complex and redundant, but also vulnerable. For instance, an animal model recently showed that cortical lesions had a greater percent improvement at 8 weeks than striatal lesions (Karthikeyan, Jeffers, Carter, & Corbett, 2019), potentially due to the redundancy in the cortical motor system (Jones & Adkins, 2015; Karthikeyan et al., 2019).

Complex motor behavior involves connectivity between specialized regions. Subcortical regions are involved in complex motor feedback systems that include the putamen, the thalamus, and the striatum. With the exception of the sensorimotor cortex, cortical structures are thought to play a role in movement initiation. The cerebellum, although a smaller structure compared to the cerebrum, is highly connected and is involved in posture and temporospatial coordination, among other motor and non-motor tasks. Damage to white matter may affect not only the conduction of information from connected motor regions, but also information from other regions. Additionally, degeneration of myelin sheaths may reduce the speed of conduction, resulting in a gradation of motor deficits.

1.6.1   CORTICOSPINAL TRACT

The corticospinal tract is the major descending white matter pathway and it is associated with motor control. It begins in the motor cortex, descends to the cerebral peduncle, and crosses to the other hemisphere via the pons as it connects with lower motor neurons in the spinal cord. In stroke, direct damage to it (lesion load) and the integrity of it after cortical damage has been associated with motor impairment, strength, coordination, and recovery (Koyama & Domen, 2017; Puig et al., 2013; Schulz, Braass, et al., 2015).

1.6.2   COMMISSURAL PATHWAYS

The corpus callosum is a major commissural pathway that connects cortical regions interhemispherically. It can be subdivided in the rostral-caudal direction, and is

related to motor, sensory, and cognitive functions as it integrates information from one hemisphere to the other. In stroke, it has been related to motor function (Hayward et al., 2017; Mang et al., 2015), and its damage is related to damage of the corticospinal tract (Liu, Qin, Zhang, Zhang, & Yu, 2015). It has also been implicated in interhemispheric inhibition—a process in which one hemisphere inhibits the other, primarily during unilateral motor tasks (van der Knaap & van der Ham, 2011).

1.6.3   CEREBELLAR PATHWAYS

The cerebellum is involved in many aspects of sensorimotor function, such as processing error (Seidler, Noll, & Thiers, 2004), timing of complicated movements (Boyd & Winstein, 2004), proprioception (Bhanpuri, Okamura, & Bastian, 2013), and the coordination of movements involving multiple degrees of freedom (Charles, Okamura, & Bastian, 2013). The cerebellum connects to the contralateral supratentorial cerebrum via the middle and superior cerebellar peduncles. In particular, the superior cerebellar peduncles—the main outflow tract—originate in the cerebellar nuclei and connect to the contralateral mid-brain. The middle cerebellar peduncle is the major inflow tract that connects the contralateral pontine nuclei to the cerebellar cortex. Its involvement in non-motor tasks (Schmahmann, MacMore, & Vangel, 2009) emphasizes the cerebellum's importance to the brain's network and—due to its high connectivity to the brain—its connection's vulnerability to supratentorial lesions.

1.6.4   DIASCHISIS AND NETWORK DAMAGE

Diaschisis was first defined in 1914 as the presence of a focal lesion, distal reductions in excitability, disconnections between the lesioned core and remote regions, and clinically observable progression of the 'schism' (von Monakow, 1914; Carrera & Tononi, 2014); however, until advancements in non-invasive imaging techniques and the implementation of graph analysis on the human brain network, measurement of diaschisis was unfeasible.

Regions remote to the lesion core exhibit loss of connectivity and function after stroke, and damage to network hubs produces extensive damage elsewhere in the brain. For instance, removing critical regions such as those in the superior parietal and frontal lobes causes the largest change in the network's global efficiency (Iturria-Medina et al., 2008). Damage to regions remote from the lesion can occur in the absence of direct connections. This suggests that damage to areas connecting to a region can be as important to network connectivity as damage to the region itself, which can lead to disruptive effects on the network and subsequent impairment and recovery post-stroke (Borstad et al., 2016; He et al., 2007).

1.6.4.1 *FUNCTIONAL DIASCHISIS*

The brain's response to focal lesion damage is also dependent on whether the brain is at rest or at task. Resting state functional connectivity in MRI shows reduced interhemispheric connectivity in people with stroke, and interhemispheric connectivity is related to 90-day outcome (Puig et al., 2018). Additionally, the connectivity of the default mode network—a resting-state network including the posterior cingulate cortex, medial prefrontal cortex, and the posterior inferior parietal lobe—is reduced after focal ischemic

lesions in stroke patients (Tuladhar et al., 2013). During unilateral task, activation patterns become less localized and exhibit increased activation in the contralesional hemisphere (Cramer, Finklestein, Schaechter, Bush, & Rosen, 1999; Du et al., 2018; Kalinosky, Vinehout, Sotelo, Hyngstrom, & Schmit, 2019). Additionally, functional diaschisis is also task-dependent (Kalinosky et al., 2019; Vinehout, Schmit, & Schindler-Ivens, 2019). Lastly, functional connectivity shows reduced connectivity between the lesioned sensorimotor cortex and the contralesional cerebellum (Kalinosky et al., 2019).

1.6.4.2 *Cross Cerebellar Diaschisis*

Other diaschisis terms, such as "cross-cerebellar diaschisis" (Feeney & Baron, 1986) describe specific remote damage to cerebellar structures following focal damage to supratentorial regions. The cerebellum has decreased perfusion after ischemic lesions affecting areas in the cortico-cerebellar loop (Förster et al., 2014; Sommer et al., 2016), likely the result of reduced excitatory signals from the cortex (Gold & Lauritzen, 2002). Similarly, gray matter atrophy has been measured in regions that are structurally connected to the primary lesion location (Cheng et al., 2015; Dang et al., 2013; Yassi et al., 2015). White matter tissue is also affected by stroke as oligodendrocytes, a key supporting neuroglia of the white matter architecture, are sensitive to ischemia and excitotoxicity (Domercq et al., 2007; Husain & Juurlink, 1995), and axonal degeneration extends beyond the area of direct injury (Jirjis et al., 2016; Wang et al., 2012). Thus, stroke-induced changes to neural structure extend throughout the brain, including gray and white matter structures distant from the injury site.

1.6.4.3 *INDIRECT CONNECTIVITY TO MEASURE STRUCTURAL DIASCHISIS*

Imaging techniques can measure resting and task-related diaschisis after stroke by measuring functional activity and connectivity, and tissue perfusion. Measuring the underlying anatomical and white matter structure mechanisms that could lead to these observations requires novel computational techniques. For instance, functional connections exist without the presence of structural connections (Honey et al., 2009) because two regions can be functional connected via indirect connections. Developing measures that assign the connectome information from direct and indirect connections at every region or voxel could reveal white matter pathways associated with motor deficits and relate tolocal and global changes in functional connectivity. Initial results are promising. Network loss in distant and contralesional areas of the brain can be detected via indirect connections (Crofts & Higham, 2009; Griffis, Metcalf, Corbetta, & Shulman, 2019; Kalinosky et al., 2013).

1.7 **SPECIFIC AIMS**

The purpose of this dissertation is to develop imaging biomarkers that are sensitive to identifying whole brain structural networks that are damaged after subacute and chronic stroke. We also aim to determine the influence of these remotely connected gray matter regions and white matter pathways on motor impairment. Typical analyses have related direct white matter pathways to post-stoke motor impairment; however, gray matter volume, functional connectivity, and perfusion imaging studies have shown the brain exhibits global changes after stroke. Our three aims will implement different

imaging biomarkers based on indirect connectivity and complex connectome measures in order to identify global changes in brain connectivity after stroke.

1.7.1 AIM I: DETERMINE IF INDIRECT STRUCTURAL CONNECTIVITY CAN DETECT CHANGES IN BRAIN NETWORKS AFTER STROKE

In order to determine if whole-brain indirect structural connectivity can detect changes in brain networks after stroke, we will use diffusion MRI, probabilistic tractography, and a region-level implementation of the voxel-wise indirect structural connectivity, (VISC), (Kalinosky et al., 2013), to measure how connections to remote regions change after stroke. *Our hypothesis is that probabilistic tractography and an indirect connectivity analysis will be able to detect changes to brain networks after stroke, in particular to cerebellar regions.*

1.7.2 AIM II: DETERMINE THE INFLUENCE OF REMOTE WHITE MATTER INTEGRITY ON STROKE IMPAIRMENT

In order to characterize the role remote white matter connections have on stroke impairment, we will scan chronic stroke participants with unilateral lesions. Global structural connectivity and integrity will be assessed using probabilistic tractography and a novel structurally weighted white matter integrity algorithm that weighs a location's white matter integrity by that of its direct connections. Lastly, white matter tracks associated with motor control will be compared to stroke impairment. *Our hypothesis is that disruption to commissural and cerebellar WM connections will be related to stroke impairment.*

1.7.3   A IM III: I DENTIFY C HANGES IN I NDIRECT S TRUCTURAL C ONNECTIVITY IN THE
         F IRST S IX M ONTHS A FTER S TROKE

In order to identify white matter fiber tracts damaged after stroke and their

differences in connectivity in subacute and chronic stroke, we will obtain diffusion MR

scans and sensorimotor impairment measurements for subacute and chronic stroke

participants. Indirect connectivity, methods to compare network topology, and lesion

effect simulation based on lesion volumes will be implemented. Lastly, connectivity of

motor-related white matter fiber tracks will be compared with improvements in motor

impairment score. *Our hypothesis is that the white matter connectivity will be more*

sensitive to neurodegenerative changes in white matter structure during stroke, and that

the connectivity of cerebellar-cerebral connections in subacute stroke will predict

improvement in chronic stroke motor impairment.

2   *C HAPTER 2: I NDIRECT STRUCTURAL CONNECTIVITY IDENTIFIES CHANGES IN BRAIN NETWORKS AFTER STROKE*

2.1   I NTRODUCTION

In this study, we investigated brain structural connectivity in people with stroke

using indirect connectivity metrics based on diffusion magnetic resonance imaging

(dMRI). In general, measures obtained from dMRI in acute stages of stroke might

provide clinically important tools to predict functional outcomes and personalize

rehabilitation strategies. In this study, we postulated that dMRI measures of indirect

connectivity, in which two brain regions are structurally connected through a third region,

would provide important information about the functionality of the brain after stroke.

While the impact of stroke on direct connections has been established, its effects on the broader connectome might be particularly important to recovery. Thus, the purpose of this study was 1) to provide evidence of changes in indirect structural connectivity after stroke, and 2) to relate changes in indirect connectivity to post-stroke impairment.

The effects of stroke on the brain are not limited to the area of the lesion. Ischemic stroke produces both rapid neuronal degeneration at the epicenter and cytotoxic cellular reactions that result in injury outside the lesion core (Domercq et al., 2007). Effects extend beyond regions adjacent to the lesion as well. For example, the cerebellum has decreased perfusion after ischemic lesions affecting areas in the cortico-cerebellar loop (Sommer et al., 2016), likely the result of reduced excitatory signals from the cortex (Gold & Lauritzen, 2002). Additionally, white matter (WM) degeneration extends beyond the area of direct injury, (Jirjis et al., 2016; Wang et al., 2012) and gray matter (GM) atrophy has been observed in regions that are structurally connected to the primary lesion location (Cheng et al., 2015; Yassi et al., 2015). Thus, stroke-induced changes to the neural structure extend throughout the brain, including gray and white matter structures distant from the injury site.

The functional connectivity of the brain depends on indirect structural connections (Sporns, 2011), which could play a key role in functional recovery after stroke. In the uninjured brain, indirect connections can account for resting state functional connectivity that is unexplained by direct connections (Honey et al., 2009). Consequently, our laboratory previously developed a voxel-level measure of indirect connectivity (VISC) in order to take into account the effects of indirect connections on functional connectivity, resulting in a structural connectivity metric that correlates with

motor impairment in people with stroke (Kalinosky et al., 2013). In addition, the VISC identified changes in connectivity of voxels distant from the stroke epicenter, reflecting the more widespread impact of stroke on brain connectivity through indirect connections. While this voxel-based approach provides an unbiased assessment of brain connectivity, it can be difficult to relate the results to observations of loss of functional connectivity in specific regions of the brain after stroke. As an example, we recently found reduced structurofunctional connectivity between the prefrontal cortex and the cerebellum that correlates with arm function (Kalinosky et al., 2017). A region-based approach could provide additional interpretive information about the impact of structural connectivity on brain function.

In this study, we modified the VISC in order to detect region-specific changes in connectivity after ischemic stroke. We integrated probabilistic tractography into an indirect connectivity measure and applied the technique to the whole-brain using a region-level analysis. We hypothesized that in comparison to direct connectivity and WM integrity, measures of indirect connectivity would detect more regions with reduced connectivity after stroke, including the cerebellum and other gray matter (GM) nodes with high centrality. Additionally, we hypothesized that reduced structural indirect connectivity of GM regions combined with WM integrity within the corticospinal tract (CST) would better predict stroke impairment compared to either measure alone.

2.2 MATERIALS AND METHODS

2.2.1 DATA COLLECTION

2.2.1.1   *SUBJECT RECRUITMENT*

Thirteen chronic stroke survivors (at least six months after stroke) (7 female) and 16 age-matched control participants (8 female, age 63.4, range 47 to 78) participated in this study. Each participant provided written consent to the experimental protocol, which was approved by the Institutional Review Boards at Marquette University and the Medical College of Wisconsin. The inclusion criteria included a minimum age of 18 (stroke mean age: 66.9, control mean age: 63.4 years), and the ability to independently answer questions, follow directions, and provide informed consent. Contraindications included claustrophobia, other known brain pathology, and MRI incompatibility. For participants with stroke, there were no restrictions with regard to the stroke location or severity.

A measure of upper extremity motor impairment was obtained for stroke participants using the Fugl-Meyer (FM, maximum of 66 points) upper extremity motor test, (Fugl-Meyer et al., 1975). Lower values indicate greater motor impairment. Table 2.1 contains information on the study participants.

Table 2-1: Stroke Participant Information

Stroke participant information, including identification number, sex, age, Fugl-Meyer score, lesion location and hemisphere. For the participants that had multiple lesions, the larger lesion is listed first.

Subject ID	Sex	Age	Fugl-Meyer (UE, out of 66)	Lesion Location	Lesion hemisphere
S02	F	64	55	Cortical	L/R
S04	M	65	64	Cortical	R
S05	M	57	59	Subcortical	L
S07	F	83	36	Pons	L
S08	M	66	62	Subcortical	L/R
S10	M	69	64	Cortical	L

S12	F	65	47	Cortical	R
S14	M	64	60	Cerebellar	L
S15	F	80	66	Subcortical	R/L
S18	M	66	64	Subcortical	L
S19	F	60	45	Subcortical	R
S20	F	73	29	Subcortical	R
S21	F	57	25	Subcortical	R

M = Male; F = Female; R = Right; L = Left

2.2.1.2 *MRI SCANS*

All MRI scans were performed using a short bore 3T GE Discovery MR750 scanner. Axial T1-weighted images were acquired using the fast spoiled gradient recall (FSPGR) 3D pulse sequence, with the following parameters: TE=3.2ms, TR=8.16ms, flip angle=12 degrees, FOV=240mm, at 156x1mm slices with an in-plane axial matrix of 256x240. Axial diffusion scans were acquired using the Q-ball high angular resolution diffusion imaging (HARDI) sequence using a single-shot echo planar imaging (ssEPI) protocol, with the following parameters: TE=72.3ms, TR=5700 ms, FOV=256mm at 59x2.5mm slices with an in-plane axial matrix of 128x128. There were 150 gradient directions (b-value=1500 s/mm^2) and five b=0 images.

2.2.2 MRI DATA PROCESSING

2.2.2.1 *IMAGE PRE-PROCESSING*

Raw Digital Imaging and Communications in Medicine (DICOM) images were converted to NIFTI image format (Neuroimaging Informatics Technology Initiative) using *mricron* (Rorden et al., 2007). All preprocessing was done using the FMRIB Software Library (FSL) (Jenkinson et al., 2012). MR bias field correction and skull

stripping were performed on the raw T1-weighted images. The diffusion images were corrected for eddy-currents and skull stripped. Eddy current correction also corrected for intra-scan motion using affine registration. Additionally, the fractional anisotropy (FA) of each stroke participant was calculated from the HARDI.

2.2.2.2 *LESION IDENTIFICATION*

Lesions were automatically identified using the Lesion Identification with Neighborhood Data Analysis (LINDA) algorithm, (Pustina et al., 2016). The algorithm requires the lesions to be on the left hemisphere; therefore, prior to pre-processing, all raw T1 and diffusion weighted images with right-hemisphere lesions were flipped to the left hemisphere, and the diffusion gradient vector file was flipped in the X-direction. One participant had a lesion on the left hemisphere of the cerebellum. Most cerebellar afferent and efferent connections cross hemispheres to connect to the contralateral cortex (Allen & Tsukahara, 1974). Because of this, the stroke participant with the left-cerebellar lesion was flipped to reflect a right-cerebellar lesion.

2.2.2.3 *IMAGE REGISTRATION*

Linear registration transformed the diffusion images to the native T1 space in 6 degrees of freedom, and the T1-weighted images to the 152-MNI brain average space in 12 degrees of freedom (FSL's *flirt* function). Non-linear registration warped the affine-registered T1-image to the standard 152-MNI space (FSL's *fnirt* function). Lesion masks alleviated registration in the area of the lesion, and registration quality was assessed visually.

2.2.2.4 *STRUCTURAL CONNECTIVITY*

2.2.2.4.1 NETWORK NODES

Cortical and subcortical volume segmentation was performed on the 152-MNI standard brain using the *recon-all* tool in the Freesurfer image analysis suite, (http://surfer.nmr.mgh.harvard.edu/). This produced 34 cortical and 8 subcortical volumes in each hemisphere, in addition to cerebral spinal fluid and ventricular estimations which were combined to form a 'non-brain' volume. A probabilistic atlas of the human cerebellum was obtained from FSL which contains 28 cerebellar nodes (Diedrichsen et al., 2009). Including 2 brain stem volumes, a total of 114 GM nodes were incorporated into the connectome.

2.2.2.4.2 DIFFUSION TRACTOGRAPHY

Diffusion direction and orientation estimates were obtained from the eddy-corrected images using the FSL *bedpostx* function (Behrens, Woolrich, et al., 2003). Three fibers were estimated per voxel, each with a range of diffusivities. Probabilistic diffusion tractography was performed using the *probtrackx2* function in the 152-MNI space. Each voxel from the GM nodes was seeded, and streamline samples were randomly drawn from a 1-mm sphere centered at the voxel. The connectivity results from all voxels in a given GM node were summed to produce a 114-by-114 connectivity matrix. Default parameters were used for the number of steps, step length, curvature threshold. Fibers were terminated if the streamline entered a 'non-brain' exclusion mask.

In order to reduce the processing time and memory load when seeding all voxels in the 114 GM nodes (782,454 voxels), processing was parallelized by sending smaller jobs to more processors using the *--rseed* option in *probtrackx2*. This option randomly selects different samples from the orientation distribution function such that no two parallel jobs were the same. We determined that sampling 500 streamline fibers per voxel was sufficient. This was determined by measuring the effect on the connectivity matrix (percent change in the mean degree in the brain) by adding 10 more streamlines per voxel. The percent change curve was an exponentially decreasing curve, and it stabilized at approximately 0.25% change at approximately 500 streamlines per voxel seeding the whole-brain gray matter. We split up the 500 streamlines per voxel into 50 processors, each sampling 10 streamlines per voxel—parallelizing this way sped up computation time, while calculating 500 rather than the recommended 5000 streamlines per voxel reduced RAM. As a result, each subject had 50 connectivity matrices, each with 114 nodes.

2.2.2.5 *POST-PROCESSING*

MATLAB (R2017a) was used to post-process the network connectivity matrices. The resulting 50 weighted and non-symmetric connectivity matrices were summed for each subject. The diagonal in the connectivity matrix is zero (a region cannot be connected to itself). A weight in the matrix is the probability of one of the 500 streamlines connecting any two nodes, and the matrix is non-symmetric as a result of the probabilistic nature of the tractography (and not due to anatomy nor the raw diffusion signal). Thus, the resulting merged matrix was forced symmetric by averaging the matrix

by its transpose. Additionally, we normalized the connectivity matrices in order to compare connectivities across subjects. The normalization technique has an effect on the overall topology – normalizing matrices to maintain the degree of the matrix may over-emphasize weak connections in matrices with overall low degree and under-represent strong connections in denser matrices. We chose to normalize by the average number of successful streamlines generated by the edge's endpoints. We averaged the total number of successful streamlines generated by two endpoints, i and j (w_i and w_j) and used that to normalize every edge, A_{ij} in the matrix, A (Equation 1).

$$A_{ij} = 2 * A_{ij}/(w_i + w_j) \hspace{3cm} \text{Equation 2.1}$$

Data from the probabilistic tractography were used to assemble a weighted connectivity matrix and a series of binary connectivity matrices. Probabilistic tractography produces dense matrices, with many edges containing low-probability connections, and thresholding is used to remove spurious connections. However, selecting the threshold may also affect the topology of the matrix. Gong et al., (2009) used a range of thresholds and this methodology is less sensitive to the subjective selection of thresholds on the matrix topology. Thus, we determined the maximum edge for every participant's normalized and symmetric connectivity matrix, and thresholded to maintain connections above a range of 0.5%-5% of the determined maximum in intervals of 0.125% (a total of 37 thresholds). The resulting 37 each had varying sparsities (a measure of the densitiy of connections in the matrix).

2.2.2.6 *NETWORK PARAMETERS*

Network parameters were calculated for all 37 connectivity matrices (A for the binary matrix, and W for the weighted matrix) for every subject and for all regions, N. Measures of direct connectivity (node degree and clustering coefficient) were calculated at each GM node, i, using the Brain Connectivity Toolbox, (Rubinov & Sporns, 2010). We calculated the node degree, K_i, as the total number of edges connected to a node (Equation 2.2), where A_{ij} represents the connection between nodes i and j.

Equation 2.2

$$K_i = \sum_{j \in N} A_{ij}$$

The clustering coefficient, C_i, was calculated as a measure of the extent a node's direct connections are connected to each other; this is a function of the number of triangles, t_i, (Equations 3 and 4). A represents the binary connectivity matrix, t_i is a measure of the number of triangles, and C_i is the clustering coefficient at node i.

Equation 2.3

$$t_i = \frac{1}{2} \sum_{j,h \in N} A_{ij} \, A_{ih} A_{jh}$$

Equation 2.4

$$C_i = \frac{1}{n} \frac{2t_i}{k_i(k_i - 1)}$$

Lastly, the weighted indirect structural connectivity (WISC) is introduced as the number of weighted connections to indirect connections. This metric was derived from the voxel-wise indirect structural connectivity (VISC) (Kalinosky et al., 2013), which was originally designed to amplify lesion-induced effects on prominent white matter tracts at the voxel-level in the entire brain. First, a binary indirect connectivity matrix, Y,

classifies two regions as being indirectly connected if the *ith* and *jth* regions share at least one common direct connection, *k*, but are not directly connected to each other (Equation 5). The VISC is the sum of the direct connections to the indirect connections, divided by the total number of indirect connections (Equation 6, Kalinosky et al., 2013). The numerator is the product of indirect connections of node *i*, Y_i (n-columns) multiplied by the weighted connectivity matrix, W (n-by-n), and multiplied by a vector of ones (n-rows) in order to perform the sum. Similarly, the denominator is the product of the indirect connection vector (n-columns) by a vector of ones (n-rows).

Equation 2.5

$$Y_{ij} = \begin{cases} (1 - A_{ij})(1 - \prod_{k=1}^{N}(1 - A_{ik}A_{kj})), & i \neq j \\ 0, & otherwise \end{cases}$$

Equation 2.6

$$WISC_i = \frac{\sum_{j \in N}\left(Y_{ij} \sum_{k \in N} W_{jk}\right)}{\sum_{j \in N} Y_{ij}} = \frac{Y_i W 1}{Y_i \, 1}$$

We calculated the *weighted* indirect structural connectivity, *WISC*, at each GM region in order to assess its ability to identify connectivity changes to distant GM regions after stroke. Our implementation calculated the binary indirect structural connectivity matrix, Y, (Equation 5), using the binary direct connectivity matrix, A, for all 37 sparsity levels. The WISC calculation in Equation 6 used probability-weighting, W. For every region at each of the 37 sparsity levels, the WISC was defined as the sum of the probability weights of the direct connections to the indirect connections, divided by the total number of indirect connections. The normalized weighted matrix, W, has a maximum normalized value of 1. The WISC's numerator is the sum of normalized

connectivity weights of the direct connections of indirect connections; thus, the numerator is greater than one. The denominator is the sum of indirect connections. Thus, the WISC *can* have values greater than one.

2.2.3 STATISTICAL ANALYSIS

Non-parametric permutation testing was performed at each GM region to test whether the stroke group mean for the network parameters (degree, clustering coefficient, or WISC) differed from the mean of the control group (FSL's *randomize*). This test was performed 37 times (once for each sparsity level) for all 114 regions; thus, the p-value was corrected twice. For every sparsity level, false-discovery rate corrected for multiple comparisons of all 114 regions, which provided corrected p-values. Only regions with p<0.0014 were identified as significant (p-corrected=0.05, Bonferroni-corrected for 37 observations). The resulting 37 images showing regions in which the metric (degree, clustering coefficient or WISC) had a statistically lower value in the chronic stroke group as compared to the control group were combined into one image for visualization and interpretation purposes.

Single and multiple linear regressions were performed in order to determine the correlation between WM integrity of the CST, the volume of GM with reduced connectivity, and motor impairment. A Pearson correlation test between the Fugl-Meyer score and the FA within the CST was first calculated. The volume of affected GM was defined as the total number of regions (vaGM), or number of motor-related gray matter regions (vaGM$_{motor}$), with a connectivity value (degree, clustering coefficient, WISC) significantly lower than the average of the control group. This was done by assuming a t-

distribution of the values within the control group, and a critical t-value corresponding to

an alpha value of 0.05. A Pearson's correlation was performed between motor

impairment and the vaGM or vaGM$_{motor}$ using the three metrics. Lastly, a multiple linear

regression was performed between motor impairment and the linear sum of the FA within

the CST and the vaGM or vaGM$_{motor}$ using degree, clustering coefficient and WISC. Out

of the 114 regions used in this study, thirty (30) were selected as motor-related (Table 2-

2).

Table 2-2: Gray Matter Motor Regions

Thirteen (13) regions are shown here to indicate the total 30 motor-related regions used in the regression analysis. There are two sets of cortical and subcortical regions—with the exception of the Brain Stem—in addition to the cerebellar I-IV, V, (left and right hemisphere)..

Regions		Motor-related function	Reference
Cortical	Paracentral gyrus	Part of the sensorimotor cortex; controls motor and sensory innervations, mainly lower extremity	(Frigeri, Paglioli, de Oliveira, & Rhoton, 2015)
	Precentral gyrus	Contains the primary motor cortex, (Brodmann's area 4), associated with movement generation including limb movement, speech control	(Itabashi et al., 2016)
	Postcentral gyrus	Contains the primary somatosensory cortex, and parts of Brodmann's areas 1, 2, and 3	(Caldwell et al., 2019)
	Superior parietal cortex	Contains Brodmann's areas 5 and 7, involved in spatial orientation and connected with the postcentral gyrus. Also involved in working memory	(Manuweera, Yarossi, Adamovich, & Tunik, 2019)
Subcortical	Thalamus	Information hub for every sensation system (except olfaction), and motor and language systems	(Sakayori et al., 2019)
	Putamen	Involved in motor planning, learning, and preparation, in addition to determining movement amplitudes and executing simple and complex movement sequences. Has been implicated in Parkinson's disease.	(Marchand et al., 2008)
	Pallidum	Mainly an inhibitory structure that counteracts excitatory action of the cerebellum and helps execute smooth targeted movements. Involved in voluntary and involuntary movements. Damage here can result in dystonia. Has been implicated in Parkinson's disease.	(Suryanarayana, Hellgren Kotaleski, Grillner, & Gurney, 2019)
	Diencephalon	Contains part of the pons and lower thalamus in this study. Relays motor impulses between	(Morecraft et al., 2018)

		the spinal cord and medulla oblongata and cerebellum.	
	Brain Stem	Contains the medulla oblongata and projection white matter pathways in this study (such as the CST). The gray matter is responsible for basic functions such as breathing and eating.	(Nicholls & Paton, 2009)
Cerebellar	I-IV	Reciprocal connections with primary motor cortex and exhibits somatotopic organization. Mainly lower extremity	(Diedrichsen & Bastian, 2013)
	V	Reciprocal connections with primary motor cortex and exhibits somatotopic organization. Mainly lower extremity	(Diedrichsen & Bastian, 2013)
	VI	Complex limb movements, showing bilateral activation for unilateral hand movements. May have connections with cortical secondary motor areas. The vermis part is associated with eye movements	(Buckner, Krienen, Castellanos, Diaz, & Yeo, 2011)
	VIII	Form part of the secondary motor cortical-cerebellar loop, similar to anterior lobe regions	(Diedrichsen & Bastian, 2013)

2.3 **RESULTS**

2.3.1 CHRONIC STROKE LESION DISTRIBUTION

Thirteen chronic stroke participants were recruited; most lesions were near the

internal capsule area and inferior parietal lobe (7 participants), one was near the pons, and

another in the left cerebellum. Four participants had predominantly cortical lesions. A

summary of the lesion locations is shown in Figure 2.1.
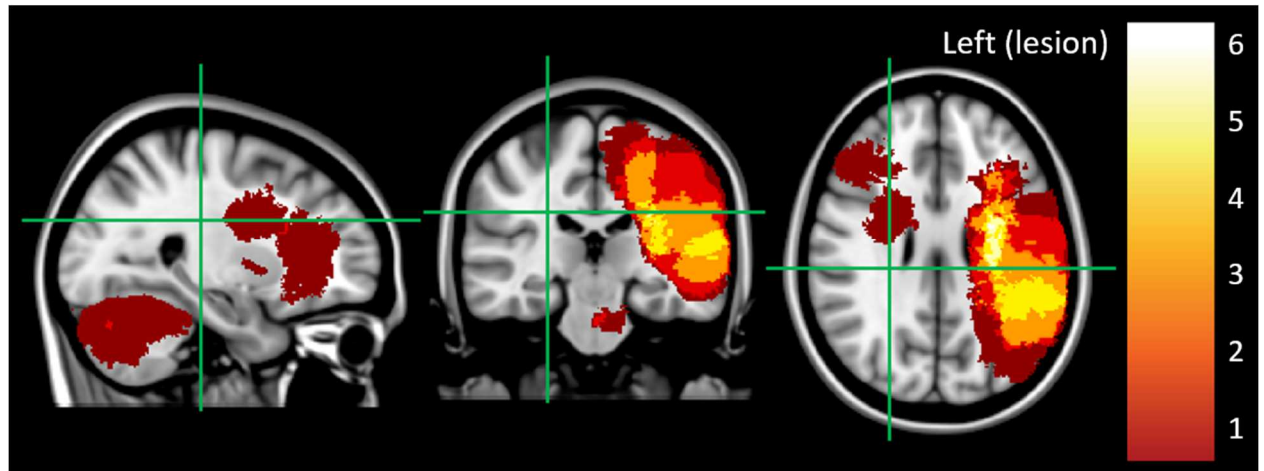
Figure 2-1: Stroke Lesion Distirbution

Heat map showing the lesion distribution of 13 chronic stroke participants in the right sagittal, frontal coronal, and the neurological axial view (green cross-hair shows location). The color bar on the right indicates one subject had a lesion in the brain stem and the cerebellum (dark red), and six participants had lesions near the internal capsule region (bright yellow).

2.3.2 CONTROL GROUP VARIATION IN WISC

The variation of WISC within the control group was calculated in order to ensure

that our measure of indirect connectivity was consistent in neurologically intact

participants. At each sparsity level (for the 37 binarizing thresholds), the WISC at each of

the 114 regions was summed to obtain a whole-brain WISC. The whole-brain WISC

decreased exponentially as the network sparsity increased. The within-group standard

deviation also decreased as the matrix sparsity increased; however, the coefficient of

variation was similar (12.7% at the lowest sparsity level, and 14.4% at the highest

sparsity level).

2.3.3   INDIRECT CONNECTIONS REVEAL LARGER EXTENT OF CONNECTIVITY POST STROKE

The WISC identified broad regions of indirect connectivity loss in participants with stroke compared to controls in regions in, around, and far from the lesion (p-corrected<0.0014). The WISC identified regions with reduced connectivity directly affected by the lesion (see Figure 2.2, rows 1 and 4). These regions included the ipsilesional precentral gyrus, rostral-middle-frontal gyrus, the post-central gyrus, superior-parietal gyri, regions in the temporal lobe, the ipsilesional pallidum and putamen, and bilateral caudate nucleus. The WISC also identified regions with reduced connectivity neighboring the lesion distribution. In particular, cortical gyri in the ipsilesional superior-frontal lobe, anterior and posterior segments of the cingulum, and the bilateral diencephalon were identified. Perhaps most important, however, was that the WISC identified regions with reduced connectivity far from the lesioned volume including the contralesional post-central gyrus, the brain stem, and cerebellar regions on both hemispheres, including the right (contralesional) region IX, and the left region VIIb.

Graph metrics of direct connectivity also differed between the stroke and control groups, but to a lesser spatial extent (p-corrected<0.0014). When compared to neurologically intact participants, the degree indicated reduced connectivity in stroke only in the ipsilesional cortical gyri, including the precentral gyrus, the rostral-middle-frontal gyrus, the superior-parietal gyrus, and parts of the bilateral caudal anterior cingulate gyrus (Figure 2.2, row 2). The clustering coefficient indicated lower connectivity in the anterior and posterior cingulate gyrus, the superior temporal gyrus, and the ipsilesional diencephalon (Figure 2.2, row 3).
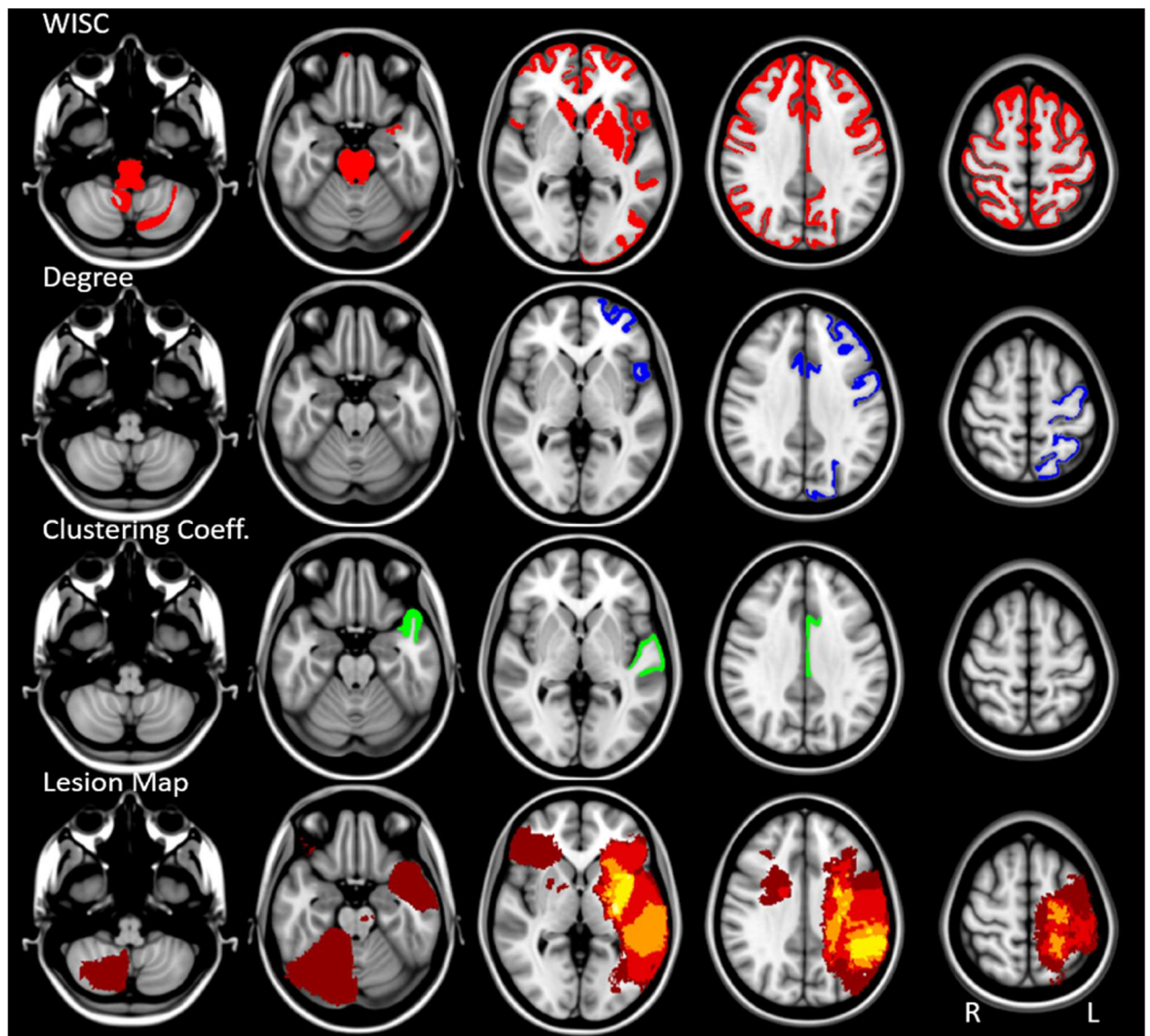
Figure 2-2: Indirect and Direct Connectivity Changes after Stroke

*Regions with statistically significant (p-corrected < 0.0014) reduction in indirect (red)
and direct (blue and green) connections. WISC identified reduced connectivity in the
cortical, subcortical, and some cerebellar regions, while measures of direct connectivity
identified reduced connectivity only in cortical regions. The fourth row shows the lesion
distribution (n=13).*

2.3.4   MEASURES OF CONNECTIVITY AND INTEGRITY PREDICT MOTOR IMPAIRMENT

The average fractional anisotropy within the CST (FA_{CST}) significantly correlated with motor impairment (R^2=0.52, p<0.05); the vaGM calculated by the WISC and degree trended, but did not significantly (p<0.1) correlate with motor impairment (R^2=0.24, R^2=0.16, respectively). When only counting the volume of affected motor-related gray matter ($vaGM_{motor}$), the reduction in gray matter connectivity calculated by WISC significantly correlated with motor impairment ($R^2 = 0.31$, p<0.05), while reduced connectivity of gray matter identified by degree did not significantly correlate with motor impairment (Table 2.3).

Adding vaGM or $vaGM_{motor}$ to regression of FA_{CST} with motor impairment produced a significant improvement (p<0.05) in the correlation, suggesting connectivity analyses can improve prediction of motor impairment. As shown in Figure 2.3 (top) and Table 2.3, using the FA_{CST} and the vaGM as independent variables, the multiple regression with motor impairment improved by 27% (R^2=0.66, p<0.05) when using the degree, and by 37% (R^2=0.71, p<0.05) when using the WISC. When only including motor-related regions in the analysis, the multiple regression of the FA_{CST} and the vaGM-motor with motor impairment improved the correlation by 12% (R^2=0.58, p<0.05) when using the degree, and by 33% (R^2=0.69, p<0.05) when using the WISC (Figure 2.3, bottom), although the improvement in the model was only significant when adding the WISC (p<0.05). As a reference, four stroke participant's vaGM is shown in Figure 2.4. These participants were selected due to their lesion location (subcortical, cortical, brian stem, and cerebellum).

Table 2-3: Multiple Linear Regression With Motor Impairment

The adjusted R^2 and p-values are listed for single linear regression (FA_{CST} and Connectivity) and multiple linear regression (MLR) (FA_{CST} + Connectivity) with the

upper extremity Fugl-Meyer. The connectivity values are the WISC and the Degree in the volume of affected GM (vaGM) and volume of affected motor-related GM (vaGM$_{motor}$). The p-value for the slope coefficients in the multiple linear regression are listed for the FA and the Connectivity measures. Significant models (p<0.05) are underlined, and MLR models with significant contributions of Connectivity values are highlighted (*)

FA$_{CST}$		Connectivity			FA$_{CST}$ + Connectivity			
R^2	p-value	Measure	R^2	p-value	R^2	p-value	FA$_{CST}$ p-value	Connectivity p-value
0.52	0.003	WISC vaGM	0.24	0.05	0.71	0.001	0.002	0.02 *
		Degree vaGM	0.16	0.1	0.66	0.002	0.002	0.04 *
		WISC vaGM$_{motor}$	0.31	0.03	0.69	0.001	0.003	0.02 *
		Degree vaGM$_{motor}$	0.05	0.22	0.58	0.005	0.003	0.13
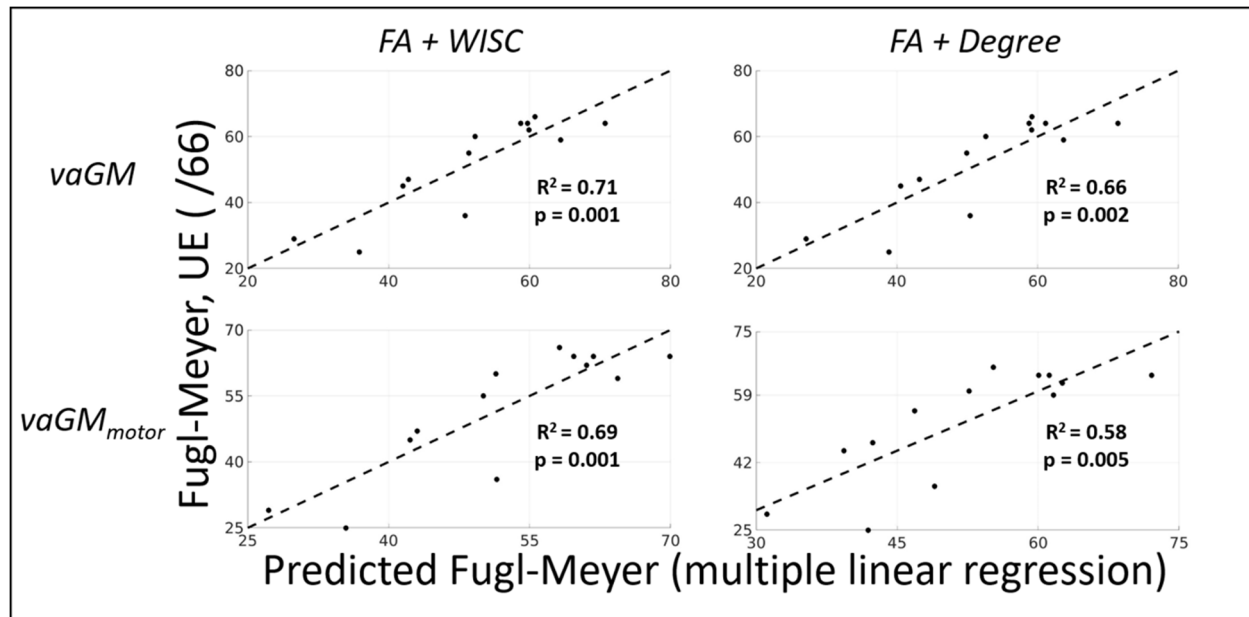
Figure 2-3: White Matter Connectivity and Integrity Correlations with Fugl-Meyer score

Multiple linear regression results with motor impairment, using the FA within the CST (FA$_{CST}$) and the volume of affected gray matter (vaGM) as the independent variables. The R^2 and p-values are displayed for the full model fit, and ^{Ŧ} indicates the addition of the

*connectivity measure significantly improved the model. The Fugl-Meyer is shown in the
y-axis and the predicted Fugl-Meyer is shown in the x-axis. The columns show
the vaGM calculated by the WISC (left) and the Degree (right). The rows show the total
number of affected regions (vaGM) and the total number of motor-related affected
regions (vaGM$_{motor}$)*
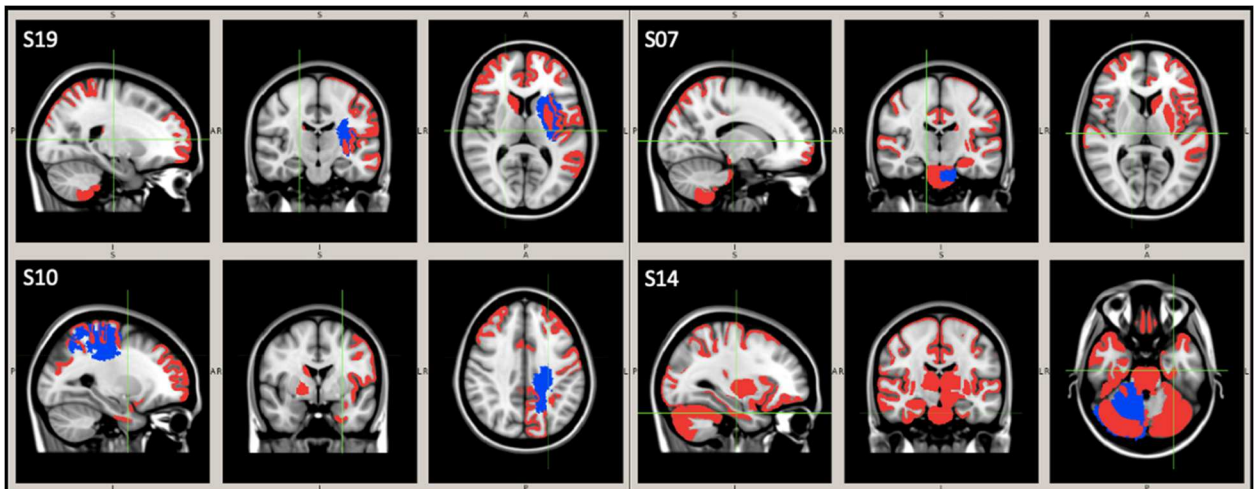
*Figure 2-4: Four stroke participants and their respective volume of affected gray matter
measured by WISC*

*Four stroke participant examples and their volumes of affected gray matter (vaGM)
calculated by the WISC. This is calculated as the number of regions with a reduced WISC
compared to the t-distribution created by the control participants in our cohort. In blue is
the lesion location, and red shows the vaGM. Stroke participant label is shown in the top
left corner of each figure. Figures panels show the sagital, coronal, and axial view from
left to right.*

2.4   DISCUSSION

The purpose of this study was to provide evidence of changes in indirect

structural connectivity after stroke, and to relate changes in white matter integrity and

connectivity to motor impairment. Direct connectivity metrics were only able to identify

changes in connectivity within the lesion distribution and in the motor cortex adjacent to

the lesion. In contrast, indirect connectivity identified regions within, near, and far from

the lesion distribution. In particular, regions in the parietal and frontal lobe, subcortical

regions, and the cerebellum saw reduced indirect connectivity after stroke. Additionally, WM integrity within the CST and the measures of indirect connectivity significantly predicted motor impairment.

2.4.1   REDUCED STRUCTURAL CONNECTIVITY IN MOTOR NETWORKS

2.4.1.1   *THE FRONTO-PARIETAL AND SUBCORTICAL NETWORK*

Our study found reduced structural connectivity in regions important to sensorimotor function such as the ipsilesional fronto-parietal cortex and subcortical regions after stroke. Measures of direct connectivity were reduced in the precentral gyrus, rostral-middle-frontal gyrus, the superior-parietal gyrus, and parts of the cingulum. In contrast, indirect connectivity detected reduced connectivity in the aforementioned regions, in addition to the bilateral postcentral gyrus and the superior frontal gyrus (Figure 2.2). These findings suggest that regions in the frontal and parietal lobes are hubs in the brain connectome, and that connectivity of these regions can be altered by stroke, regardless of lesion location. This is consistent with a centrality and vulnerability analysis using diffusion MRI measures of connectivity, where iteratively removing critical regions such as those in the superior parietal and frontal lobes cause the largest change in the network's global efficiency (Iturria-Medina et al., 2008).

Indirect connectivity can be sensitive to changes in connectivity to network hubs. Our results indicate that indirect connectivity is reduced in cortical and subcortical regions both directly and indirectly affected by the lesion, (Figure 2.2). This suggests that damage to areas connecting to a region can be as important to network connectivity as damage to the region itself, which can lead to disruptive effects on the network and

subsequent impairment and recovery post-stroke (Borstad et al., 2016; He et al., 2007). In a similar analysis, the caudate nucleus and thalamus have a reduced direct connectivity (Bosnell et al., 2011), and reduced weighted communicability after subcortical stroke (J. Crofts et al., 2011). The latter also found reduced connectivity in the bilateral caudate nucleus, mirroring our results, (Figure 2.2). Our study is unique in demonstrating that changes in connectivity in the contralesional hemisphere extend to sensorimotor cortical regions, and that these changes occur after lesions in areas other than the internal capsule.

2.4.1.2 *CEREBELLAR REGIONS*

Our measures of indirect connectivity indicated changes in connectivity to the cerebellum in people with supratentorial lesions (Figure 2.2). While the subject with the cerebellar lesion likely reduced the stroke group's average WISC in the cerebellum, the differences in direct connectivity, measured using degree, were not significant. Instead, it is likely that reduced WISC in the brain stem and cerebellum is caused by a reduced number of indirect connections from supratentorial brain structures.

Diffusion MRI changes beyond the lesion site have been found in supratentorial WM tracks. For example, fiber pathways directly above and below the main lesion volume degenerate after stroke (G. Liu et al., 2015), and similar observations have been reported after spinal cord injury (Jirjis et al., 2016). Perfusion and gray matter thickness studies suggest that the cerebellum changes shape and connectivity after stroke (Sommer et al., 2016) and diffusion MRI measures of WM connectivity support the idea that focal ischemic lesions produce progressive degeneration of major WM tracks (Kalinosky et al.,

2013; Schulz, Frey, et al., 2015). Our approach using indirect connectivity could have the sensitivity needed to detect changes to cerebellar connectivity after supratentorial stroke.

Two studies highlight changes in cerebellar connectivity after stroke and their relationship with post-stroke impairment. Kalinosky et al., (2017) developed a novel structurofunctional metric that weighted functional BOLD connections by their residual WM connectivity, and found that cerebellar-prefrontal cortical connectivity correlates with arm function after stroke. Additionally, Schulz et al., (2015) found a positive correlation between the WM integrity of the major cerebellar tracts and residual motor output and fine-motor control. The lack of additional evidence of losses in connectivity to the cerebellum may be due to complex fiber organization in the pons and the cerebellum. Our results highlight the importance of calculating indirect connections from the entire connectivity matrix (Kalinosky et al., 2013) because it amplifies remote-region connectedness and highlights vulnerability of connectivity to a focal lesion.

2.4.2   WM INTEGRITY AND CONNECTIVITY PREDICT MOTOR IMPAIRMENT

We found that a multiple linear regression model of WM connectivity and integrity better predicted motor impairment, and that using indirect connectivity performed better than direct connectivity. The linear model of WM integrity within the corticospinal tract (FA_{CST}) moderately but significantly correlated with motor impairment, which is consistent with prior studies (Koyama & Domen, 2017; Mang et al., 2015; Schulz et al., 2012; Wen et al., 2016). Adding the total number of regions with significantly reduced WISC or degree to the model significantly improved the ability to

predict motor impairment and better explained the variance seen in post-stroke impairment (Figure 2.3, top).

It should be pointed out that adding the number of *motor-related* regions with reduced connectivity significantly improved the regression model of upper extremity motor impairment for only the measure of indirect connectivity (Figure 2.3, bottom). Indirect connections could be more sensitive to loss in connectivity to motor-related regions, as shown in Figure 2.2 and 2.3. Stroke induces changes in integrity in the CST and changes in the connectome. By measuring direct and indirect connections, the WISC was able to identify significant losses in connectivity in motor-related regions in the cortex and subcortical regions, and these changes in connectivity better predicted motor impairment in a multiple linear regression model. In a similar study, Mang et al., (2015) used hierarchical regressions using the integrity of WM tracks and transcranial magnetic stimulation to predict motor impairment. Integrity of the CST and indirect connectivity both appear to be important motor function and the combination may be a useful imaging marker of functional recovery.

2.4.3 LIMITATIONS AND FUTURE DIRECTIONS

The current study utilized an anatomical and tractography-based parcellation to establish gray matter nodes for connectivity analysis, which could have impacted the results. The effects of node selection should be taken into consideration when interpreting results (Zalesky et al., 2010). Although the reproducibility of connectivity measures across time scales, tractography techniques, and scanners is high, (Meskaldji et al., 2013;

Welton, Kent, Auer, & Dineen, 2015), node selection, processing techniques, and interpretation should be considered carefully.

A voxel-based approach for calculating indirect connectivity is appealing due to its objective classification of network nodes (Kalinosky et al., 2013); however, there are computational constraints and methodological considerations to account for. For instance, at fine parcellation resolutions some nodes may have little to no connectivity, resulting in a sparse and noisy connectivity matrix. Unless more streamlines are calculated, which would further increase the computational burden, the connectivity matrix may not be reproducible (Zalesky et al., 2010). Additionally, probabilistic tractography algorithms could be sensitive to artificial increases in connectivity probabilities (Carrera & Tononi, 2014) due to decreases in probabilities elsewhere (J.J Crofts, et al., 2010). During fiber track estimation, a decrease in anisotropy, or an increase in dispersion, in the lesion would decrease the number of tracks passing through the lesion volume and might artificially increase the number of tracks to alternative routes. However, our study did not find increases in connectivity or graph measures in the stroke group when compared to the neurologically intact individuals.

It is difficult to interpret increases or decreases in graph metrics when probabilistic tractography is used. Probabilistic tractography implemented in FSL calculates probabilities of a single fiber connecting two regions, and thus the edge number in the connectivity matrix should not be interpreted as the number of fibers connecting two regions (Behrens et al., 2007). Although subjective, employing techniques that binarize connectivity matrices based on pre-selected probability thresholds could be the preferred method of comparing connectivity graphs; in this case,

the existence of connections is assessed. However, we point out that the selection of the thresholds may influence our results. We used a range of thresholds in order to account for this; stronger and more reliable connections would be represented more frequently regardless of the threshold used. Another approach would be to use principle component analysis in order to find the most reliable network per participant.

Probabilistic tractography might underestimate the number of indirect connections in a region. For example, cerebellar output from the dentate nucleus ends at the contralateral thalamus where a second set of axons send efferent signals to the cortex (Allen & Tsukahara, 1974). However, probabilistic tractography could directly connect the cerebellum to the cortex; the low anisotropy and high uncertainty in a voxel diverges downstream streamlines and reduces their individual probabilities. Similarly, unconstrained probabilistic tractography potentially increases the number of incorrect connections to a seed region. For example, our approach connects the right cerebellar hemisphere to the left and the right thalamus. This might explain why the right cerebellar lesion caused bilateral changes in connectivity in the supratentorium (Figure 2.2). A way to mediate these methodological issues would be to add waypoint constraints for each of the 114 seed regions; however, this would impose a bias on our reconstructed fiber tracks based on our subjective selection of waypoint regions. We addressed these issues by selecting a range of probability thresholds that preserved physiologically relevant streamlines. Future implementations could employ more objective methods of thresholding.

A limitation to WISC is that the calculation is sensitive to either a loss in direct connections to indirect connections, or due to an increase in indirect connections (see

Equation 2.6). However, our implementation of VISC counts the probabilities of the direct connections to indirect connections (the degree of the indirect connections). Therefore, this number, the numerator of the WISC calculation, increases faster as more indirect connections (the denominator) are added. This slight modification to the VISC makes a decrease in the WISC due to an increase in the denominator less likely.

2.5   CONCLUSION

The major finding of this study is evidence of the ability of indirect connectivity to uniquely identify remote changes in brain connectivity after stroke, and its ability to explain variance in post-stroke impairment. When compared to measures of direct connectivity, our indirect connectivity analysis detected changes in connectivity in contralesional cortical areas, ipsilesional subcortical regions and the thalamus, brain stem, and cerebellum. These areas are regions with high centrality in the brain, are near large white matter tracks that connect, and are clinically important in behavior and sensorimotor function. The clinical implication of our study is that changes in structural connectivity extend beyond the lesion volume, and that these changes in connectivity can be used along with white matter integrity to predict motor impairment. This highlights the need to analyze white matter connectivity when considering the effects of stroke on the brain, and adds evidence that suggests the fronto-parietal lobe, subcortical regions, and the cerebellum are important nodes in the brain's connectome. The methodological implications of our study emphasize the need to calculate indirect connections in order to capture global effects of a brain lesion on the connectome.

3   CHAPTER 3: WHITE MATTER INTEGRITY AND CONNECTIVITY IN MOTOR PATHWAYS RELATE TO MOTOR IMPAIRMENT AFTER STROKE

3.1   INTRODUCTION

In this study, we combined measures of white matter (WM) connectivity and integrity to characterize the relationship between WM structure and upper extremity motor impairment after stroke. Measures of WM orientation obtained from DWI can characterize global connectivity of the brain, which could provide neuroimaging tools to prognosticate clinical outcomes of stroke rehabilitation. Developing and testing algorithms that can integrate both WM integrity and connectivity could help detect subtle changes in WM structure distant from the lesion that may predict motor impairment. Thus, the purpose of this study was to 1) develop a novel biomarker that informs a voxel's local WM integrity by its global connections, to 2) provide evidence of changes in global connectivity and integrity after stroke, and to 3) relate these changes in WM structure to post-stroke motor impairment.

Traditional stroke neuroimaging tools of brain WM structure do not take into account the effect a focal lesion has on global brain connectivity. Although stroke produces local damage within the lesion volume and surrounding penumbra, cellular, WM, and gray matter (GM) degeneration occurs outside the lesion core (Cheng et al., 2015; Förster, Kerl, Goerlitz, Wenz, & Groden, 2014; Jirjis et al., 2016; Lee, Grabb, Zipfel, & Choi, 2000; Sommer et al., 2016; Wang et al., 2012; Yassi et al., 2015). The most common diffusion measure of post-stroke WM integrity is the fractional anisotropy (FA) (Basser et al., 1994), and integrity within the corticospinal tract (CST) has been related to post-stroke function, strength, impairment and recovery (Koyama & Domen,

2017; Mang et al., 2015; Puig et al., 2010; Schulz et al., 2012; Wen et al., 2016).
However, there are three main limitations to using FA: 1) it does not explain all variance
in post-stroke outcome, 2) it is affected by complex fiber structures (Behrens et al.,
2003), and 3) it is only locally sensitive to lesion volume (Kalinosky, Schindler-Ivens, &
Schmit, 2013).

Measures of global connectivity could provide additional information about
changes in WM structure after focal lesions. For example, weighted communicability
was found to be sensitive to changes in WM connectivity in the contralesional
hemisphere after stroke (Crofts et al., 2011). Additionally, our lab recently developed a
measure of indirect connectivity that related to upper extremity motor impairment
(Kalinosky et al., 2013). We also developed a measure of connectivity that weighs the
BOLD functional MRI signal from a voxel by its structural WM connections (Kalinosky,
Berrios Barillas, & Schmit, 2017), and it was shown to correlate with post-stroke motor
function of the arm. Identifying damaged WM tracks after stroke (Yeh et al., 2013) could
be used as regions of interests for correlation analyses with post-stroke impairments (Li
et al., 2017). Thus, DWI measures of WM connectivity and integrity could identify
damaged WM tracks distant from the lesion volume, and relate these changes in
connectivity to function.

In this study, we developed a novel measure of brain structure in order to identify
global changes in WM integrity and connectivity after stroke, and we related these
changes to motor impairment. Using voxel-level probabilistic tractography, we
calculated the average FA of connected voxels to estimate changes in post-stroke WM
structure with the aim of extending local changes in WM integrity along connected

pathways. We compared our combined measure of WM structure with measures of WM integrity (FA) and connectivity (degree), and related WM structure to motor impairment. We hypothesized that our measure would detect a larger volume of affected white matter after stroke, and that this would relate to post-stroke motor impairment in the CST in addition to commissural and cerebellar pathways associated with sensorimotor function.

3.2 METHODS

3.2.1 DATA COLLECTION

3.2.1.1 SUBJECT RECRUITMENT

Thirteen chronic stroke survivors (>6 months after stroke) (10 female, average age 63.2) and sixteen age-matched control participants (8 female, average age 63.4) participated in this study. Each participant provided written consent to the experimental protocol, which was approved by the Institutional Review Boards at Marquette University and the Medical College of Wisconsin. The inclusion criteria included a minimum age of 18 (mean age 64.4 years for the stroke group, 63.4 years for the neurologically intact group), and the ability to independently answer questions, follow directions, and provide informed consent. Contraindications included a history of multiple strokes, history of claustrophobia, other known brain pathology, and MRI incompatibility. This cohort is similar to those in chapter two, with the exception that stroke participants with history of multiple lesions were removed. Participants in the neurologically intact group were age- and sex-matched to the stroke group.

A measure of upper extremity motor impairment was obtained for stroke participants using the Fugl-Meyer (FM, maximum of 66 points) upper extremity motor test, (Fugl-Meyer et al., 1975). Lower values indicate greater motor impairment. Table 3.1 contains information on the stroke study participants.

Table 3-1: Stroke Participant Information

Stroke participant information, including identification number, sex, age, lesion location, lesion hemisphere, and the Fugl-Meyer upper extremity motor score (out of 66). For the subjects that had multiple lesions, the larger lesion is listed first. M = Male; F = Female; R = Right; L = Left

Subject ID	Sex	Age	Lesion Location	Lesion hemisphere	Fugl-Meyer (/66)
C01	M	65	Cortical	R	64
C02	M	57	Sub Cortical	L	59
C03	F	83	Brain Stem	L	36
C05	M	69	Cortical	L	64
C06	F	65	Cortical	R	47
C07	M	64	Cerebellum	L	60
C09	F	62	Sub Cortical	L	64
C11	F	60	Sub Cortical	R	45
C13	F	73	Sub Cortical	R	29
C14	F	57	Sub Cortical	R	25
C15	M	58	Sub Cortical	L	26
C16	F	42	Sub Cortical	L	19
C18	F	67	Cortical	R	9

3.2.1.2 *MRI Scans*

All MRI scans were performed using a short bore 3T GE Discovery MR750 scanner. Axial T1-weighted images were acquired using the fast spoiled gradient recall (FSPGR) 3D pulse sequence, with the following parameters: TE=3.2ms, TR=8.16ms, flip angle=12 degrees, FOV=240mm, at 156x1mm slices with an in-plane axial matrix of 256x240. Axial diffusion scans were acquired using the Q-ball high angular resolution diffusion imaging (HARDI) sequence using a single-shot echo planar imaging (ssEPI) protocol, with the following parameters: TE=72.3ms, TR=5700 ms, FOV=256mm at 59x2.5mm slices with an in-plane axial matrix of 128x128. There were 150 gradient directions (b-value=1500 s/mm^2) and five b=0 images.

3.2.2   MRI DATA PROCESSING

3.2.2.1   *IMAGE PRE-PROCESSING*

Raw Digital Imaging and Communications in Medicine (DICOM) images were converted to NIFTI image format (Neuroimaging Informatics Technology Initiative) using *mricron* (Rorden et al., 2007). All preprocessing was done using the FMRIB Software Library (FSL) (Jenkinson et al., 2012). MR bias field correction and skull stripping were performed on the raw T1-weighted images. The diffusion images were corrected for eddy-currents and skull stripped. Additionally, the fractional anisotropy (FA) of each stroke participant was calculated from the HARDI.

3.2.2.2   *LESION IDENTIFICATION*

Lesions were automatically identified using the Lesion Identification with Neighborhood Data Analysis (LINDA) algorithm, (Pustina et al., 2016). The algorithm

requires the lesions to be on the left hemisphere; therefore, prior to pre-processing, all raw T1 and diffusion weighted images with right-hemisphere lesions were flipped to the left hemisphere, and the diffusion gradient vector file was flipped in the X-direction. One participant had a lesion on the left hemisphere of the cerebellum. Most cerebellar afferent and efferent connections cross hemispheres to connect to the contralateral cortex (Allen & Tsukahara, 1974). Because of this, the stroke participant with the left-cerebellar lesion was flipped to reflect a right-cerebellar lesion.

3.2.2.3 *IMAGE REGISTRATION*

3.2.2.3.1 BRAIN TEMPLATE CREATION

All study participants' diffusion images were registered to a template space in order to statistically compare WM integrity and connectivity metrics in the same space; however, for visualization purposes we display our final results in MNI standard space. The template space was selected as the control participant with characteristics (as determined by registration) closest to all other control participants. The template space was determined by non-linearly registering all control participant's FA images to each other in order to determine the most representative brain using *tbss_2_reg* (S. M. Smith et al., 2006). Afterwards, all control participants' T1-weighted images were non-linearly registered to the target space using ANTs' (Advanced Normalization Tools) SyN algorithm (Avants et al., 2008). The final brain template image was calculated as the average warped T1-weighted image of all control participants in our target space (Figure 3.1-a). The transform that warps our template space to MNI space was obtained using the ANTs' SyN algorithm.
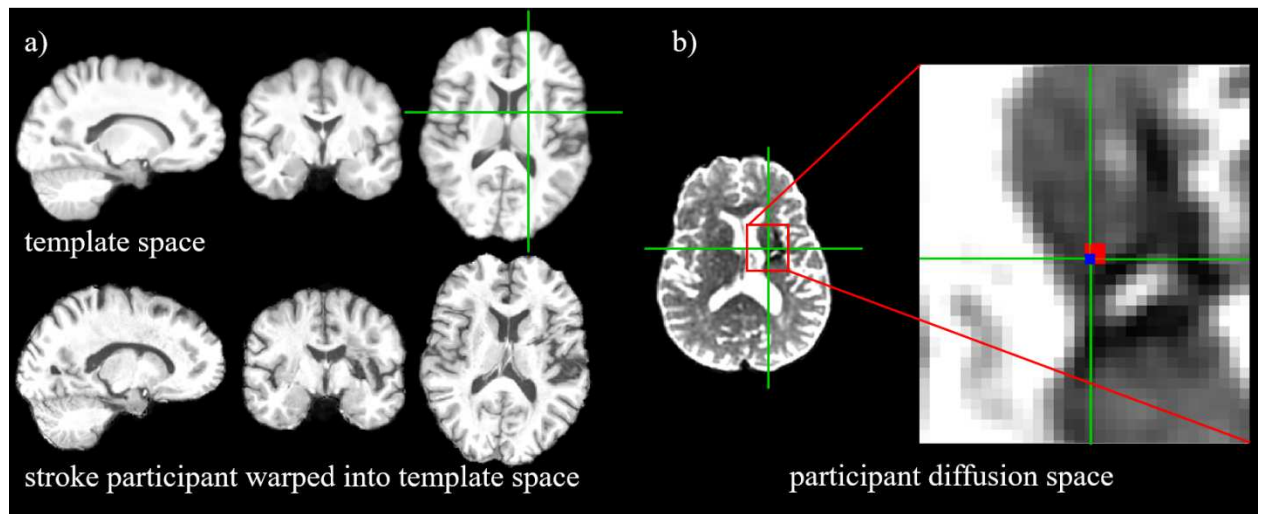
Figure 3-1: Template Space and Registration to Diffusion Space

Panel a shows two T1-weighted images: our study's template space (top) and a stroke participant (C02) warped into the template space. The green cross-hair indicates the coronal and sagittal slice, in addition to a representative voxel. Panel b shows the stroke participant's diffusion space with the corresponding location of the representative voxel (enlarged on the right). Note: when applying a transform on an image, the single voxel in template space has been interpolated into 4 voxels (shown in red), whereas applying a transform on a list of physical points results in a single warped voxel (shown in blue)

3.2.2.3.2   REGISTRATION TO TEMPLATE SPACE

Each participant's diffusion image was linearly registered to its T1-weighted image using FSL's linear registration (*flirt*) using 6 degrees of freedom. Linear and diffeomorphic non-linear registration warped each participant's T1-weighted image onto template space using ANT's SyN algorithm with Gaussian regularization, histogram matching, and lesion masking. The diffusion-to-structural, and the structural-to-template transforms were concatenated, and the final result was a set of invertible linear and non-linear transforms that mapped every physical point in diffusion space to template space. An example stroke participant warped into the template space is shown in Figure 3.1-a.

3.2.2.4   *STRUCTURAL CONNECTIVITY*

3.2.2.4.1   TRACTOGRAPHY MASKS

Our WM seed mask was determined as the maximum overlap of all of our control participants' WM volumes. Each control participant's WM and cerebral spinal fluid (CSF) volumes were obtained using *fast* in FSL. After warping to template space, binarizing, and adding the volumes, a threshold of 16 (our total number of control participants) determined the maximum overlap.

The CSF mask prevented streamlines from entering non-brain areas, and a gray matter (GM) mask was created in order to only include streamlines that connect gray matter regions and ignore streamlines that prematurely end within the WM (R. E. Smith et al., 2012). Our GM mask was estimated in MNI space, which includes cortical and subcortical volumes obtained from Freesurfer (Fischl et al., 2004, 2002), and cerebellar GM volumes obtained from FSL (Diedrichsen et al., 2009). The CSF and GM masks were warped into each participant's diffusion space.

A common tractography approach is to iteratively seed a voxel in the template space, warp seed points to the native diffusion space and perform tractography, and warp the final result back to template space (Kalinosky et al., 2013). At the time of this study, a method to convert ANT's warps into the format FSL requires for tractography had not been developed. We therefore warped our entire WM mask to each participant's diffusion space, seeded and performed tractography in native space, and warped the final result back to template space after tractography.

We observed that warping a single voxel from our template image to a single participant's diffusion image did not result in a one-to-one mapping of physical points in diffusion space due to image voxel interpolation and smoothing (Figure 3.1-b). In order to decrease the variability in the number of seed voxels in each participant's diffusion image, we transformed a list of physical seed points from the target space to diffusion space, resulting in a one-to-one mapping of physical point (*ImageMath* and *antsApplyTransformsToPoints* functions in ANTs). Our in-house MATLAB (R2017a) package then converted the list of transformed physical points in diffusion space into transformed voxel locations in native diffusion space.

3.2.2.4.2   DIFFUSION TRACTOGRAPHY AND CONNECTIVITY

Diffusion direction and orientation estimations were obtained from the eddy-corrected images using the FSL *bedpostx* function (Behrens, Woolrich, et al., 2003). Three fibers were estimated per voxel, each with a range of diffusivities. In addition to the seed (white matter) and the exclusion (CSF) masks, an inclusion (gray matter) mask was specified in our tractography algorithm, similar to the anatomically constrained tractography (ACT) algorithm described in Smith et al., (2012). Probabilistic tractography was performed using the *probtrackx2* function (Behrens et al., 2007) in each participant's native diffusion space, with distance correction. We estimated 2,500 streamlines per voxel, split into 50 cores using the *–rseed* option in *probtrackx2*. The output was 50 sparse connectivity matrices that represent the probability of connectivity between every WM voxel seeds. The average size of our connectivity matrix was roughly 200,000 voxels.

An in-house MATLAB package combined the 50 sparse connectivity matrices for each participant, and the final matrix was forced symmetric. Typically, the weights of the connectivity matrix can either be binarized (all connection weights forced to equal one) or normalized between a value of zero and one. Although probabilistic tractography can increase the number of true positive fiber connections, it also produces false positives (Maier-Hein et al., 2017) which could justify the use of a normalization technique and appropriate thresholding (Gong et al., 2009). On the other hand, normalization procedures that can control for the topology of the network have not yet been developed satisfactorily (Meskaldji et al., 2013; van Wijk, Stam, & Daffertshofer, 2010; Zalesky et al., 2010), and our methodology further complicated this issue; although we attempted to standardize the number of seed voxels in order to keep the number of nodes in our connectivity matrices consistent, every participant still had a different-sized matrix. For this study, we performed all connectivity measures on a binary and symmetric connectivity matrix. Thus, our connectivity matrix represents the volume of possible connections to a voxel, rather than the volume of the most probable connections.

3.2.2.5 *POST-PROCESSING - DIFFUSION BIOMARKERS*

The 'normalized' degree, k_i, (Rubinov & Sporns, 2010) was calculated using our in-house MATLAB package as the sum of all values of columns, j, in our connectivity matrix, a, divided by the number of voxels, N (**Error! Reference source not found.**).

$$k_i = \frac{1}{N}\sum_{j \in N} a_{ij}$$
Equation 3.1

Additionally, the FA was calculated from our HARDI data at each voxel, i, (section **Error! Reference source not found.**). Lastly, the structurally-weighted

fractional anisotropy (SWIFT) was defined as the average FA of connected voxels. This was accomplished by matrix-multiplying the binary connectivity matrix with the FA image in vector form (Figure 3.2). The resulting vector was then divided by the number of direct connections, Nk_i, to produce the average FA of direct connections (**Error! Reference source not found.**). This algorithm was developed independently from Buchanan et al., (2014), where they similarly averaged the FA across streamlines to create an FA-weighted brain network based on 84 regions.

$$SWIFT_i = \frac{1}{Nk_i} \sum_{j \epsilon N} a_{ij} \cdot FA_j \qquad \text{Equation 3.2}$$
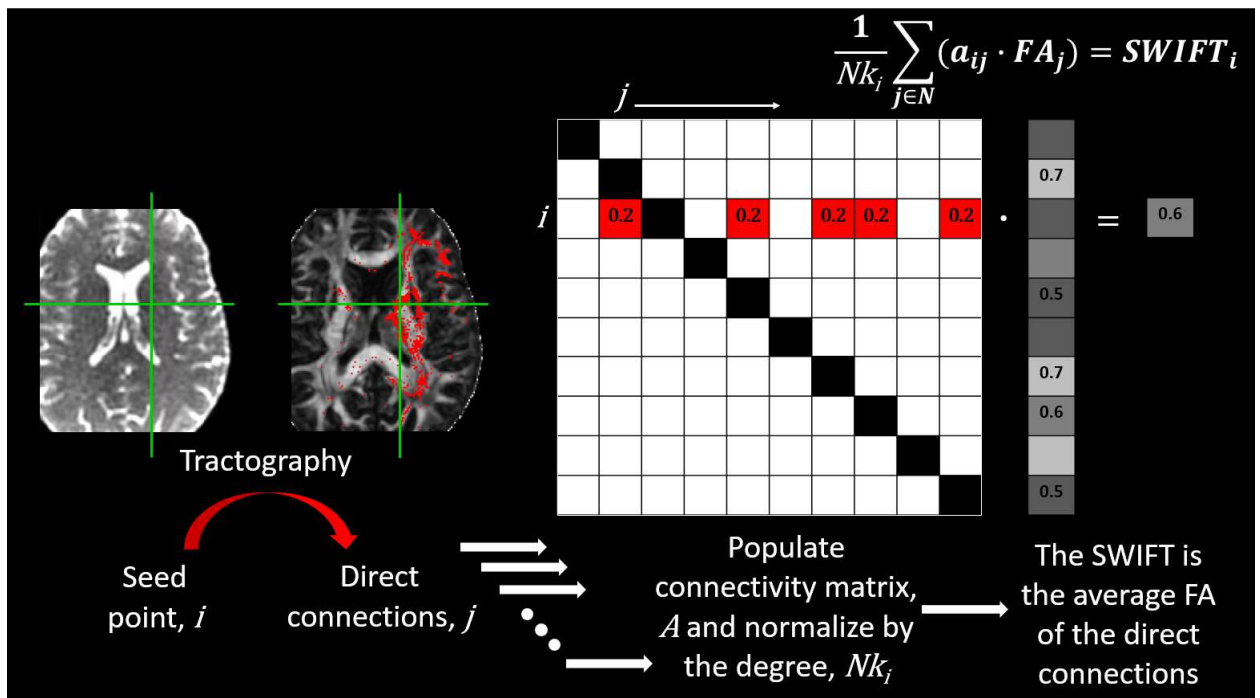
Figure 3-2: Structurally-weighted Fractional Anisotropy Calculation

*After warping the seed image, a single voxel, i (centered at the cross-hair), seeded probabilistic tractography to create a list of possible direct connections, j, which then populated a connectivity matrix, **A**. The SWIFT was then calculated by matrix-multiplying a 'degree-normalized' connectivity matrix by a vectorized FA image. Similarly, the product of a binary connectivity matrix and the vectorized FA image was divided by the degree (Equation 3.2).*

3.2.3 STATISTICAL ANALYSIS

We performed non-parametric permutation tests (FSL's *randomize*, threshold-free cluster enhancement) in order to compare the chronic stroke group with the control group. Lesion volumes were removed from the analysis. The resulting images were then thresholded (p-corrected<0.05) to show volumes where the stroke group had significantly reduced values in our three biomarkers, and then warped to MNI space for visualization purposes.

In order to determine the relationship between our biomarkers (FA, degree and SWIFT) and stroke impairment (Fugl-Meyer score), we conducted a Pearson correlation test between the Fugl-Meyer score and the volume of affected WM (vaWM), defined as the number of voxels less than the critical t-value (Kalinosky et al., 2013), assuming a t-distribution of the values in the control group and a critical t value corresponding to an alpha of 0.025. The vaWM for each biomarker was then considered a possible predictor of Fugl-Meyer.

3.2.4 POST HOC CORRELATION WITH MOTOR IMPAIRMENT IN TRACKS OF INTEREST

In order to identify which WM tracks were damaged after stroke, we calculated the lesion load of our stroke group significantly reduced FA, degree, and SWIFT volumes on predefined WM ROIs (henceforth to be referred to as "percent WM damage", Figure 3.3). This is the overlap of the damage in connectivity after stroke (measured by the FA, SWIFT, and the Degree) with a WM ROI. We also identified the contribution of each WM ROI—normalized by its size—to the overall volume of significantly reduced FA,

degree, and SWIFT (henceforth to be referred to as "percent contribution", Figure 3.3).

The percent contribution is the overlap a white matter track has on the volume of reduced

integrity/connectivity. Supratentorial WM ROIs were obtained from the Laboratory of

Brain Anatomical MRI at John Hopkins University (Hua et al., 2008; Wakana et al.,

2007), and the cerebellar tracts were obtained from the Neurosurgical Centre Nijmegen in

The Netherlands (van Baarsen et al., 2016). This analysis produced four WM ROIs, and

the vaWM within these were then correlated with the Fugl-Meyer scores.
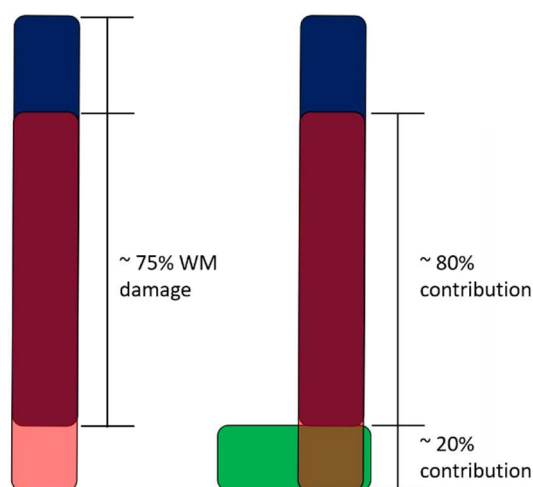
Figure 3-3: Percent WM Damage and Percent Contribution Calculation

*Visual representation of 'percent WM damage' and 'percent contribution'
calculations noted in Table 2. In red (transparent) is the statistically reduced SWIFT, FA,
and degree depicted in Figure 3.4 (p-corrected < 0.05). In blue and green are
representative white matter tracks depicted in Figure 3. The 'percent WM damage' is the
overlap the volume of reduced white matter integrity/connectivity (red) has on
a particular white matter track (blue, for instance). In this example, 75% of
the blue white matter track has reduced integrity. The 'percent contribution' is
the overlap a white matter track has on the volume of reduced integrity/connectivity. In
this example, 80% of the volume of reduced integrity resides in the blue white matter
track, while 20% resides in the green white matter track.*

3.3   **RESULTS**

The thirteen (13) stroke participants in our analysis included five participants with lesions in the internal capsule and the putamen, three participants with lesions in the parietal lobe, one brain stem lesion, and one cerebellar lesion (Table 3.1 and Figure 3.4).

The volume with reduced degree detected a 44.3% damage of the ipsilesional anterior thalamic radiation (ATR), and the volume of reduced FA detected a 17.4% damage of the ipsilesional cortico-spinal tract (CST). The volume of reduced SWIFT detected a 48.8% damage of the ATR and 53.1% of the CST, in addition to 33.1% of the corpus callosum (CC) and 19.1% of the contralesional superior cerebellar tract (SCP) (Table 3.2). Thus, for our post hoc analysis we used the ipsilesional ATR and CST, the CC, and the contralesional SCP; these tracts are shown in the second column of Figure 3.4.

It should be noted that the SWIFT detected a 49.1% and 36.4% damage in association tracts. However, we focused our results and interpretation on projection and commissural fibers because their contribution accounted for 84.4%, 76.3%, and 73.9%, of the total volume of reduced connectivity (degree), integrity (FA), and SWIFT, respectively.

Table 3-2: White Matter ROI based on Percent Damage and Percent Contribution

Percent WM damage and percent contribution is indicated for three biomarkers (SWIFT, FA, Degree) across WM ROI's. Bolded numbers indicate our selected WM tracks for our WM ROI analysis. ATR-l, ATR-r: left / right anterior thalamic radiation; CST-l, CST-r: left / right corticospinal tract; CC: corpus callosum; SCP-r: right superior cerebellar peduncle; MCP-r: right middle cerebellar peduncle; ICP-r: right inferior cerebellar peduncle; Association fibers include the superior, inferior longitudinal fasciculus, uncinated fasciculus, and the inferior fronto-occipital fasciculus.

	SWIFT	FA	Degree

		%WM damage	% contribution	%WM damage	% contribution	%WM damage	% contribution
Projection Fibers	ATR-l	48.8	15.0	8.1	18.2	44.3	42.3
	ATR-r	27.0	8.3	0.6	1.4	0	0
	CST-l	53.1	16.3	17.4	39.1	13.8	13.1
	CST-r	23.6	7.3	0.1	0.1	0	0
Commissural Fibers	CC	33.1	10.1	4.7	10.6	4.3	4.1
Cerebellar peduncles	SCP-r	19.1	5.9	0.9	2.0	25.7	24.5
	MCP-r	16.9	5.2	0.9	2.0	0	0
	ICP-r	18.8	5.8	1.3	2.9	0.4	0.4
Association Fibers	Left	49.1	15.1	9.4	21.2	16.3	15.6
	Right	36.4	11.2	1.0	2.3	0	0

3.3.1   THE FA AND DEGREE DETECT ISOLATED DAMAGE TO PROJECTION FIBERS

Our analysis revealed extensive WM changes in projection and commissural tracts after stroke (p-corrected<0.05). Ignoring the lesion location, 39.1% of the volume of reduced FA was in the CST; this can best be seen in Figure 3.4, where reduced FA (red, column 4) outlines the left CST (blue, column 2). The ATR has an 18.2% contribution. Interestingly, the FA also identified parts of the corpus callosum as seen in the sagittal view (10.6% contribution). The FA also revealed a sparse collection of voxels in the contralesional cerebellum as having reduced integrity; however, this only accounted for about 6% of the total volume of reduced FA (Table 3.2). The volume of

reduced degree was mostly concentrated along the left ATR (42.3% contribution), which is mostly concentrated in the thalamus. The left CST was also identified by the degree (13.1% contribution).

3.3.2 THE SWIFT HIGHLIGHTS LOSS OF INTEGRITY IN PROJECTION, COMMISSURAL, AND CEREBELLAR FIBERS

Similar to the FA and degree, the SWIFT revealed an extensive loss of integrity in major projection and commissural fibers; however, the SWIFT detected damage along these projection fibers, extending superiorly to WM voxels that neighbor the primary motor cortex. This contrasts with the FA where only sparse clusters of voxels were detected within the CST (Figure 3.4). Bilaterally, the SWIFT also identified homologous WM volumes in the non-lesioned hemisphere, although to a lesser extent.

In a similar way, the SWIFT extended the volume of damage from the FA to highlight changes in integrity along the corpus callosum (Figure 3.4). The CC accounted for 10.1% of the total volume of changes in SWIFT after stroke. Although this is similar to that of the FA (10.6%), the SWIFT detected 33.1% damage to the CC, while the FA only detected 4.7% damage. In other words, roughly 10% of the group-level reduction in the FA and the SWIFT was found in the CC; however, the SWIFT was more sensitive to detecting reduction in WM integrity in the CC as seen by the percent WM damage.

Lastly, the SWIFT extended the affected area relative to the FA highlighting changes along the contralesional SCP. Similarly, the degree indicated changes in 25.7% of the contralesional SCP, which accounted for 24.5% of the degree's total volume of reduced connectivity (Table 3.2). As seen in Figure 3.4, however, the extent of overlap

between volume differences in degree and the SCP is supratentorial (thalamic afferents) and not within the cerebellum. In contrast, the SWIFT was able to detect changes in integrity within the cerebellum's efferent portion of the SCP.
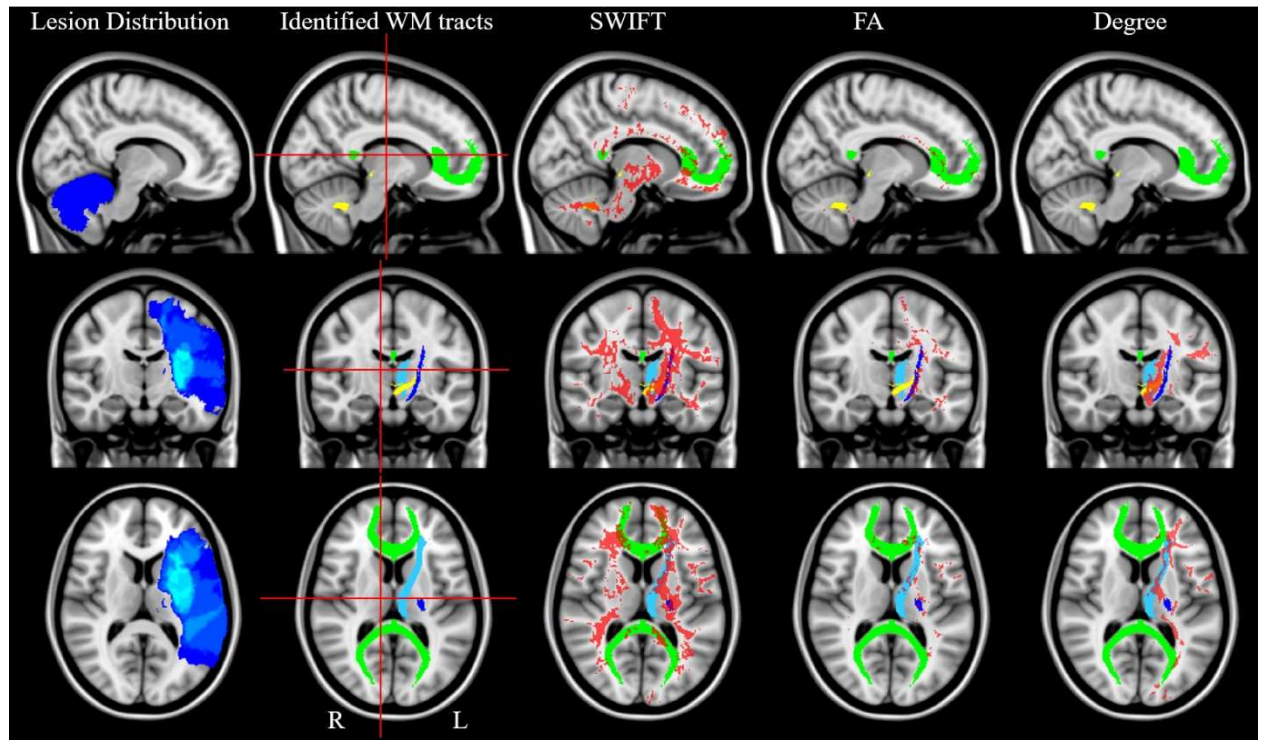
Figure 3-4: SWIFT, FA, and Degree changes after Stroke

Volume of significantly reduced (translucent red, p-corrected < 0.05) SWIFT (column 3) FA (column 4) and Degree (column 5) in stroke vs control. The lesion distribution is shown in column 1 with brighter colors indicating a higher lesion prevalence (n=13). The four WM ROIs from Table 2.2 are shown in column 2 (CC: green; ATR-l: light-blue; CST-l: blue; SCP-r: yellow). Column 2 shows right and left hemisphere, in addition to a cross hair indicating sagittal, coronal, and axial views.

3.3.3   SWIFT CORRELATES WITH UPPER MOTOR IMPAIRMENT

Our measure of upper extremity stroke motor impairment significantly ($p<0.05$) and negatively correlated with whole-brain vaWM integrity (FA: $R^2=0.55$, SWIFT: $R^2=0.63$), but not with measures of connectivity (degree) (Figure 3.5).

Figure 3-5: Regression of SWIFT, FA, Degree with Motor Impairment

Scatter plots displaying correlations between the upper extremity motor impairment (FM, Fugl-Meyer, out of 66), and the whole-brain volume of affected white matter for the SWIFT (top left), FA (top right), and the Degree (bottom left), with the linear model shown as a dashed line. A summary table displaying the R^2 value and the model's significance is shown on the bottom right.

The WM ROI analysis revealed that the SWIFT correlated better with motor impairment than FA in supratentorial projection fibers and the efferent cerebellar tracts, while the FA correlated better than the SWIFT in the corpus callosum (Figures 3.5 and 3.6). The SWIFT's vaWM correlated with the Fugl-Meyer better than the FA within the CST (R^2=0.82, R^2=0.58, respectively), (top row, Figure 3.6). The FA's vaWM correlated slightly better with the Fugl-Meyer than the SWIFT within the corpus callosum (bottom row, Figure 3.6), (R^2=0.53, R^2=0.41, respectively). Although the linear model was significant for the FA, the correlation might be driven by two samples, as can be seen by the scatter plot on the bottom right of Figure 3.6.
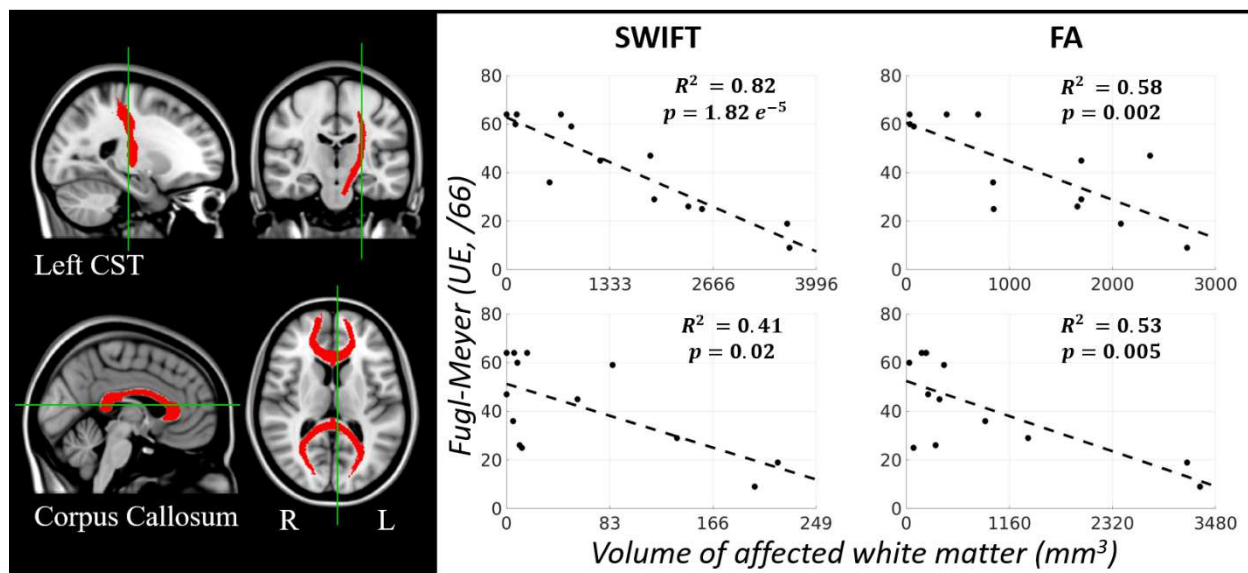
Figure 3-6: SWIFT and FA in CST and CC Regression with Motor Impairment

Scatter plots displaying correlations between the upper extremity motor impairment (FM), and the volume of affected white matter within the left corticospinal tract (CST, top) and the corpus callosum (bottom) for the SWIFT (left scatter plots) and the FA (right scatter plots). Summary results are displayed within the scatter plots (R^2 and p-values). The WM ROIs are shown in MNI space on the left two brain images, in red. The vertical and horizontal green lines indicate the coronal, sagittal, or axial views for that image pair. The left and right hemispheres are indicated in the bottom-right axial image.

Within the SCP, only the SWIFT significantly correlated with motor impairment (R^2=0.57), (Figure 3.7). Additionally, the SWIFT significantly correlated with the Fugl-Meyer within the ipsilesional ATR (R^2=0.43). Although the correlation of the FA with the Fugl-Meyer was not significant (p=0.08), the correlation was moderate to low.
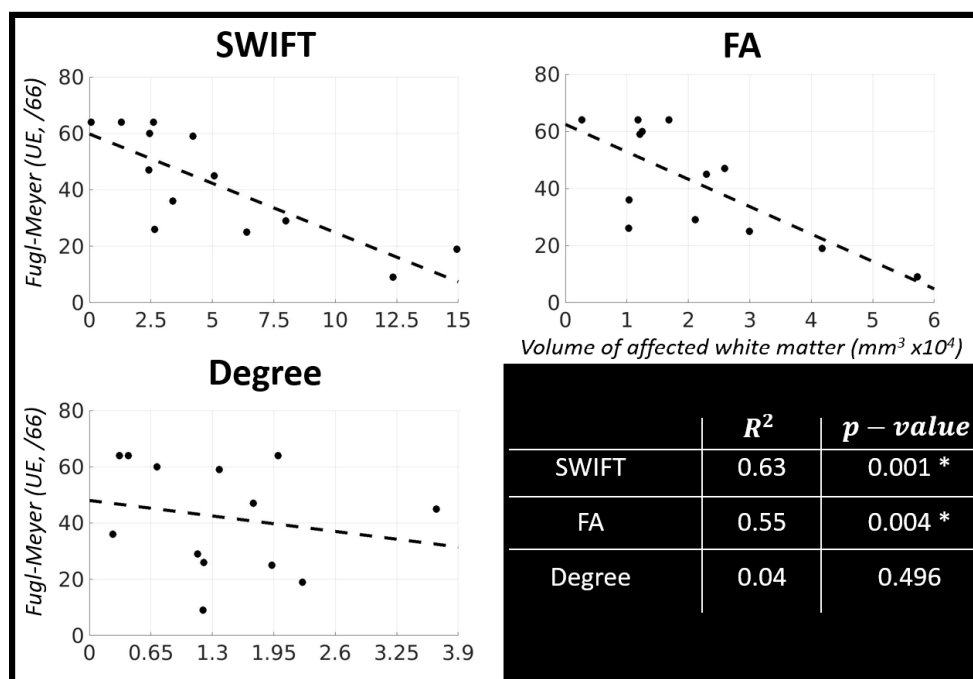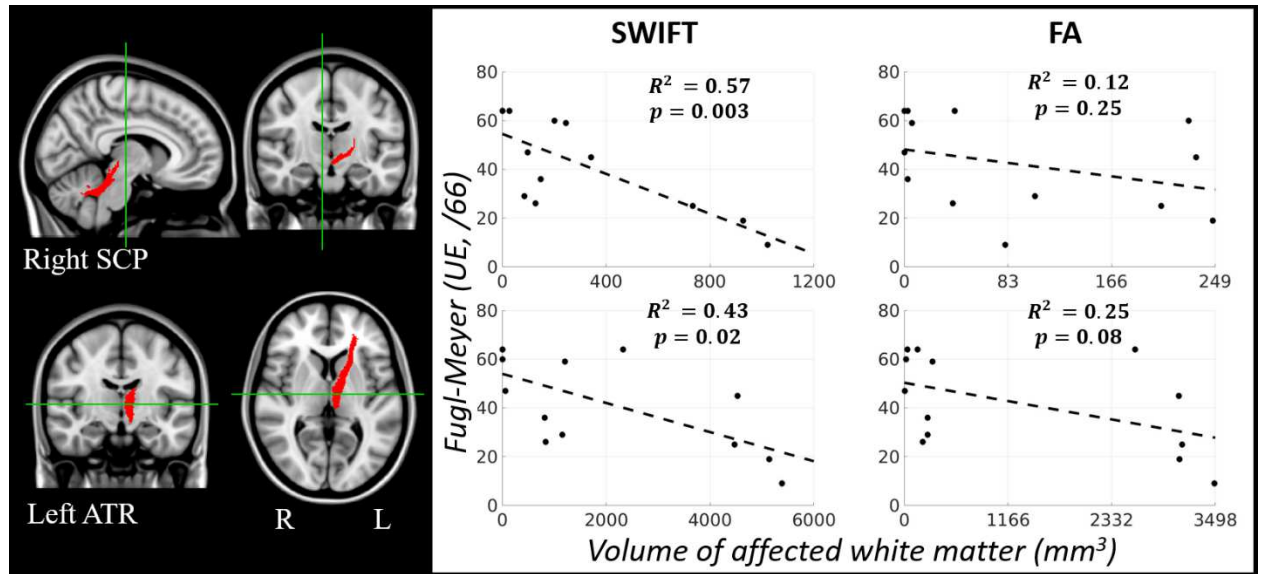
Figure 3-7: SWIFT and FA in SCP and ATR Regression with Motor Impairment

Scatter plots displaying correlations between the upper extremity motor impairment (FM), and the volume of affected white matter within the right superior cerebellar peduncle (SCP, top) and the ipsilesional anterior thalamic radiation (ATR, bottom) for the SWIFT (left scatter plots) and the FA (right scatter plots). Summary results are displayed within the scatter plots (R^2 and p-values). The WM ROIs are shown in MNI space on the left two brain images, in red. The vertical and horizontal green lines indicate the coronal, sagittal, or axial views for that image pair. The left and right hemispheres are indicated in the bottom-right axial image.

3.4   DISCUSSION

3.4.1   WHITE MATTER INTEGRITY PREDICTS MOTOR IMPAIRMENT

3.4.1.1   *PROJECTION FIBERS*

All three biomarkers used in this study detected reduced WM structure in the ipsilesional projection fibers after stroke. The degree revealed loss in WM connectivity in areas primarily outside the lesion distribution, in particular the anterior thalamic radiation (ATR). The FA, on the other hand, more closely outlined the CST. The unique

contribution of the SWIFT was that it identified damage to both these WM projection tracks (Figure 3.4).

To our knowledge, this is the first study to implement degree at the voxel level as a measure of structural centrality. A striking result was that over 40% of the volume of damaged degree was in the ATR (Table 3.2). Damage to the ATR after stroke has been associated with deficits ranging from memory deficits (Ghika-Schmid & Bogousslavsky, 2000) to the ability for basic movement (Tamari, Umeki, Goto, & Kawano, 2018) and semantic and phonological fluencies (Li et al., 2017). The thalamus is a highly interconnected hub in the brain; it projects to the frontal lobe and is involved in behavioral functions ranging from cognition to sequential motor planning and basic movement. The ability of the voxel-wise degree to detect changes in integrity of a track with high centrality underscores its usefulness in stroke brain imaging.

Additionally, our study found reduced integrity and connectivity in the CST. Damage to the CST after stroke and its relation to impairment and function has been reported using lesion load (Habegger et al., 2018; Lam et al., 2018), FA (Koyama & Domen, 2017; Mang et al., 2015; Puig et al., 2010; Schulz et al., 2012; Wen et al., 2016), and fiber count (Maraka et al., 2014). The correlations between the FA and the Fugl-Meyer within the CST are consistent with these prior studies. We also found that the SWIFT within the CST correlated with motor impairment (R^2=0.82, Figure 3.6). The ability of our metric to better predict motor impairment may be due to the weighting of WM integrity by its direct connections. This is especially true for stroke participants with lesions surrounding the CST, but with normal appearing WM. The SWIFT extended local, lesion-induced reductions in integrity along major WM tracks. The

ability of the SWIFT within the CST to better predict the Fugl-Meyer may be due to the CST being a major, highly-connected WM track with projections to the main lesion distribution.

3.4.1.2 *COMMISSURAL FIBERS*

Our study found reduced WM integrity in the CC (Figure 3.4) and the vaWM within the CC (SWIFT and FA) correlated with the motor impairment (Figure 3.6). Although the regression with the FA might be driven largely by two data points, our results are consistent with other reports of a correlation between the FA within the CC and post-stroke impairment and function (Hayward et al., 2017; Mang et al., 2015). The extent of damage to the CC is reportedly related to lesion location (Koh et al., 2018), especially when there is damage to the CST (Cunningham et al., 2015; J. Liu et al., 2015) and the internal capsule (J. Crofts et al., 2011). It has also been associated with track degradation over time due to processes such as Wallerian degeneration (Gupta et al., 2006). The lesion distribution for our stroke participants and our finding of callosal damage supports these findings.

Damage to the CC can induce changes in sensorimotor functional connectivity, contributing to poor recovery after stroke (X. Yu et al., 2018). The influence of the CC on post-stroke motor function and impairment may be due to interhemispheric inhibition (see van der Knaap & van der Ham, (2011), for a review). For instance, Murase et al., (2004) found that interhemispheric inhibition of the ipsilateral primary motor cortex to the homologous region in the contralateral side was facilitatory in neurologically intact participants, but detrimental and persistent in stroke participants during movement of the

paretic hand. In contrast, interhemispheric inhibition was similar in stroke participants to neurological controls when moving the non-paretic hand (Duque et al., 2005).

3.4.1.3 *CEREBELLAR EFFERENT FIBERS*

A unique property of the SWIFT was its ability to detect areas of reduced integrity within the cerebellum. Although the FA detected reduced integrity in small clusters of cerebellar WM, the SWIFT identified a much larger region of affected tissue (SCP, Figure 3.4). Detecting a larger region of affected WM—although less specific— can be more sensitive to detecting subtle changes to WM after stroke. Additionally, the SWIFT within the SCP significantly correlated with motor impairment (Figure 3.7).

The cerebellum is involved in many aspects of sensorimotor function (Bhanpuri et al., 2013; Boyd & Winstein, 2004; Charles et al., 2013; Seidler et al., 2004), and direct or indirect damage to the cerebellum can result in ataxia and deficits in muscle control and coordination. Ataxic hemiparesis has been reported after lesions to the posterior limb of the internal capsule, pons, corona radiate, and the thalamus (Fisher, 1978; Marek et al., 2015; Schonewille, Tuhrim, Singer, & Atlas, 1999). Additionally, changes to the cerebellum after a supratentorial lesion, (cross cerebellar diaschisis), (Feeney & Baron, 1986), have been observed in perfusion (Förster et al., 2014; Sommer et al., 2016), metabolism (Kushner et al., 1984), gray matter volume (Dang et al., 2013), and electrophysiological studies (Gold & Lauritzen, 2002). It is possible that the chronic loss of afferent activation to neurologically intact brain regions (Lewerenz & Maher, 2015) and mechanisms such as Wallerian degeneration lead to a long-term loss of connectivity and integrity in normal appearing WM. A measure that weighs a voxel's WM integrity

by its direct connections may be sensitive to these subtle changes in WM integrity distant from the lesion.

Changes in cerebellar connections after supratentorial lesions can be detected using diffusion imaging. For instance, Schulz et al., (2015) related the loss of integrity of the efferent cerebellar WM tracts to general motor output and fine motor skills. Additionally, Kalinosky et al., (2017) related a combined measure of structural and functional connectivity in cerebellar-prefrontal cortex connections with fine motor control after stroke. Similarly, our study found that a combined measure of integrity and connectivity within the contralesional SCP correlated with motor impairment. Although the SWIFT within the SCP correlated with motor impairment, this should be interpreted carefully. With the exception of a six-point coordination and speed examination, the Fugl-Meyer measure of stroke upper extremity motor impairment is not a measure of cerebellar function. It is possible that the correlation of the SWIFT to the Fugl-Meyer motor impairment within the SCP may be driven by the voxels near the thalamus. Future studies that correlate WM connectivity with measures of cerebellar dysfunction, such as ataxia out of proportion to weakness, could reveal the influence cerebellar WM integrity has on post-stroke motor impairment and function after stroke.

3.4.2 LIMITATIONS AND FUTURE DIRECTIONS

A limitation to this study is the small sample size in both groups. With the small sample size, lesions variability would complicate damaged WM track identification. We mitigated this by 1) normalizing lesion location, and 2) removing participants with

multiple lesions in both hemispheres. An ideal biomarker would not require a careful selection of participants based on the number of lesions they have.

The Fugl-Meyer assessment was performed by three different examiners. This may have introduced variability; however, the effect is expected to be minimal due to the high inter-rater reliability of the Fugl-Meyer assessment (Sanford, Moreland, Swanson, Stratford, & Gowland, 1993).

A considerable limitation to the study was connectivity matrix normalization. We performed whole-brain tractography in the native diffusion space. Although the number of physical points was kept consistent in each subject, the resulting number of voxels depended on brain size. A future implementation of this algorithm would convert the ANTs diffeomorphic warp into an FSL-warp. The FSL software would then seed and display tractography results in a template space. By standardizing the number of seeds, the connectivity matrix could be normalized by sparsity level or degree; however, these solutions could modify the topology of the matrix by enforcing non-significant connections in stroke participant's networks (van Wijk et al., 2010). Thresholding at a probability level could be a better alternative; however, this requires careful normalization that maintains the original topology, and can be implemented at the whole-brain scale. Fulfilling the second point requires each voxel (row in the connectivity matrix) to have the total number of attempted streamlines from that voxel; however, that information is not readily available. Even with a probability-weighted connectivity matrix, one cannot interpret a higher probability of connectivity between two voxels as a "stronger" connection, due to the possibility that less streamlines were propagated in one direction, therefore artificially preferring another direction (Carrera & Tononi, 2014).

Due to not being able to normalize our connectivity matrix adequately, a binarized matrix was used. This produced a connectivity matrix of possible connections, rather than of probable connections. As a result, the SWIFT at a given voxel may be influenced by false positive connections. The SWIFT detected reduced integrity in the contralesional projection fibers (Figure 3.4). Although changes in integrity and gray matter structure have been reported in the contralesional hemisphere after stroke (Dacosta-Aguayo et al., 2014; Grefkes & Ward, 2014; Yassi et al., 2015), it is possible that the reduced SWIFT in the contralesional projection fibers is due to false connections. With adequate normalization and probability thresholding, the SWIFT could be the average FA of probable connections. Normalizing and thresholding a connectivity matrix while maintaining the topology of the network remains an unsolved problem. Future studies dedicated to developing a normalization and thresholding technique could provide a way to improve the SWIFT calculation by controlling seed placement, normalizing and thresholding the connectivity matrix, and weighing the SWIFT by probability of connectivity.

3.5   **C**ONCLUSION

The major contribution of this study is the development of a combined measure of WM integrity and connectivity, and its ability to identify damaged WM tracks and better relate these changes to post-stroke motor impairment. When compared to FA and degree, the SWIFT identified damaged projection, commissural, and cerebellar fibers. Additionally, the SWIFT vaWM related with motor impairment within these identified fiber tracks to a greater extent than the FA and degree. The methodological implication of

our study is the development of a biomarker more sensitive to WM damage and post-stroke impairment than typical measures of WM integrity. Our study also adds to the clinical understanding of post-stroke WM damage and motor impairment; we corroborate evidence of global and remote changes in WM structure after focal lesions which are related to motor impairment, particularly in fiber tracks connecting hubs such as the fronto-parietal lobe, thalamus, and the cerebellum.

4 CHAPTER 4: INDIRECT CONNECTIVITY IDENTIFIES DIFFERENCES IN CEREBELLAR CONNECTIVITY BETWEEN SUBACUTE AND CHRONIC STROKE

4.1 INTRODUCTION

In this study, we investigated the differences in white matter structure in people with subacute and chronic stroke and compared them to neurologically intact individuals using direct and indirect connectivity metrics based on diffusion magnetic resonance imaging (dMRI). Measures of indirect connectivity are sensitive to global damage to white matter (WM) structure (Kalinosky et al., 2013), may better relate to functional connectivity (Honey et al., 2009), and could be useful diagnostic biomarkers for post-stroke outcome, rehabilitation, and recovery. In this study we postulated that measures of WM structure and indirect connectivity would detect larger reductions in brain connectivity in motor pathways in people with chronic stroke than in subacute stroke when compared to control participants, reflecting a progressive degeneration in white matter integrity.

Stroke recovery has been associated with network changes in functional connectivity and white matter integrity in the corticospinal tract; however, it is not well

understood how structural connectivity changes during the first six months after stroke. For instance, interhemispheric functional connectivity measured by fMRI during the first week after stroke has been related to motor outcome, impairment severity, and motor recovery (Chi et al., 2018; De Bruyn et al., 2018; Park et al., 2011; Puig et al., 2018). Additionally, the activation of the contralesional cerebellum at three months post stroke is related to stroke recovery (Small, Hlustik, Noll, Genovese, & Solodkin, 2002). The primary finding in stroke longitudinal studies using dMRI is a degeneration in FA during the first 2-12 weeks, and a stabilization after that (Groisser, Copen, Singhal, Hirai, & Schaechter, 2014; Liang et al., 2008; Thomalla, 2005; Thomalla et al., 2004; C. Yu et al., 2009). Although the time-course of MR-related signal intensities has been defined during the normal time-course after stroke (Allen, Hasso, Handwerker, & Farid, 2012), the effect of local degenerative changes on structural connectivity—a measure that could help describe changes in network connectivity after stroke—is not yet well understood.

Direct and indirect structural connectivity—in which regions are connected via an intermediate region—relates to motor impairment after stroke (Crofts et al., 2011; Kalinosky et al., 2017) and may provide the key to explaining changes in functional connectivity and motor outcome post stroke because two regions may be functionally connected even if they are not directly connected by structural paths (Honey et al., 2009). In order to ascertain the local and global changes in connectivity after stroke, indirect structural connectivity and probabilistic tractography are necessary. This is particularly important when estimating the connectivity of long-distant connections, such as those to the cerebellum. However, structural connectivity has only been simulated in the acute/subacute stage of stroke based on connectome deletion based on lesion location

(Kuceyeski et al., 2014). Although diffusive and microstructural changes in the lesion volume occur during reperfusion and normal recovery (Allen et al., 2012), and lesion volume growth has been reported in the early hours and days after stroke (Rocha et al., 2019; Schwamm et al., 1998) lesion volumes defined at the late-acute / subacute stage and subsequently in the chronic stage do not change dramatically because infarcts do not enhance after 1-6 weeks (Allen et al., 2012). This motivates studies that estimate fiber tractography in the subacute and chronic stage, rather than simulating the connectome based on lesion location.

Our main goal is to identify differences in direct and indirect structural connectivity between people with subacute and chronic stroke. Understanding changes in structural connectivity after stroke is important to the development of prognostic indicators of functional recovery after stroke. Thus, the purpose of this study is to compare the structural connectivity of subacute and chronic stroke participants, with the aim of developing the analyses needed for a longitudinal study. We hypothesize that indirect structural connectivity will be more sensitive to differences between subacute and chronic stroke than measures of white matter integrity due to white matter degeneration. We also hypothesize that cerebellar white matter connections will exhibit a reduction in connectivity and play an important role in recovery, reflecting neurodegenerative changes in connectivity remote from the lesion, and its importance in motor recovery.

4.2 METHODS

4.2.1 DATA COLLECTION

4.2.1.1 *SUBJECT RECRUITMENT*

The study enrolled ten subacute stroke participants, and screened potential data from 29 chronic (>6 months) stroke and 32 neurologically intact participants obtained from other studies in our laboratory. Each participant provided written consent to the experimental protocol, which was approved by the Institutional Review Boards at Marquette University and the Medical College of Wisconsin. Inclusion criteria for the subacute stroke participants included a minimum age of 18 and the ability to independently answer questions, follow directions, and provide informed consent. Contraindications included a history of multiple strokes, history of claustrophobia, other known brain pathology, and MRI incompatibility. Participants in the neurologically intact group were age- and sex-matched to the stroke group.

This study aimed to collect longitudinal imaging and behavioral data from people with stroke at the subacute (2 weeks) and chronic (>6 months) stage. Out of the ten recruited participants, four completed the study and one subacute scan was excluded due to poor imaging quality in the cerebellum. The subacute stroke group consisted of nine stroke survivors (6 female, average age 62) measured on average 14 days after stroke admission date (standard deviation 3.5 days). In addition to the four paired (participants also in the subacute group) chronic stroke participants, we assessed the lesion location of 29 chronic stroke participants and selected a cohort with lesion distributions most similar to the subacute group. This was done by iteratively calculating a Dice coefficient (Zou et al., 2004) between each subacute stroke lesion and the 29 chronic stroke lesions. A Dice coefficient of 25% was heuristically chosen as a threshold, and the chronic stroke

participants meeting this criterion were included. Ten out of the 29 chronic stroke

datasets were included in our chronic stroke group, resulting in a total of 14 participants

in the chronic stroke group (10 female, average age 62). Out of the 32 neurologically

intact participants, 13 were excluded due to improper imaging of the cerebellum in the

diffusion scan, resulting in 19 participants (10 female, average age 61).

A measure of upper extremity motor impairment was obtained for stroke

participants using the Fugl-Meyer (FM, maximum of 66 points) upper extremity motor

test, (Fugl-Meyer et al., 1975). Lower values indicate greater motor impairment. Table

4.1**Error! Reference source not found.** contains information on the stroke study

participants.

Table 4-.1: Paired stroke samples. subacute and chronic stroke demographics

Subacute subjects are listed along with their gender, time post stroke and between scans, the Fugl-Meyer upper extremity (out of 66) and the age at the first scan. For those who completed the study, the respective information is also provided

Subject	Gender	Time Post Stroke (days)	Time between scans (days)	FM-UE at scan 1	FM-UE at scan 2	Age
101	F	18	NA (Deceased)	29	NA	63
102	F	17	242	6	45	59
103	F	16	NA	47	NA	72
104	M	8	282	56	64	67
105	F	13	198	12	29	73
106	F	18	201	20	25	56
107	M	11	NA	55	NA	68
108	F	13	NA	45	NA	48
109	M	12	NA	5	NA	52

Table 4-.2: Chronic stroke participant demographics

Subjects 102, 104, 105, 106 are chronic stroke participants from Table 4.1. The age, gender, and Fugl-Meyer are listed for all chronic stroke participants in this study

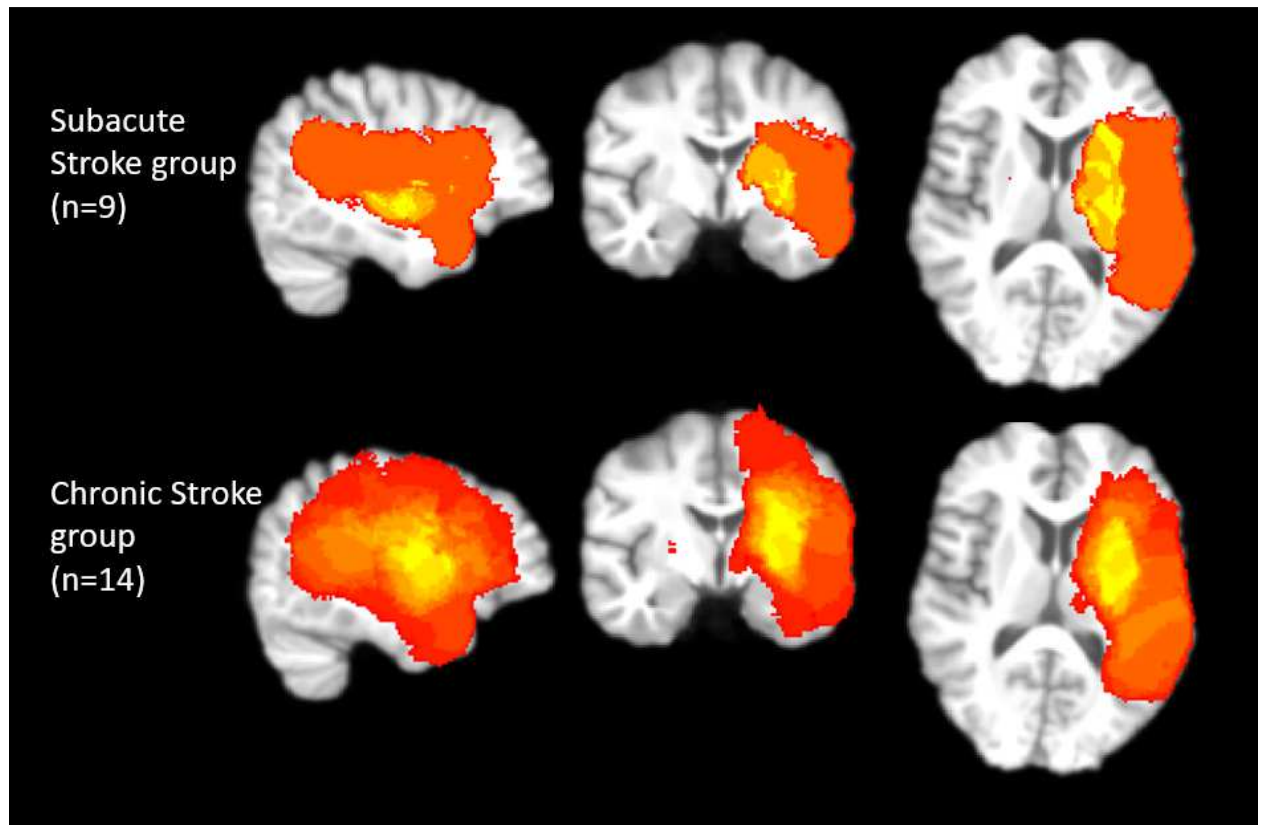| Subject	Gender	Age	FM-UE
102	F	60	45
104	M	67	64
105	F	73	29
106	F	57	25
C01	M	65	64
C02	M	57	59
C03	F	83	36
C06	F	65	47
C15	M	58	26
C16	F	42	19
C18	F	67	9
C19	F	60	23
C21	F	69	NA
C23	F	45	NA

Figure 4-.1: Stroke Lesion Distribution: Subacute and Chronic

Lesion distribution for the subacute and chronic stroke subjects used in this study. The chronic stroke subjects were selected to best match the subacute stroke (lesion-matched). Yellow/white indicates high lesion prevalence. Red/orange indicates low lesion prevalence. Lesion distribution was concentrated in internal capsule

4.2.1.2   *MRI Scans*

All MRI scans were performed using a short bore 3T GE Discovery MR750 scanner. Axial T1-weighted images were acquired using the fast spoiled gradient recall (FSPGR) 3D pulse sequence, with the following parameters: TE=3.2ms, TR=8.16ms, flip angle=12 degrees, FOV=240mm, at 156x1mm slices with an in-plane axial matrix of 256x240. Axial diffusion scans were acquired using a q ball high angular resolution diffusion imaging (HARDI) sequence using a single-shot echo planar imaging (ssEPI) protocol, with the following parameters: TE=72.3ms, TR=5700 ms, FOV=256mm at 59x2.5mm slices with an in-plane axial matrix of 128x128. There were 150 gradient directions (b-value=1500 s/mm^2) and five b=0 images.

4.2.2   MRI Data Processing

4.2.2.1   *Image Pre-Processing*

A series of standard pre-processing steps were applied to the acquired images. Raw Digital Imaging and Communications in Medicine (DICOM) images were converted to NIFTI image format (Neuroimaging Informatics Technology Initiative) using *mricron* (Rorden et al., 2007). MR bias field correction and skull stripping were performed on the raw T1-weighted images using *N4BiasFieldCorrection* (Tustison et al., 2010), and *ROBEX* (Iglesias, Liu, Thompson, & Tu, 2011), respectively. Preprocessing for diffusion

images was done using the FMRIB Software Library (FSL) (Jenkinson et al., 2012), including eddy-currents correction, skull stripping, and fractional anisotropy (FA) estimation.

4.2.2.2   *LESION IDENTIFICATION*

Lesions were automatically identified using the Lesion Identification with Neighborhood Data Analysis (LINDA) algorithm, (Pustina et al., 2016). For stroke participants, all raw T1 and diffusion weighted images with right-hemisphere lesions were flipped to the left hemisphere, and the diffusion gradient vector file was flipped in the X-direction. Lesion masks alleviated registration in stroke participants.

4.2.2.3   *IMAGE REGISTRATION TO TEMPLATE SPACE*

All study participants' diffusion images were registered to a template space in order to statistically compare WM integrity and connectivity metrics in the same space; however, for visualization purposes we display our final results in MNI standard space. The template space creation was previously described (chapter 3). All registration was done with the *antsRegistrationSyN.sh* tool using the ANTs (Advanced Normalization Tools) SyN algorithm (Avants et al., 2008). Each participant's diffusion image was rigidly registered to its T1-weighted image using a rigid transform (ANTs). Rigid, affine, and deformable non-linear registration warped each participant's T1-weighted image onto template space using gaussian regularization, histogram matching, and lesion masking The diffusion-to-structural, and the structural-to-template transforms were concatenated, and the result was a set of invertible linear and non-linear transforms that

mapped diffusion space to template space. The final diffusion-to-template warps were converted from the ANTs format to FSL format using *c3d* from ITK-SNAP (Yushkevich et al., 2006).

4.2.2.4   *STRUCTURAL CONNECTIVITY*

4.2.2.4.1   DIFFUSION TRACTOGRAPHY AND CONNECTIVITY

We used WM seeding, GM waypoints, and CSF exclusionary masks to perform tractography. Prior to tractography, WM, GM and CSF masks were created to constrain the tracts. Our WM seed mask was previously defined (chapter 3) as the maximum overlap of all control participants' WM volumes. Similarly, a CSF mask prevented streamlines from entering non-brain areas, and a gray matter (GM) mask was created in order to only include streamlines that connect gray matter regions and ignore streamlines that prematurely end within the WM, similar to the anatomically constrained tractography (ACT) algorithm described in Smith et al., (2012). Unlike the aforementioned study, all masks were kept in template space.

Sparse connectivity matrices for data subsets were obtained using probabilistic tractography. Diffusion direction and orientation estimations were obtained from the eddy-corrected images using the FSL *bedpostx* function (Behrens, Woolrich, et al., 2003). Three fibers were estimated per voxel, each with a range of diffusivities. Probabilistic tractography was performed using the *probtrackx2* function (Behrens et al., 2007), seeding in template space with distance correction. We estimated 2,500 streamlines per voxel, split into 50 cores using the *–rseed* option in *probtrackx2*. The output was 50

sparse connectivity matrices that represent the probability of connectivity between every WM voxel seed.

An in-house MATLAB package merged the 50 sparse connectivity matrices for each participant, and the final matrix was forced symmetric by averaging the merged matrix with its transpose. Probabilistic tractography produces erroneous tracts, and these are typically removed by thresholding based on probability weight, or by carefully selecting waypoints. Since we are performing whole-brain tractography, the latter was not an option. Prior to thresholding, each merged and symmetric connectivity matrix was normalized by multiplying by the number of seed voxels and dividing by the total number of successfully completed streamlines (*waytotal*). The approach was adapted from chapter 3. The waytotal divided by the number of seed points gives an approximation of the average number of successfully completed streamlines, and we normalized the merged and symmetric matrix by dividing by this number. In this study, the number of seed voxels was the same. We heuristically removed all streamlines that had a cumulative probability below 0.25. This was determined by selecting thresholds and extracting corticospinal, corpus callosum, and superior cerebellar peduncle tractography-based fiber tracks from the symmetric and normalized connectivity matrix of five randomly selected control participants, and selecting the threshold that qualitatively best minimized aberrant pathways. This resulted in a symmetric, normalized, and thresholded matrix.

4.2.2.4.2   TEMPLATE MATRIX CREATION AND LESION EFFECT SIMULATION

A template matrix was calculated in order to simulate the effects of lesions on the connectivity matrix, and to calculate a new measure called the connectome similarity

metric (COSMIC). Every control participant's symmetric, normalized, and thresholded matrix was binarized at connections greater than zero. The 19 control participant binarized connectivity matrices were then summed; the entries in the sum matrix were between 0 (no connectivity found in any control participant) to 19 (all 19 participants showed connectivity in that pair of voxel nodes). We thresholded the matrix to include the 75% overlap (connectivity in that pair of voxel nodes found in 14 of the 19 control participants). The weighted template connectivity matrix was the average of the 19 control weighted matrices in that 75% overlap span. Since the input binary matrices that created the template matrix were already thresholded to reduce aberrant tracks, thresholding the template matrix was not necessary. However, we still dissected for, the connectivity matrix the CST, CC, and the SCP in order to ensure the connectivity matrix had the right topology.

The connectivity matrices calculated from probabilistic tractography were compared to simulated connectivity matrices calculated from artificial lesions placed in the weighted template connectivity matrix (lesion effect simulation, LES). We aimed to compare the simulated connectivity losses to the subacute and chronic stroke data to determine whether simple anatomical information about a lesion can account for most of the loss in connectivity. Alternatively, degeneration outside of the lesion location could further influence connectivity measurements, especially in chronic stroke. The simulated connectivity matrix for LES was calculated by identifying the nodes of the template connectivity matrix residing in the lesion volume, and zeroing all edges connected to those nodes.

The analysis on the connectome from the connectivity matrices derived from tractography and from LES focused on the network defined by the template connectivity matrix. In other words, we ensured the comparison between the connectivity matrices for the subacute and chronic stroke groups and the LES matrices measured the same topology by only analyzing the set of connections determined by the template matrix. The template connectivity matrix masked out every participant's tractography-derived connectivity matrix by zeroing out every edge that was not included in the template connectivity matrix. This was done in order to ensure that networks can be compared across groups (comparing stroke and controls, and subacute and chronic stroke) and across methods (comparing the connectivity results between the fiber tractography connectivity matrix and the LES connectivity matrix). In this way, the focused on network connectivity reductions when compared to controls.

4.2.2.5 *POST-PROCESSING – WM STRUCTURE MEASURES*

White matter integrity and connectivity were assessed at the voxel level. The fractional anisotropy (FA) was calculated from HARDI data at each WM voxel, i, (section **Error! Reference source not found.**) as a surrogate measure of local WM integrity. Similarly, the volume fractions for the first and second sticks from the ball-sticks model were used as a surrogate measure of WM integrity. This aimed to assess changes in WM integrity at the voxel level in the primary and secondary fiber directions.

Using the connectivity matrices obtained from LES (subacute and chronic stroke) and tractography (controls, subacute and chronic stroke), we calculated the structurally weighted fractional anisotropy (SWIFT) as an indicator of white matter integrity, the

weighted degree as a measure of direct connectivity and network centrality, and the voxel wise indirect connectivity (VISC) for indirect connectivity. We also compared each connectivity matrix to the template matrix using a novel measure, the connectome similarity metric (COSMIC), which is based on a correlation of the connectivity matrices and assesses network overlap. A description of each metric follows.

As previously described, (chapter 3), the structurally-weighted fractional anisotropy (SWIFT) was defined as the average FA of connected voxels, (Equation 4.1), where k_i is the number of directly connected voxels, and a is the binary connectivity matrix. The SWIFT aimed at measuring global, tract-specific WM integrity.

$$SWIFT_i = \frac{1}{k_i}\sum_{j\epsilon N}(a_{ij} \cdot FA_j) \hspace{2cm} \textit{Equation 4.1}$$

The 'weighted' degree, k_i, (Rubinov & Sporns, 2010) was calculated using in-house MATLAB algorithms as the sum of all values of columns, j, in our weighted connectivity matrix, a, (Equation 4.2). This is our measure of direct connectivity.

$$k_i = \sum_{j\epsilon N} a_{ij} \hspace{2cm} \textit{Equation 4.2}$$

The voxel-wise indirect connectivity (VISC, Equation 4.3) (Kalinosky et al., 2013) was implemented as a measure of indirect connectivity. This sums the total number of direct connections of indirect connections, y_i, divided by the number of indirect connections, and has been shown to be sensitive to global damage to WM connectivity.

$$VISC_i = \frac{\sum_{j\epsilon N}(y_{ij}\sum_{k\epsilon N}a_{jk})}{\sum_{j\epsilon N}y_{ij}} = \frac{y_i a\mathbf{1}}{y_i\mathbf{1}} \hspace{2cm} \textit{Equation 4.3}$$

Lastly, the connectome similarity metric (COSMIC, Equation 4.4) was calculated as the correlation between every participant's weighted matrix, $a^{participant}$, and the template weighted matrix, $a^{template}$, calculated at every node (voxel). The aim of this

measure is to summarize the overlap in the connectome between every participant and a template matrix. Every node has a summary value between 0 and 1 based on its correlation to the template matrix. Since it is a correlation, it is not affected by differences in magnitude in the connectivity weight. Additionally, it is a more specific measure of direct connectivity; rather than count the number of direct connections, as it determines whether the network's connectome at a node is similar to that of the template node.

$$cosmic_i = corr(a_i^{participant}, a_i^{template}) \hspace{3cm} Equation\ 4.4$$

4.2.3 STATISTICAL ANALYSIS

The mean measures outlined in section 4.2.2.5, excluding stroke lesion volumes, were calculated in the whole-brain WM, corticospinal tract (CST), contralesional superior cerebellar peduncle connecting the ipsilesional thalamus with the contralesional cerebellum (SCPr), and the corpus callosum (CC). These were selected due to their involvement in motor function, and because they were identified as being damaged by stroke and correlated with motor impairment in a prior study (chapter 3). The CST and CC masks were obtained from the Laboratory of Brain Anatomical MRI at John Hopkins University (Hua et al., 2008; Wakana et al., 2007), and the SCPr was obtained from the Neurosurgical Centre Nijmegen in The Netherlands (van Baarsen et al., 2016).

All statistical analyses were done in R (3.6.1). Our aim was to find differences in WM integrity and connectivity in subacute stroke, chronic stroke, and neurologically intact participants. We first performed four 1-factor MANOVAs (whole-brain, CST, SCPr, CC) to assess whether there were differences in variances between the three groups

in any of the six dependent variables: FA, Degree, Cosmic, VISC, F2, SWIFT. The four ROIs were not treated as factors because our hypothesis assessed whether there were differences in the means in any of the dependent variables in any of these non-overlapping regions. At a significance of 0.0125 ($p<0.05$, Bonferroni-corrected by four regions), all MANOVAs passed. We later ran 24 1-factor ANOVAs (four regions, six dependent variables) to assess whether there was a significant difference in variance between the groups. The only measures that did not reach significance ($p<0.05$) is the F2 and FA in the right SCP. For the comparison analysis in the next paragraph, the mean FA, Degree, Cosmic, VISC, and F2 in the whole-brain-WM, CST, SCPr, and CC were compared between the control, chronic, and subacute groups—with the exception of the F2 and FA in the rSCP since it did not reach significance in the ANOVA test.

The group comparison tested the hypothesis that the mean value of the dependent variable was significantly different between two groups in the four regions of interest. The control group was separately compared with the subacute and the chronic stroke groups using an unpaired t-test. Given that there were four overlapping (paired) participants in the subacute and chronic stroke groups, our post-hoc analysis implemented the partially-overlapping t-test approach in Derrick et al., (2017). The approach is an interpolation between the paired and the unpaired t-test. Significant differences in means were defined at $p < 0.0125$ (p-uncorrected = 0.05, Bonferroni-corrected by four regions of interests).

In order to aid in the interpretation of the partially-overlapping t-test results, non-parametric permutation tests (FSL's *randomize*, threshold-free cluster enhancement) were performed in order to compare the chronic stroke and subacute stroke group with the

control group. Lesion volumes were removed from the analysis. The resulting images were then thresholded (p-corrected<0.05 by FDR) to show volumes where the stroke group had significantly reduced values in our connectivity and integrity measures. Additionally, the paired stroke participants (those subacute participants with a subsequent chronic stroke scan) were qualitatively compared to denote changes over time in lesion size and shape.

Lastly, the change in the upper extremity Fugl-Meyer score between subacute and chronic stroke scans (6 months) was correlated with the WM integrity and connectivity measurement values at the subacute stage.

4.3   RESULTS

Nine subacute stroke, fourteen chronic stroke, and nineteen control participants were analyzed in this study. The lesion distributions for the subacute and chronic groups were concentrated in the internal capsule (Figure 4.1). The Dice coefficient between the subacute and the chronic stroke lesion distributions was 70%. The Dice coefficient between the paired (same participants measured six months apart) subacute and chronic stroke lesion was also 70%.

4.3.1   FIBER TRACTOGRAPHY COMPARED TO LESION EFFECT SIMULATION IN STROKE

Lesion effect simulation (LES) indicated reduced connectivity in stroke only in the corticospinal tract when compared to the control group. There were no differences between subacute and chronic stroke groups. In contrast, fiber tractography suggested differences between both stroke groups and the control group in the CST, CC, and SCP.

Additionally, tractography was able to identify differences between the subacute and chronic stroke groups in the three tracts of primary interest (Figures 4.2, 4.3, 4.4).

Figure 4-.2: COSMIC Fiber Tractography vs Lesion Effect Simulation

Mean COSMIC in the whole-brain, CST, SCP, and Corpus Callosum for Control (dark-gray) Subacute (gray) and Chronic (light-gray) groups calculated using fiber tractography (left) and lesion effect simulation (LES) (right). Significance between subacute and chronic are shown (*). Non-significance between control and stroke are shown (N.S) (assume significance between control and stroke if otherwise not stated). Significance is not tested in the LES plots (right)
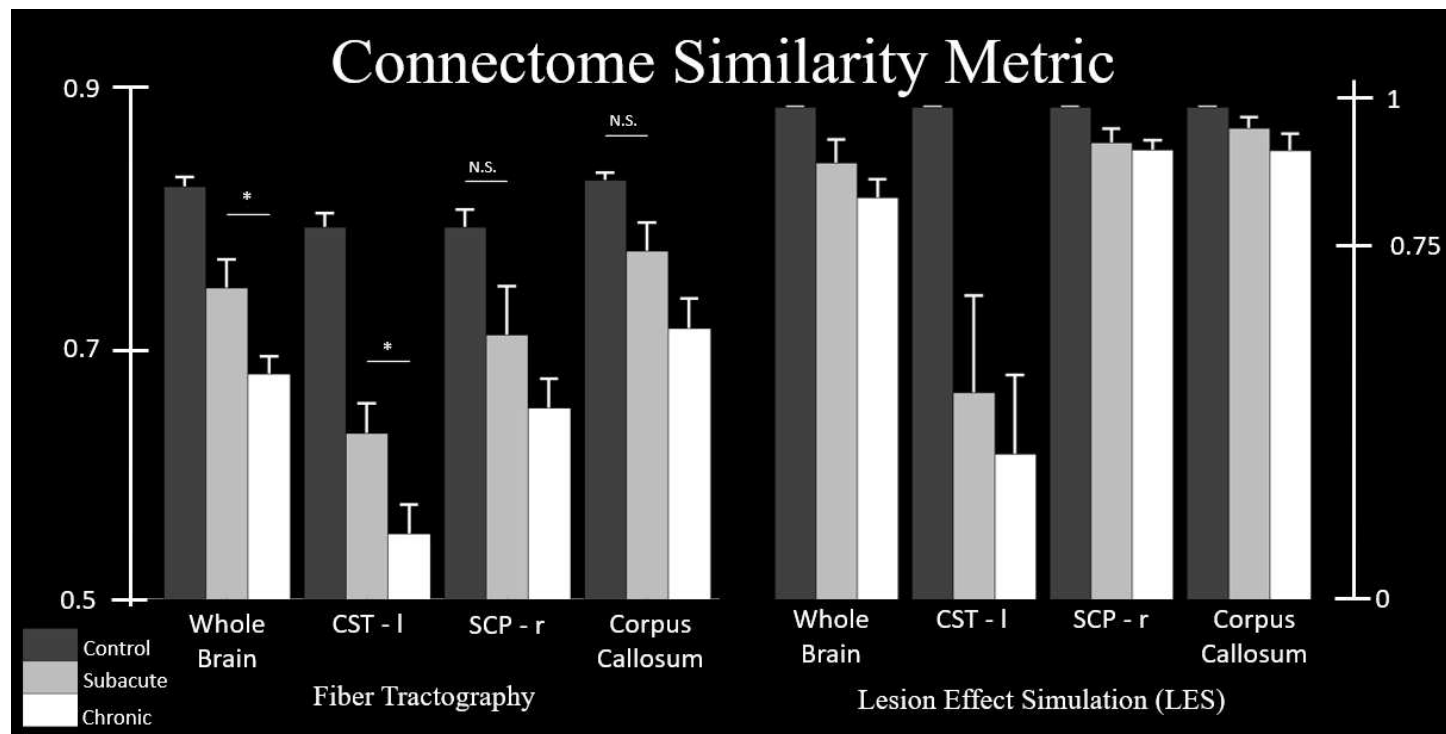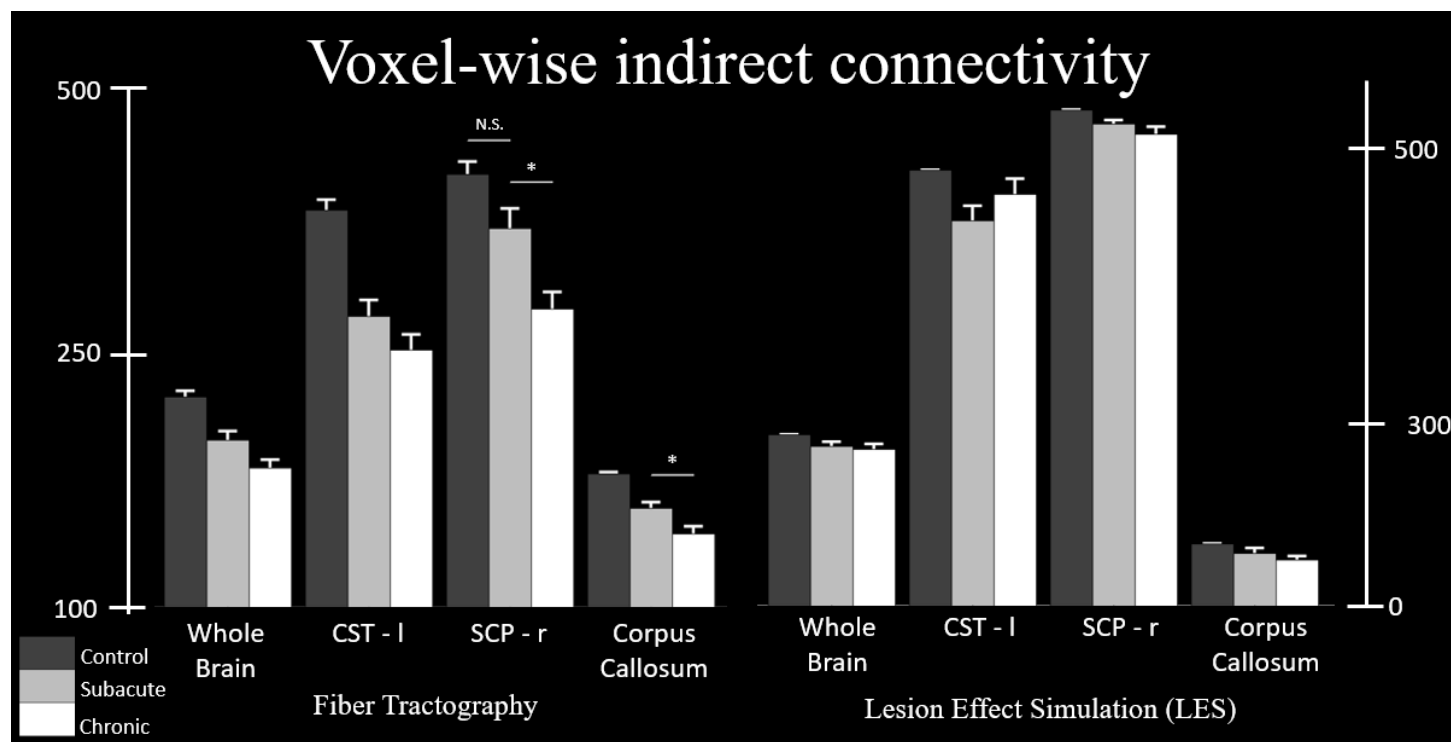
Figure 4-.3: VISC Fiber Tractography vs Lesion Effect Simulation

Mean VISC in the whole-brain, CST, SCP, and Corpus Callosum for Control (dark-gray) Subacute (gray) and Chronic (light-gray) groups calculated using fiber tractography (left) and lesion effect simulation (LES) (right). Significance between subacute and chronic are shown (*). Non-significance between control and stroke are shown (N.S) (assume significance between control and stroke if otherwise not stated). Significance is not tested in the LES plots (right)

Figure 4-.4: Degree Fiber Tractography vs Lesion Effect Simulation

*Mean Degree in the whole-brain, CST, rSCP, and CCfor Control (dark-gray)
Subacute (gray) and Chronic (light-gray) groups calculated using fiber tractography
(left) and lesion effect simulation (LES) (right). Significance between subacute and
chronic are shown (*). Non-significance between control and stroke are shown (N.S)
(assume significance between control and stroke if otherwise not stated). Significance is
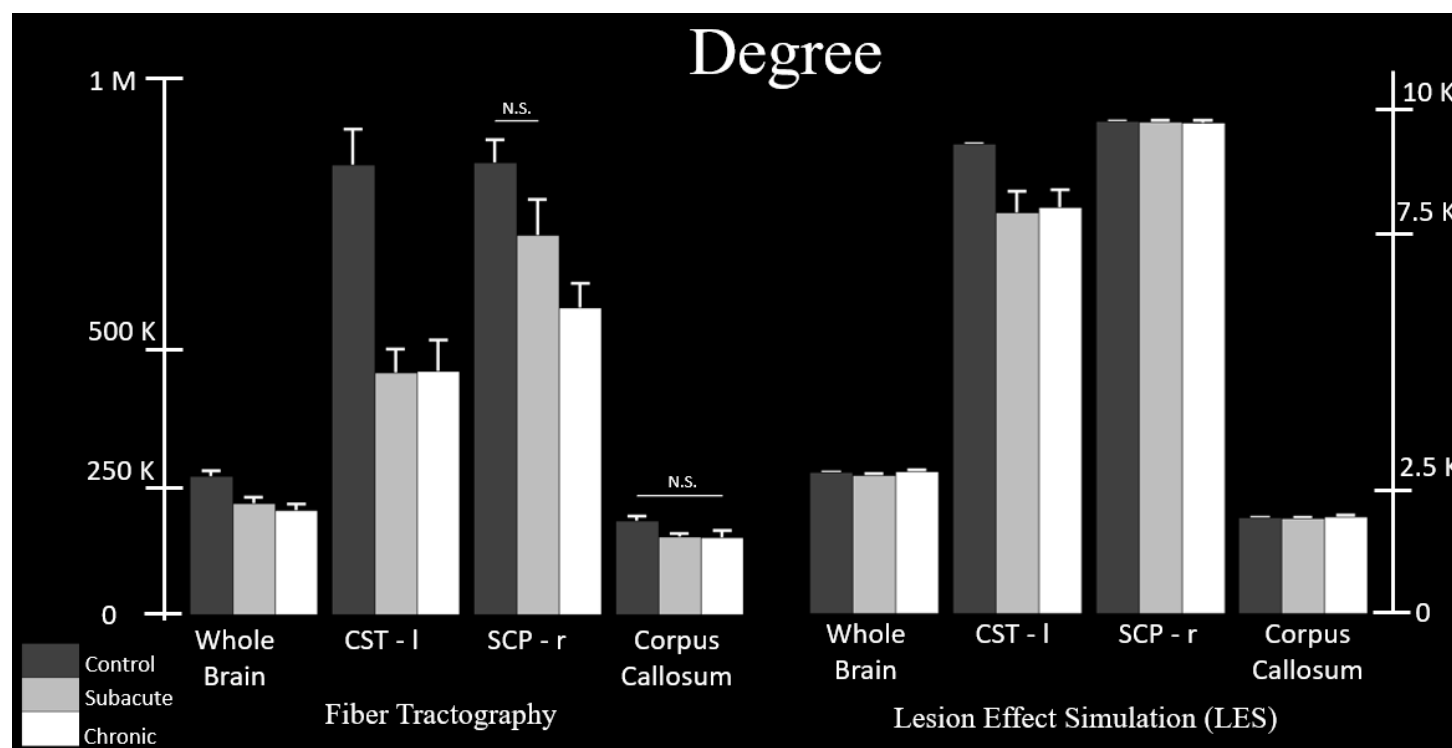not tested in the LES plots (right)*

4.3.2 DIFFERENCES IN WM INTEGRITY IN STROKE

The FA and the bedpostx F1 group results were similar to each other in the

selected WM tracts because F1 measures the strength of the primary fiber direction and

the FA within the selected white matter tracts (with the exception to the SCP at the

decussation) are large WM tracks with one primary direction. We used the FA for

subsequent analysis, and did not use F1. There was a significant decrease in all WM

integrity measures (FA, SWIFT, and F2) in the subacute and chronic stroke groups'

whole-brain WM volume and the CST when compared to the control group (FA and F2

illustrated in Figures 4.7 and 4.8). The partially-overlapping t-test identified significant differences in WM integrity between the subacute and chronic stroke groups in the whole-brain WM volume (Figures 4.7, 4.8, and 4.9). Interestingly, only the strength of the second fiber direction (F2) showed discernable differences between subacute and chronic stroke in the CST (Figure 4.8).

Out of the three WM ROIs, the control group had significantly higher average WM integrity values than the chronic group in the CST and the CC; additionally, only the SWIFT indicated significantly reduced WM integrity in the rSCP between the chronic stroke and control groups, similar to what we found in chapter 3 (Figures 4.7, 4.8, and 4.9). Interestingly, there were no significant differences in WM integrity values between the subacute stroke and the control groups in the CC. Similarly, the differences between the subacute and chronic stroke groups in the CC did not reach significance.

Nonparametric permutation testing revealed significantly reduced FA in inferior portions of the CST and the anterior CC in the subacute stroke group when compared to the control group (Figure 4.5). Differences between the subacute and control groups in the F2 parameter were minimal in our three WM ROIs (Figure 4.5). The chronic stroke group had a greater extent of reduced WM integrity in the CC and the CST when measured by FA and F2 (Figure 4.5).

Figure 4-.5: Nonparametric testing in FA and F2 between stroke and control

Control vs Subacute (top) and Control vs Chronic (bottom) nonparametric permutation results in FA (A) and F2 (B). Superior cerebellar peduncle (green), corticospinal tract (blue) and corpus callosum (yellow) are shown. Statistically significant differences shown in red.
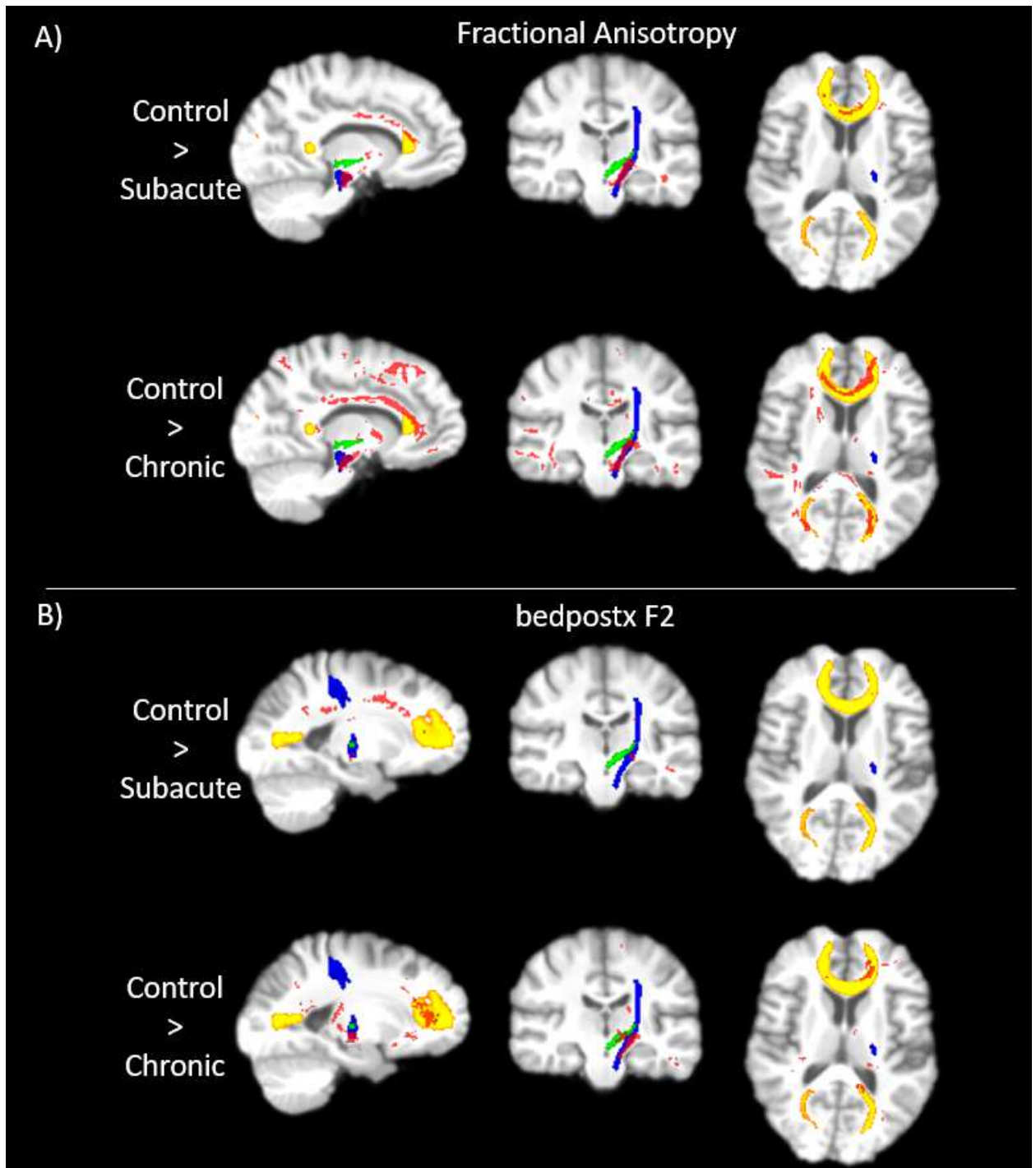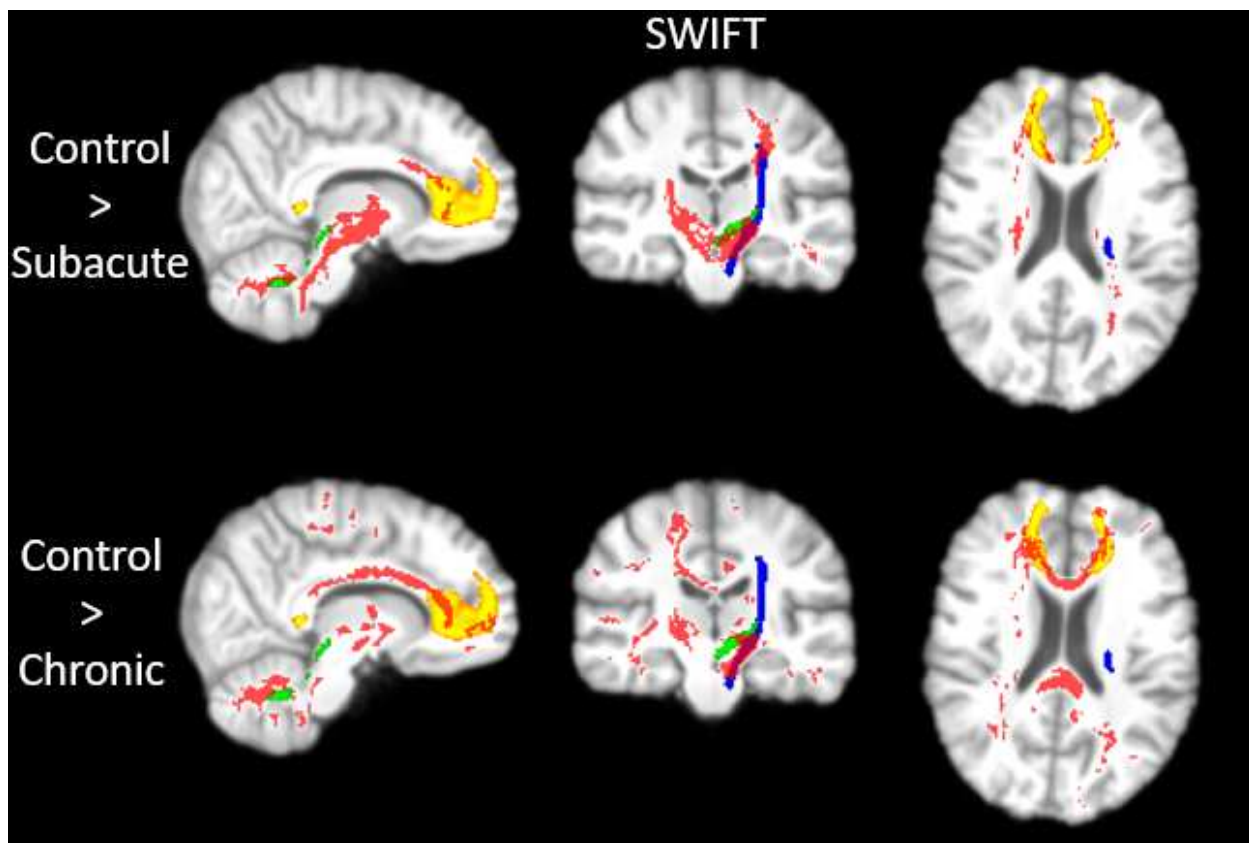
Figure 4-.6: Nonparametric testing in SWIFT between stroke and control

Control vs Subacute (top) and Control vs Chronic (bottom) nonparametric permutation results in SWIFT. Superior cerebellar peduncle (green), corticospinal tract (blue) and corpus callosum (yellow) are shown. Statistically significant differences shown in red.

Figure 4-,7: Comparison between partially-overlapping and Paired Samples for FA

Comparison between partially-overlapping (left) and paired samples (right) for FA. Control (dark-gray), Subacute (gray), and chronic (light-gray) group means in whole-brain, CST, and CC are shown for the FA. Significance between subacute and chronic are shown (*). Non-significance between control and stroke are shown (N.S) (assume significance between control and stroke if otherwise not stated)
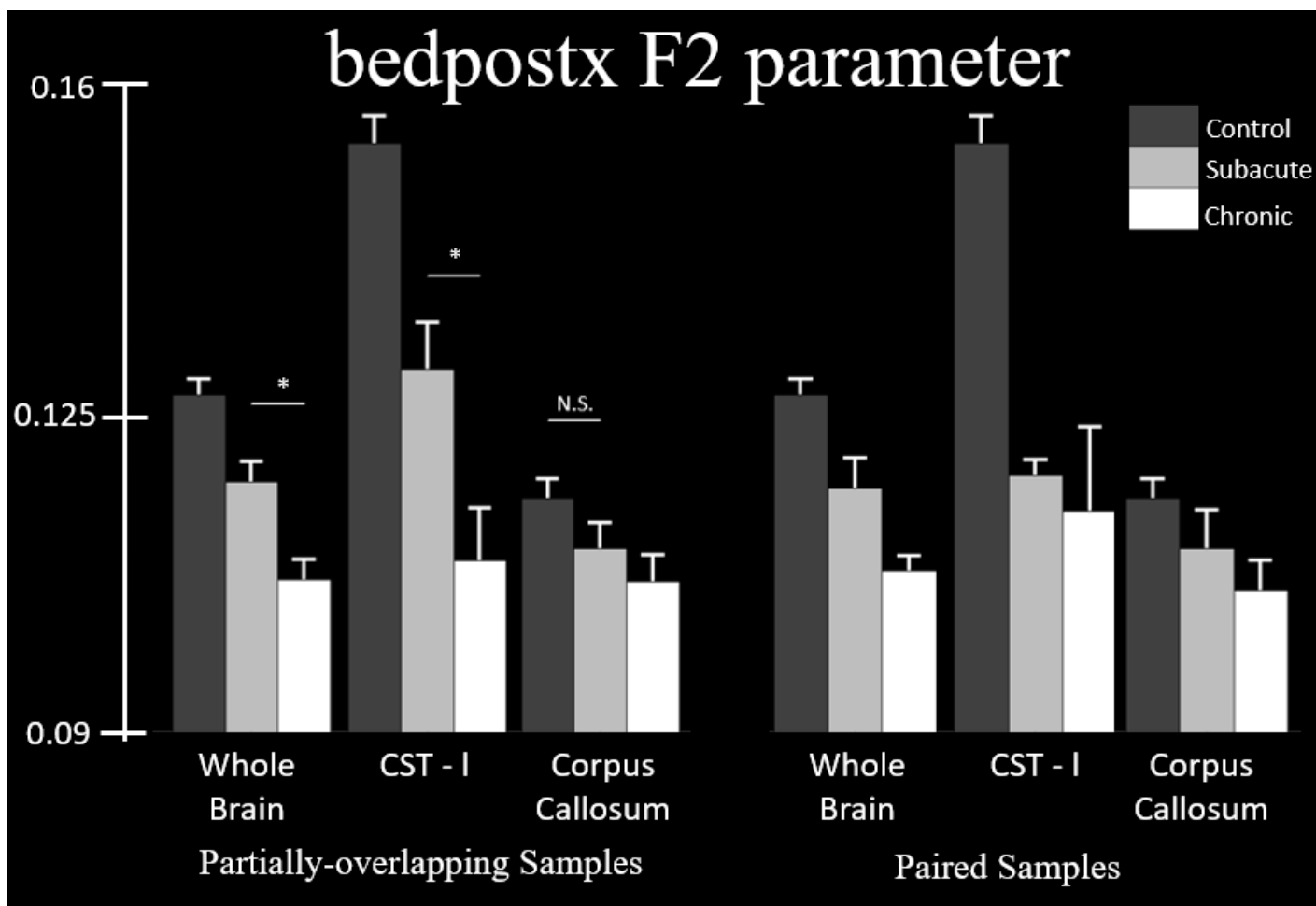
Figure 4-.8: Comparison between partially-overlapping and Paired Samples for F2

Comparison between partially-overlapping (left) and paired samples (right) for F2. Control (dark-gray), Subacute (gray), and chronic (light-gray) group means in whole-brain, CST, and CC are shown for the F2. Significance between subacute and chronic are shown (*). Non-significance between control and stroke are shown (N.S) (assume significance between control and stroke if otherwise not stated)
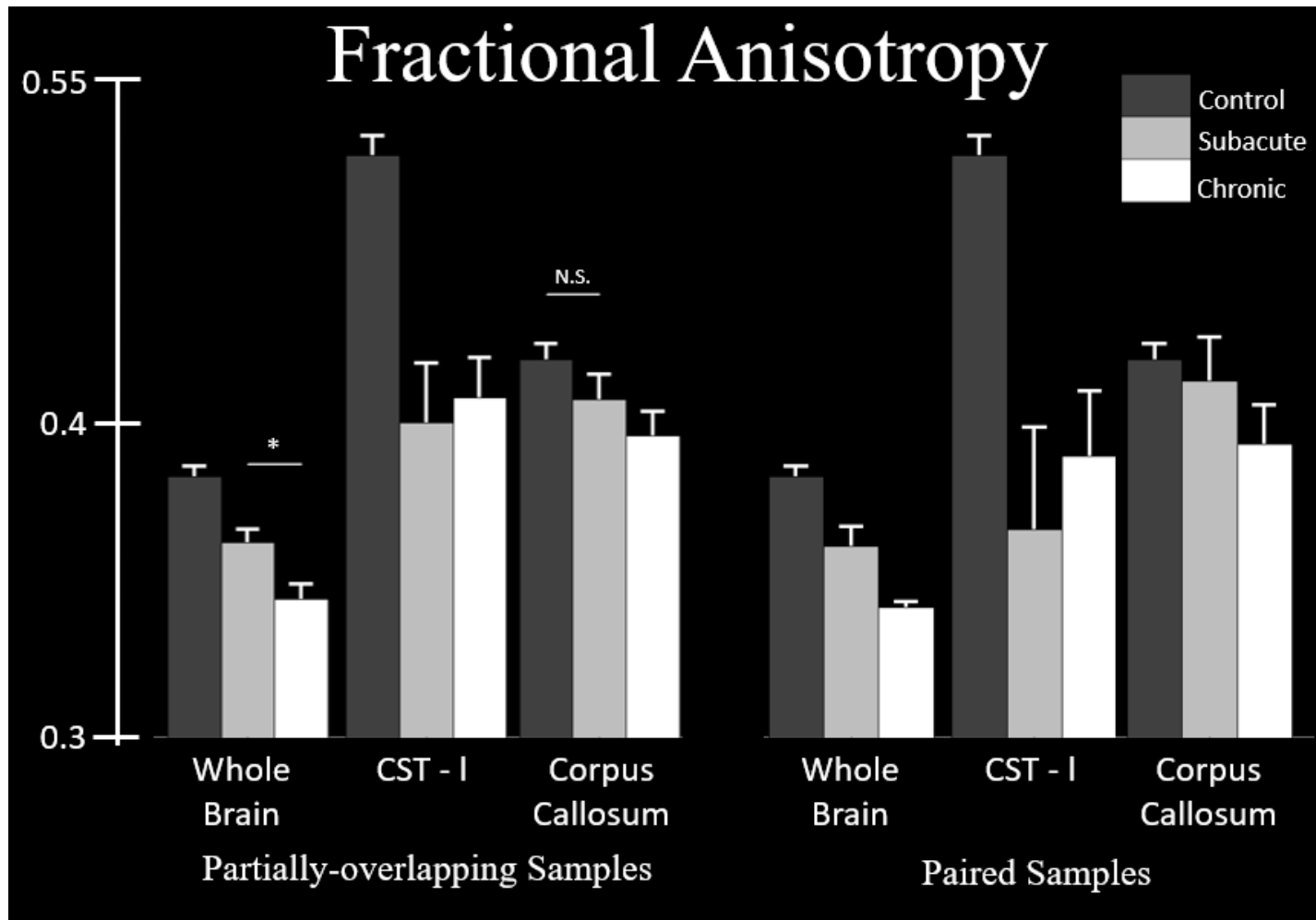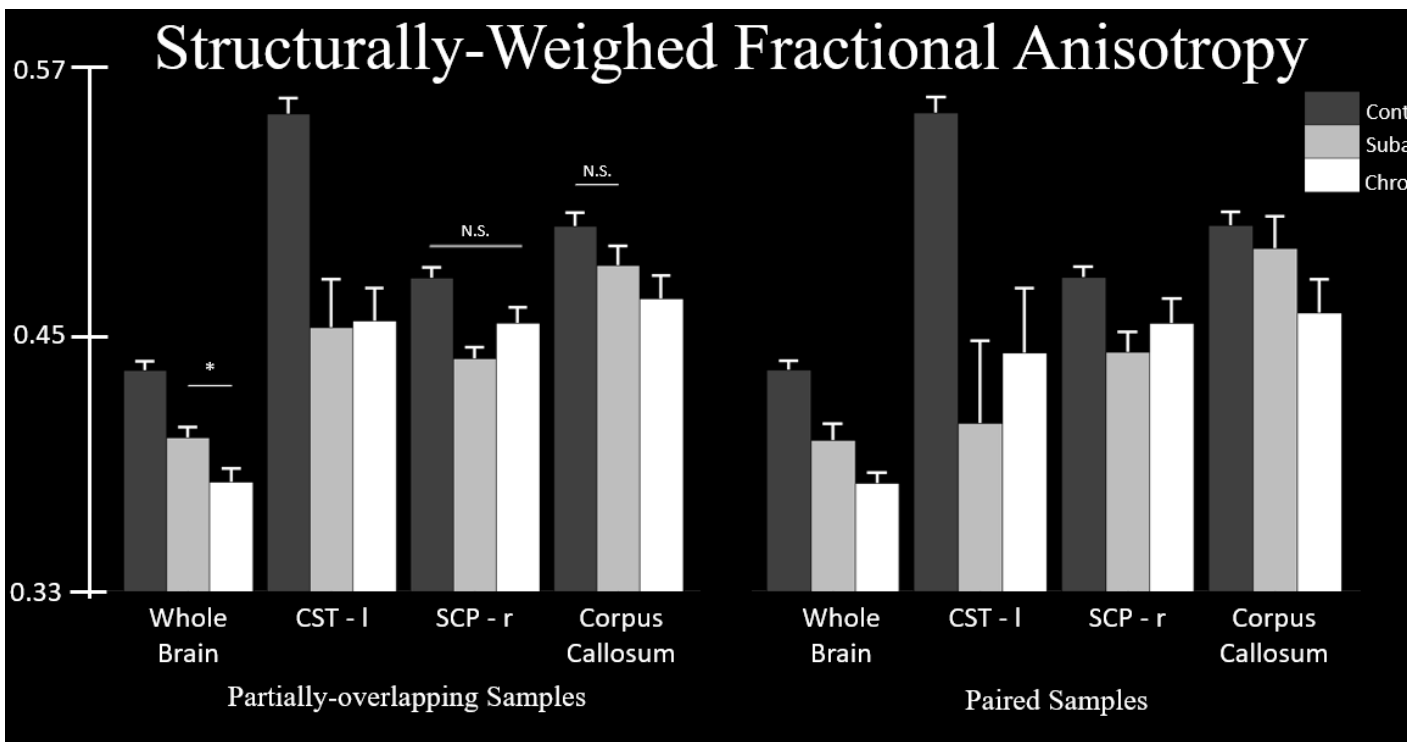
Figure 4-.9: Comparison between partially-overlapping and Paired Samples for SWIFT

Comparison between partially-overlapping (left) and paired samples (right) for SWIFT. Control (dark-gray), Subacute (gray), and chronic (light-gray) group means in whole-brain, CST, SCPr, and CC are shown for the SWIFT. Significance between subacute and chronic are shown (*). Non-significance between control and stroke are shown (N.S) (assume significance between control and stroke if otherwise not stated)

4.3.3   DIFFERENCES IN WM CONNECTIVITY IN STROKE

The lesion effect simulation (LES) approach only found discernable group differences between the control group and the two stroke groups in the CST when using COSMIC and VISC; there were no significant differences between the chronic and subacute stroke groups when the effects of a lesion were simulated (Figures 4.2, 4.3, and 4.4).

Using fiber tractography, there were significant differences between the control group and the chronic and subacute stroke groups in the whole-brain WM volume for

COSMIC and VISC (Figures 4.11 and 4.12). The chronic stroke group had significantly reduced COSMIC and VISC in the CST, rSCP, and CC when compared to the control group. In contrast, the CST had significantly reduced COSMIC and VISC in the subacute stroke group when compared to the control group; the VISC also identified reduced connectivity in the CC (Figures 4.11 and 4.12).

Although the chronic stroke group had significantly reduced connectivity in the rSCP and the subacute stroke group did not when compared to the control group, only the VISC found reduced WM connectivity in the rSCP in chronic stroke compared to subacute stroke (Figure 4.12). Interestingly, the partially overlapping t-test found reduced COSMIC in the chronic stroke compared to subacute stroke in the CST, and VISC in the CC (Figure 4.11).

Nonparametric permutation testing revealed significantly reduced COSMIC in the CST only, and reduced VISC in the bilateral CST and CC in the subacute stroke group when compared to the control group (Figure 4.10). The chronic stroke group had a greater extent of reduced WM connectivity in the CC and the CST when measured by COSMIC and VISC. The volumes of reduced COSMIC and VISC in the chronic stroke group were similar to each other (Figure 4.10).
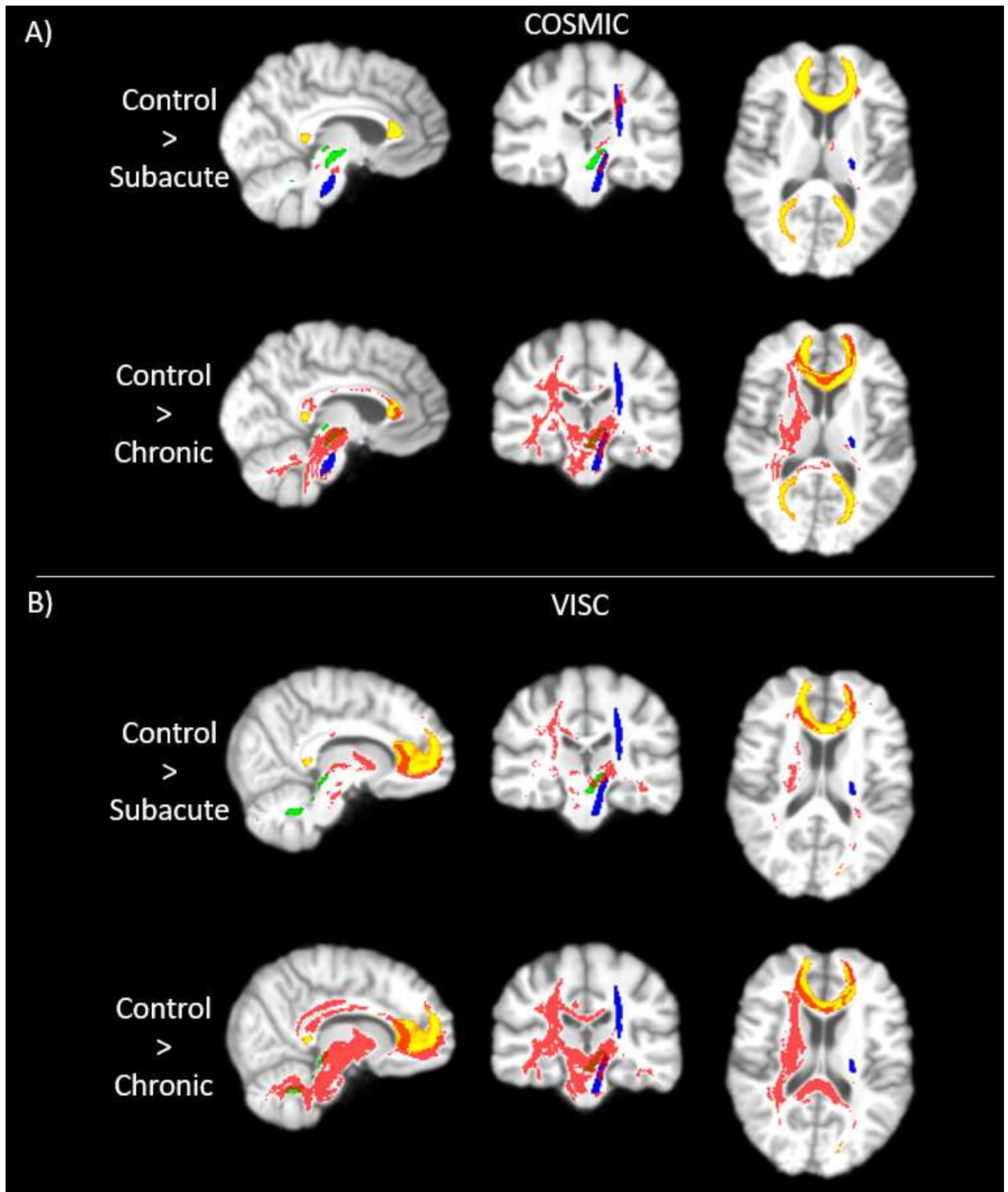
Figure 4-.10: Nonparametric testing in COSMIC and VISC between stroke and control

Control vs Subacute (top) and Control vs Chronic (bottom) nonparametric permutation results in COSMIC (A) and VISC (B). Superior cerebellar peduncle (green), corticospinal tract (blue) and corpus callosum (yellow) are shown. Statistically significant differences shown in red.
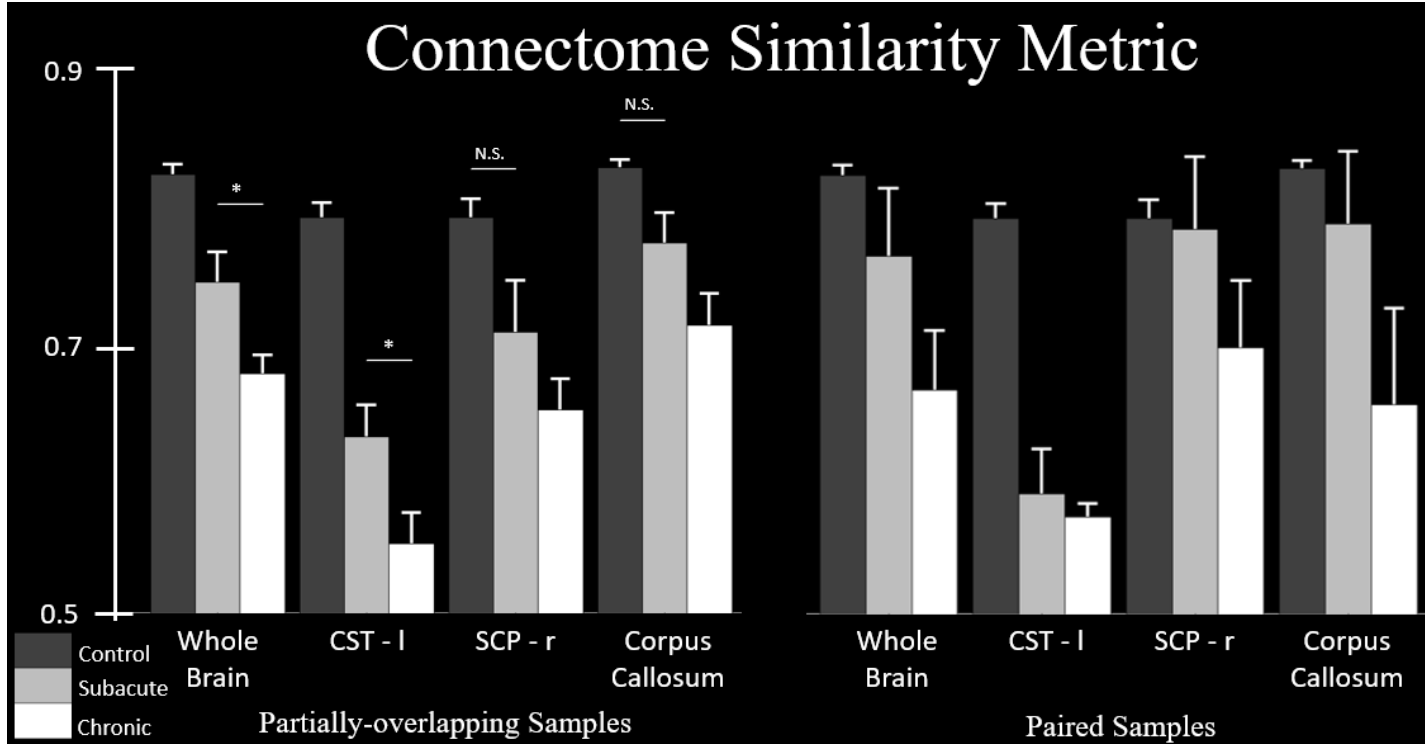
Figure 4-.11: Comparison between partially-overlapping and Paired Samples for COSMIC

Comparison between partially-overlapping (left) and paired samples (right) for COSMIC. Control (dark-gray), subacute (gray), and chronic (light-gray) group means in whole-brain, CST, SCP, and Corpus Callosum are shown for the COSMIC. Significance between subacute and chronic are shown (*). Non-significance between control and stroke are shown (N.S) (assume significance between control and stroke if otherwise not stated)
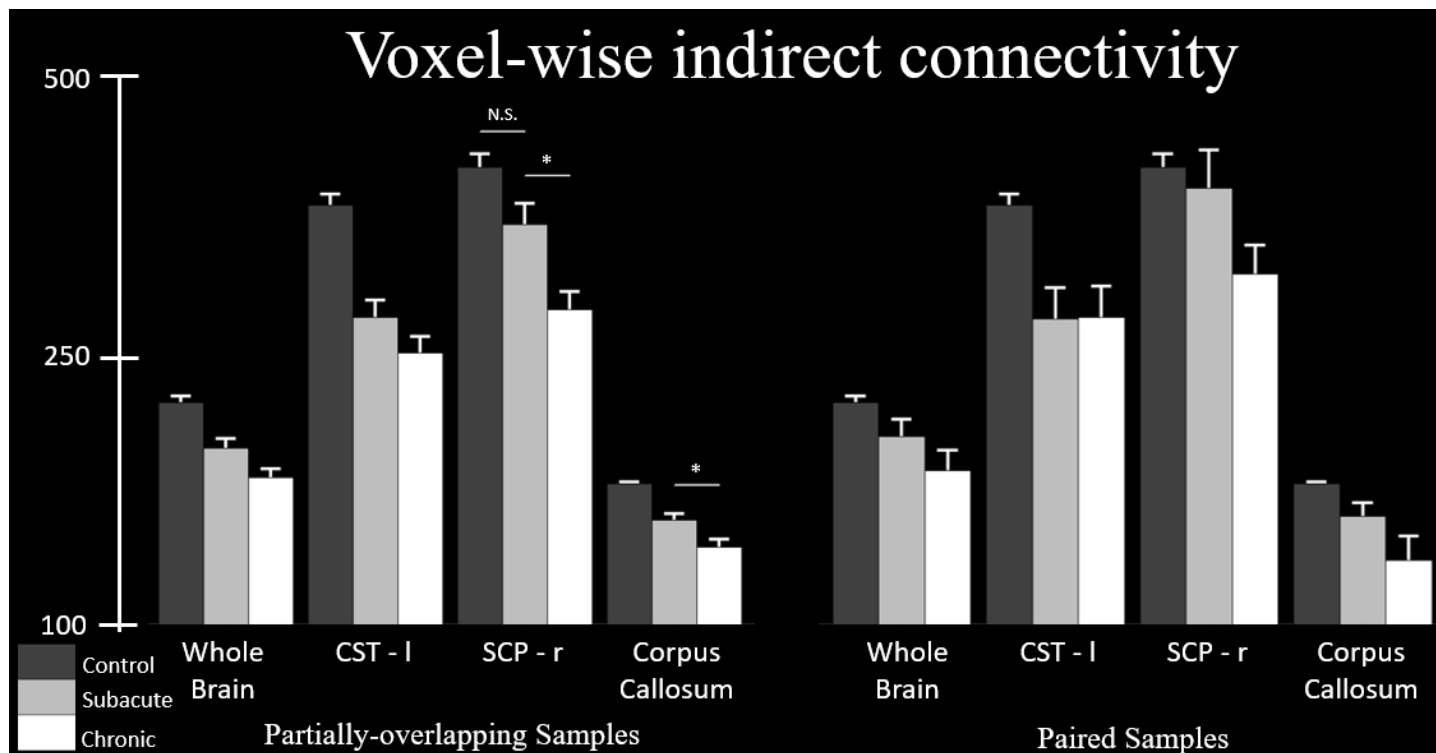
Figure 4-.12: Comparison between partially-overlapping and Paired Samples for VISC

Comparison between partially-overlapping (left) and paired samples (right) for VISC. Control (dark-gray), subacute (gray), and chronic (light-gray) group means in whole-brain, CST, SCP, and Corpus Callosum are shown for the VISC. Significance between subacute and chronic are shown (*). Non-significance between control and stroke are shown (N.S) (assume significance between control and stroke if otherwise not stated)

4.3.4 PRELIMINARY OBSERVATIONS IN SUBACUTE AND CHRONIC STROKE

In the limited sample size (n=4), an increase in the FA between the subacute and the chronic scans in the rSCP trended with an increase in upper extremity Fugl-Meyer. Additionally, an increase in the upper extremity Fugl-Meyer was related to the baseline subacute COSMIC in the CC and the whole-brain WM, and the VISC in the rSCP.

4.4 DISCUSSION

We found reduced indirect structural connectivity and white matter integrity in subacute and chronic stroke when compared to age-matched neurologically intact controls, indicating a loss of white matter structure in the whole-brain white matter, CST, SCP, and CC following an ischemic event. We found reduced connectivity and WM integrity in the whole-brain WM in chronic stroke when compared to age-matched and lesion-matched subacute stroke. Additionally, the overlap in connectome spatial map (COSMIC) in the CST, and indirect connectivity (VISC) in the SCP and CC were reduced in chronic stroke when compared to subacute stroke. The results suggest a chronic degeneration in white matter structure during the first six months after stroke. Additionally, the preliminary results on paired subjects suggest cerebellar connectivity may relate to improvement in motor impairment score.

4.4.1 FIBER TRACTOGRAPHY IS MORE SENSITIVE TO DIFFERENCES IN CONNECTIVITY COMPARED TO SIMULATED ANALYSES

As hypothesized, connectivity analysis based on fiber tractography was better able to discern differences in connectivity between stroke and control, and differences between subacute and chronic stroke, when compared to connectivity analysis based on lesion effect simulation (LES). Although LES detected differences in stroke and control in the CST—one of the major pathways of the brain—this is mostly due to direct damage to the CST (Figures 4.2, 4.3, and 4.4). Direct damage to the CST has been shown to relate to motor recovery and improvement (Habegger et al., 2018; Koyama & Domen, 2017; Lam et al., 2018; Schulz et al., 2012); however, it does not explain the complete variance in motor abilities after stroke.

Probabilistic fiber tractography propagates local and systemic changes fiber integrity and orientation uncertainty, extending reductions in connectivity along remote fiber tracts. In particular, we report reduced structural connectivity in the cerebellum and corpus callosum—in addition to the corticospinal tract—after chronic stroke compared to control and subacute stroke participants (Figures 4.10, 4.11, and 4.12). The differences between chronic and control participants is consistent with voxel and region-level diffusion MRI analyses (Crofts et al., 2011; Griffis et al., 2019; Kalinosky et al., 2017, 2013). These changes in connectivity are partly attributable to local degenerative changes in white matter integrity following focal injury, as reported in rat models (Jirjis, Valdez, Vedantam, Schmit, & Kurpad, 2017; Motovylyak et al., 2019).

These results suggest using lesion-based LES in a longitudinal stroke analysis after the lesion size and shape has stabilized would not be sensitive to tracing changes in connectivity over time (Figures 4.2, 4.3, and 4.4). By estimating structural connectivity based on fiber tractography rather than fiber simulation, we are able to detect commissural and cerebellar fibers with reduced connectivity after stroke, in addition to the CST. Although fiber tractography in pathologic brains may have shortcomings (Kuceyeski, Maruta, Relkin, & Raj, 2013), future studies that longitudinally track changes in fiber connectivity should not depend on simulation, especially if the lesion morphology is maintained.

4.4.2   EVIDENCE OF FIBER DAMAGE AND CHRONIC DEGENERATION

Our major finding was the cross-sectional difference in indirect structural connectivity between chronic and subacute stroke (Figure 4.12), indicative of Wallerian

degeneration of major white matter pathways. Similarly, the whole-brain white matter integrity measures showed reduced integrity at the chronic stage when compared to the subacute stage (Figures 4.7, 4.8, and 4.9). Although there were no statistically significant differences between the two groups in white matter integrity in specific tracts, differences in the overlap in connectome spatial map (Figure 4.11) and in indirect connectivity (Figure 4.12) suggest these markers may be more sensitive to changes in white matter structure during subacute stroke recovery.

4.4.2.1 *Global Differences in White Matter Integrity*

Wallerian degeneration is the microstructural process that degenerates a distal axon after proximal injury to an axonal fiber or neuronal body. It begins with axonal breakdown and ends in the clearance of tissue debris (Qin et al., 2012). In a rat model for spinal cord injury, damage measured by FA was shown over 7 days after spinal cord injury (Yung et al., 2019). Additionally, a decrease in the longitudinal diffusion coefficient was found throughout the spinal cord during the 25-week recovery period (Ellingson, Kurpad, & Schmit, 2008), suggesting axonal and demyelination (DeBoy et al., 2007).

Wallerian degeneration has also been measured in humans after stroke; however, the findings are mixed. The primary finding is a degeneration in FA during the first 2-12 weeks, and a stabilization after that (Groisser et al., 2014; Liang et al., 2008; Thomalla, 2005; Thomalla et al., 2004; C. Yu et al., 2009). Additionally, Puig et al., (2010) found reduced FA in the CST in the affected hemisphere compared to the unaffected hemisphere at day 30 and not three days after stroke. This is consistent with the clinical

finding that outcomes of motor impairment increase in the short term and stabilize after three weeks (Yang et al., 2019). Progressive degeneration in white matter tracts and gray matter volume was also observed in (Duering et al., 2015), where cortical regions with the highest probability of connectivity to the lesioned volume saw the most change in cortical volume 6 months post stroke, associated with a degeneration of those connecting fiber tracts. Additionally, Haque et al., (2019) saw ongoing degeneration in areas not immediately in the lesioned volume following stroke.

In contrast, Ferris et al., (2017) did not find changes over time in the FA 30 and 90 days after a transient ischemic attack, and no differences between the lesioned and healthy hemisphere at 90 days. One potential reason why Ferris and colleagues did not find differences over time in the FA is because transient ischemic attack is a temporary blockage of blood perfusion. Interestingly, Lin et al., (2018) found reduced FA in the CST at three months post-stroke, and an increase in the 3-12 month period. These findings suggest there is an initial drop in FA over time during the first three months after stroke, and a subsequent increase that tracks recovery.

Our results only found significant (p<0.025, corrected) differences in WM integrity between the cross-sectional subacute and chronic groups in the whole-brain white matter; the un-corrected SWIFT found an increase in connectivity-weighted WM integrity in the SCP in the chronic stroke group when compared to the subacute group (p<0.1 uncorrected), (Figure 4.9). General trends showed an increase in FA in the CST, and a drop in the CC (Figure 4.7), which is consistent with results found in a rat model for stroke (van Meer et al., 2012). Differences in cross-sectional chronic and subacute stroke in white matter integrity did not reach significance partly due to the variability in

time between imaging and stroke onset (24% coefficient of variance, Table 4.1) MR intensities change dynamically during subacute and subacute stroke recovery, (Allen et al., 2012), and the variability may be in part due to the subacute images being imaged at different time-points.

As a final note, we detected significantly reduced global white matter integrity in the chronic stroke group when compared to the subacute group. The non-parametric results show a larger extent of white matter degeneration in the chronic group in the anterior portion of the corpus callosum than the subacute group when compared to the control group (Figure 4.5, 4.6). This is consistent with the trend seen in the partially-overlapping t-test between the chronic and subacute group, where the chronic group had a lower (non-significant) FA in the corpus callosum (Figure 4.7). Further analysis is required to find other white matter tracts with reduced integrity that could help explain the global drop in FA in the chronic group.

4.4.2.2 *INDIRECT CONNECTIVITY CAN DETECT TRACK DAMAGE DURING STROKE*

A unique contribution of this study is the use of voxel-level measures of structural connectivity in this cross-sectional stroke analysis, and the measured reduction in connectivity map overlap (COSMIC) and indirect connectivity (VISC) in white matter tracts with relatively unchanged integrity.

Connectivity differences in stroke may be in part due to the global reduction in white matter integrity seen in chronic stroke compared to subacute stroke. The global reduction in FA is accompanied by an increase in the dispersion (uncertainty) in the first and second fiber directions. Global tractography, in the presence of a global increase in

dispersion, reduces the probability of connection at the voxel level. In other words, seeding a voxel in the CST in the presence of globally increased uncertainty decreases the probability of connection to other voxels, and applying a threshold reduces the set of possible connections. Thus, this contributes to the reduced connectome similarity and indirect connectivity at the whole-brain level and in the three tracts of interest.

Interestingly, the degree did not detect differences between both stroke groups (Figure 4.4). This supports the hypothesis that measures of *indirect* and *complex* connectivity are more sensitive to remote changes in connectivity after stroke than measures of direct connectivity. In the same manner, decreasing the set of possible connections also decreases the set of indirect connections. By reducing the set of direct connections to all direct connections (indirect connectivity), indirect connectivity accentuates local reductions in connectivity at the global scale.

We measured a reduced COSMIC in the CST in chronic stroke compared to subacute stroke (Figure 4.11). This is in part explained by a reduced strength of the second fiber (F2) in the chronic stroke group compared to the subacute stroke group (Figure 4.8). Changes over time in the parallel and perpendicular fiber directions in the CST have previously been reported (Groisser et al., 2014), and changes in the diffusivity in these fiber orientations has been theorized to be due to neurite beading, in which cytotoxic edema induce restrictions in neuronal membranes and restricts diffusion (Baron et al., 2015).

The SCP and CC saw reduced indirect connectivity in chronic stroke compared to subacute stroke. The lesion distribution is concentrated near the internal capsule, and direct damage to the CST can lead to downstream reductions in *indirect* connectivity in

remote tracts, in particular those tracts in close proximity to the CST. For instance, the CC has been shown to have damage following direct damage to the CST (Cunningham et al., 2015; Liu et al., 2015). Additionally, the cerebellum has reduced structurofunctional connectivity following stroke (Kalinosky et al., 2017), and damage to the cerebellum following supratentorial lesions to the cortico-cerebellar loop has been reported in perfusion and gray matter volume studies (Cheng et al., 2015; Dang et al., 2013; Förster et al., 2014). Thus, measures of structural connectivity that assign whole-brain network changes at the voxel level are sensitive to disruptions in connectivity to fiber tracts not directly impact by the lesion (Kalinosky et al., 2013).

4.4.3 Implications for Longitudinal Studies: Subacute Stroke Cerebellar Connectivity and Motor Recovery

The FA in the CC and the VISC in the SCP at the subacute stage related to the improvement in upper extremity motor impairment score for our four paired stroke participants. The sample size is very small; R^2 and p-values are not provided for this reason. However, the preliminary results suggest indirect cerebellar connectivity may relate to improvements in motor score. White matter integrity of cerebellar efferent and afferent fibers (Schulz, Frey, et al., 2015), and cerebellar connectivity to prefrontal areas (Kalinosky et al., 2017) have been related to fine motor control. Additionally, cerebellar activation has been related to subacute stroke recovery (Small et al., 2002). Given that indirect connectivity can detect remote regions affected by stroke, using indirect structural connectivity may improve our ability to relate the cerebellum's impact on subacute stroke recovery.

4.4.4 S<small>TUDY</small> L<small>IMITATIONS</small>

The main limitation of this study is the low sample size in the paired analysis. We used the partially overlapping t-test results to draw conclusions about white matter connectivity during stroke recovery; however, our results may be driven by those participants that were not paired in the subacute and chronic groups. We believe our results can be used to draw conclusions about changes in white matter connectivity during the first six months after stroke because the differences in the mean between subacute and chronic stroke in white matter integrity and connectivity in the paired analysis resembles that of the partially overlapping t-test results (Figures 4.7, 4.8, 4.9, 4.11, 4.12).

Another limitation is normalizing and comparing connectivity matrices across different populations. We seeded in template space and performed tractography in diffusion space. However, probabilistic tractography produces aberrant streamlines and these need to be removed. We first heuristically determined a threshold based on the normalized matrix that best removed aberrant streamlines in the corticospinal tract, the corpus callosum, and the cerebellar tracts for our control participants. This was later applied to all controls and stroke participants. Lastly, we masked out the template network from all participants in order to normalize our analysis on loss of connectivity in the template network.

Even with normalization, one cannot interpret a higher probability of connectivity between two voxels as a "stronger" connection, due to the possibility that less streamlines were propagated in one direction, therefore artificially preferring another direction (Carrera & Tononi, 2014). In the same way, lower probabilities may be difficult to

interpret. That is why we employed the connectome similarity metric (COSMIC). This measure correlates networks to determine deviations in network topology, and is not sensitive to differences in network weights.

4.5 CONCLUSION

The major finding of this study is evidence of reduced indirect connectivity after stroke, and reduced connectivity in chronic stroke compared to subacute stroke. In addition to the corticospinal tract, the corpus callosum and superior cerebellar peduncle saw reduced connectivity indicating a degeneration of motor-related white matter tracts remote from the lesion. Additionally, the paired analysis suggests the superior cerebellar peduncle may relate to improvement in motor impairment scores. The clinical implication of our study is that changes in structural connectivity extend beyond the lesion volume, and that these changes in connectivity can be used along with white matter integrity to predict motor recovery after stroke. The study highlights the need to analyze indirect white matter connectivity when considering the effects of stroke on the brain and adds evidence that suggests the cerebellum is an important node in the brain's connectome. Lastly, the results of this study motivate future studies that aim to measure changes in structural connectivity during subacute stroke recovery.

5 CHAPTER 5: INTEGRATION OF RESULTS

5.1 SUMMARY OF RESULTS

5.1.1 BRIEF SUMMARY

The purpose of this dissertation was to identify whole-brain structural networks that are damaged after subacute and chronic stroke, to develop imaging measures of white matter integrity and whole-brain connectivity that are sensitive to these changes, and to determine the influence of these remotely connected gray matter regions and white matter connections on subacute and chronic stroke impairment..

In chapter two, we improved on a measure of indirect structural connectivity in order to detect remote gray matter regions with reduced connectivity after stroke. In a region-level analysis, we found that the weighted indirect structural connectivity (WISC) was more sensitive to remote changes in connectivity after stroke than measures of direct connectivity. The WISC identified reductions in connectivity in cortical, subcortical, and cerebellar gray matter regions that play a central role in sensorimotor function. Additionally, the white matter integrity of the corticospinal tract, and the volume of affected gray matter regions detected by the WISC correlated better with motor impairment than those measures did individually.

In chapter three, we developed a unified measure of white matter structure that extends local changes in white matter integrity along remotely connected fiber tracks in order to understand the relationship between white matter integrity, connectivity, and motor impairment. Our measure, the structurally-weighted fractional anisotropy (SWIFT) uniquely identified the corpus callosum and the superior cerebellar peduncle as having altered white matter structure after stroke. Additionally, the SWIFT within the corticospinal tract predicted a larger variance in post-stroke motor impairment than the FA. Lastly, it also was able to uniquely relate white matter structure in the superior cerebellar peduncle to motor impairment.

Finally, in chapter four we used a novel connectome similarity metric (COSMIC) and the measure of indirect structural connectivity (VISC) in order to identify cross-sectional differences in white matter structure between subacute and chronic stroke. We found whole-brain reductions in white matter structure in both stroke groups when compared to neurologically intact participants. Interestingly, the chronic group had *more* reductions in indirect connectivity in the cerebellar fibers than the subacute group, and the COSMIC—a measure of connectome similarity—found similar results in the corticospinal tract. Additionally, the VISC of the superior cerebellar peduncle at the subacute stage trended with the improvement in motor impairment score for the paired subacute/chronic stroke participants.

Collectively, our work demonstrates that indirect structural connectivity and measures that summarize global network topology at the voxel level are sensitive to global changes in connectivity after stroke. Additionally, our work suggests that these measures are necessary in order to measure disruptions in cerebellar connectivity after stroke, such as detecting network loss to the cerebellum. We also documented for the first time changes in white matter structure during subacute stroke recovery. Lastly, using these measures, we were able to show that the disruption to remote gray matter regions and white matter fiber tracts, such as those in the cerebellum, relate to post-stroke motor impairment and recovery. Thus, stroke-induced changes to structural connectivity extend throughout the brain, through the corpus callosum and the cerebellar peduncles, and indirect connectivity provides an important tool to 1) measure these changes and 2) relate these changes to motor impairment.

5.1.2 NEW INSIGHTS ON REMOTE CHANGES IN INDIRECT STRUCTURAL CONNECTIVITY AFTER STROKE

A main result of our work is the evidence of remote changes to structural connectivity after stroke, as detected by indirect connectivity. Indirect connectivity may help relate changes in functional activity and connectivity, and other imaging-related findings showing changes in areas remote from the lesion after stroke. For instance, a main finding in functional activation is reduced ipsilesional activation and increased contralesional activation after stroke. Additionally, perfusion and gray matter atrophy studies have found remote damage to contralesional cerebral and cerebellar regions. Currently, the most common findings in diffusion MRI in stroke participants show reduced integrity of the corticospinal tract. Our findings corroborated the relationship the CST has on motor impairment. As expected, indirect connectivity and global measures of connectivity extended local changes in white matter integrity along fiber tracks. Perhaps more clinically important, these changes related to motor impairment and improved existing correlations in the corticospinal tract.

Figure 5.1 shows a case study of our main result. Indirect connectivity detected cortical, subcortical, and cerebellar regions with reduced connectivity after stroke. Additionally, a measure of local white matter integrity weighted by its global structural connections extended local stroke-induced changes in white matter integrity along connected white matter paths. This suggests there are subtle changes in white matter integrity along white matter pathways connected to the lesion exhibiting Wallerian degeneration. In turn, these result in an increase in fiber orientation dispersion, resulting in reduced direct connectivity and, thus, reduced indirect connectivity to gray matter

regions. The volume of affected white and gray matter related to motor impairment, which motivate future studies to further develop these measures so that they can be implemented in the clinic.
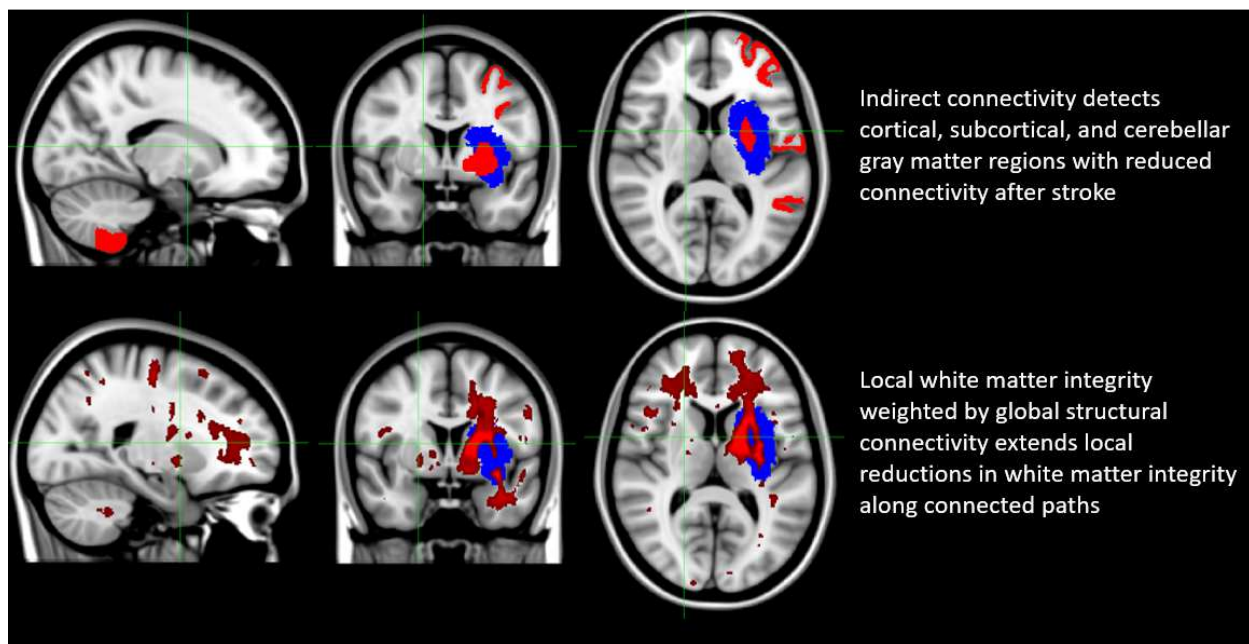
Figure 5-1: Case study of a chronic stroke participant with remote changes in indirect connectivity after stroke

This chronic stroke participant (lesion shown in blue) has reduced indirect connectivity in cortical, subcortical, and cerebellar regions (top figure, red) and reduced structurally-weighted fractional anisotropy (bottom, red).

Additionally, our results were able to distinguish the structural connectivity of chronic and subacute stroke participants. A case study is shown in Figure 5.2. The same subject is shown at the subacute stage (top) and chronic stage (bottom), and the reduced indirect connectivity compared to the mean of the control group is shown in red. Determining the connectivity profile of subacute stroke participants may become a powerful tool in stroke rehabilitation and could serve diagnostic purposes. Although the

sample size was small, the preliminary results are promising: subacute-stage indirect

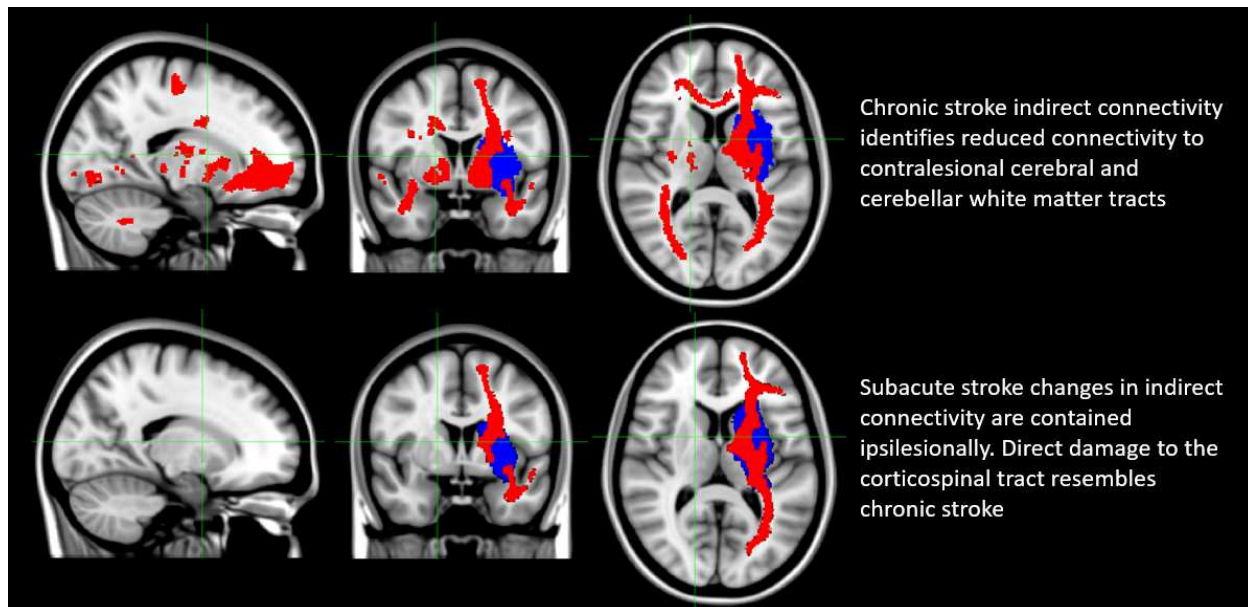connectivity of the cerebellum may predict improvements in stroke impairment.

Chronic stroke indirect connectivity identifies reduced connectivity to contralesional cerebral and cerebellar white matter tracts

Subacute stroke changes in indirect connectivity are contained ipsilesionally. Direct damage to the corticospinal tract resembles chronic stroke

Figure 5-2: Case study comparison between indirect connectivity of subacute and chronic stroke

The indirect connectivity decrease compared to the mean of the control group is shown in red for the stroke participant at the subacute (top) and chronic (bottom) stage. Lesion is shown in blue.

Lastly, we documented new evidence of changes in cerebellar structural

connectivity after stroke—a finding that has sparsely been reported in diffusion imaging

studies. Changes to cerebellar activation, functional connectivity, perfusion and gray

matter volume have been documented after lesions to the cortico-cerebellar loop, likely

due to reduced excitatory inputs. The cerebellum is indirectly connected to the cerebrum

via indirect structural connections. Using indirect structural connectivity based on

diffusion MRI has been shown in our study to be sensitive to changes in cerebellar

connectivity after stroke. We additionally related these changes to motor impairment.

Although the cerebellum is mainly involved in coordination, and our behavioral measure

is not a measure of cerebellar dysfunction, this indicates the cerebellum exhibits damages connectivity after stroke, and these changes may relate to motor deficits.

5.2   FUTURE WORK: INDIRECT CONNECTIVITY AND FUNCTIONAL CONNECTIVITY

Regions can be functionally connected even in the absence of direct structural connections. Understanding the relationship between structure and function after stroke, particularly in longitudinal studies, may be clinically important especially for prognostic purposes. Kalinosky and colleagues found reduced structurofunctional connectivity in cerebellar-cortical tracts after stroke (2017) using a method that weighted functional connections via structural connections. Chapter 3 introduced a similar approach with similar results: we weighted fractional anisotropy by structural connections. It was the residual WM structure that—when averaging the FA along the WM track—related to motor impairment. A major finding of our study was the ability of indirect connectivity to measure changes in structural connectivity to the cerebellum after stroke, in particular demonstrating differences in connectivity between subacute and chronic stroke.

The relationship between function and structure in the stroke brain, in particular using indirect structural connectivity, should be used to further investigate subacute stroke recovery. Using indirect and direct connectivity may better relate to functional connectivity, and a measure that combines direct and indirect structural connectivity, and functional connectivity should be implemented in stroke studies. This approach could elucidate mechanisms that are better able to explain the variance seen in stroke motor impairment. For example, relating the reduced structural connectivity in the cerebellum

to functional connectivity may help identify particular cerebellar structures with reduced structural-functional connectivity.

Additionally, better tests of motor impairment and function should be used. In addition to the Fugl-Meyer, clinical scores obtained longitudinally such as the Wolf-Motor score (Woodbury et al., 2010), Box and Blocks (Chen et al., 2009), gross motor output, and measures of cerebellar ataxia (Schmitz-Hubsh et al., 2006) should be investigated. For example, the cerebellum was related to motor impairment in our study; however, it would be interesting to investigate how the cerebellum modulates recovery in motor function.

The findings of this work and of future studies that combine indirect structural connectivity with functional connectivity with the aim of tracking changes in cerebellar connectivity and how they relate to motor recovery could help develop imaging techniques that can be used in the clinic. Although the work we have done has brought down computational time in diffusion imaging techniques, more work can be done such as fine-tuning the necessary streamlines required for whole-brain tractography, and running region-of-interest analyses rather than whole-brain analyses. Additionally the work demonstrated in this study and proposed here could help develop imaging techniques sensitive to identifying patients most likely to benefit from rehabilitative techniques, and prognosticating patients at the subacute stage to predict chronic stage brain connectivity and function.

6 CHAPTER 6: APPENDIX: ADDITIONAL FIGURES

Probabilistic tractography is a computational burden, requiring thousands of starting-point streamlines per voxel. In order to lessen the computational burden, we estimated the minimum required streamlines required to perform whole-brain probabilistic tractography while maintaining the same amount of information.
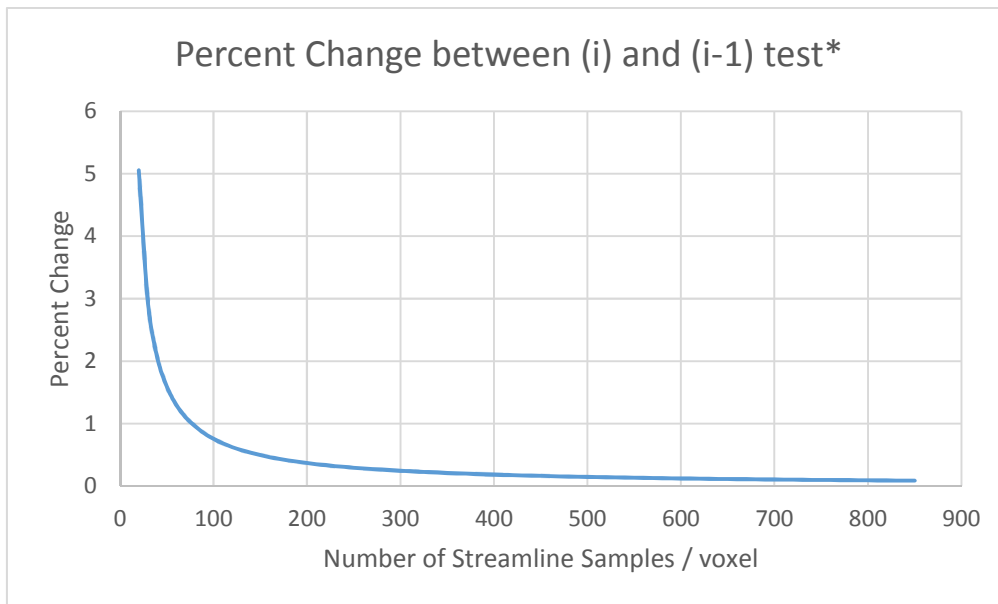

Figure 6-1: Percent change between after adding 10 more streamlines per sample vs Number of streamlines samples per voxel.

As pertaining specifically to the second chapter, we sampled the entire gray matter volume at 10 streamlines per voxel and continuously added 10 more streamlines per voxel and calculated the percent change of the average connectome probability between every two consecutive runs in order to determine the point at which adding more streamlines per voxel results in negligible change. We selected 500 streamlines per voxel as the optimal amount.

In order to properly map the connectivity of the cerebellum (physiologically connected contralaterally to the thalamus), we seeded the right cerebellum and allows unconstrainted tractography to take place. The cerebellum connects contralaterally to the thalamus in probabilistic tractography.
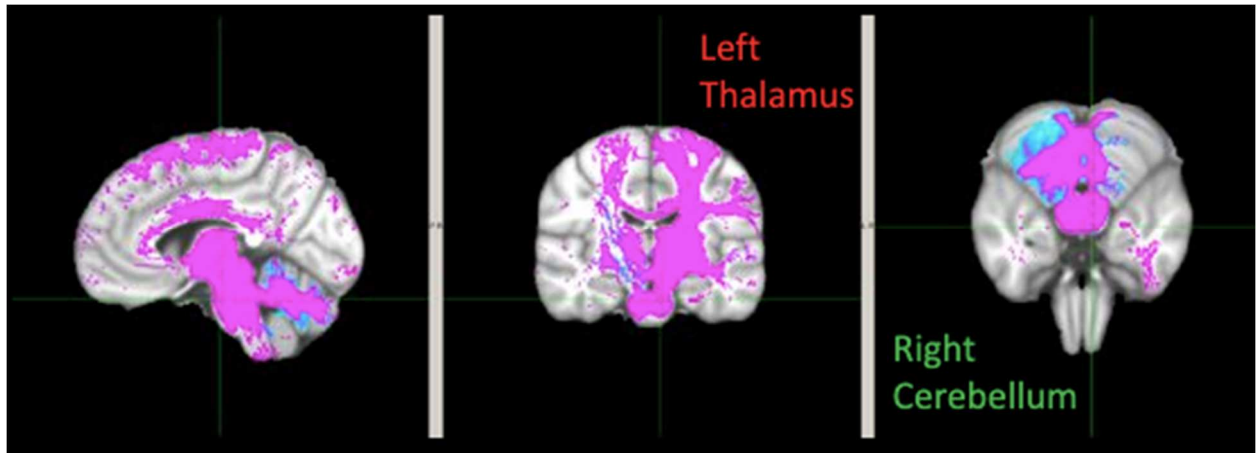
Figure 6-2: Validating cerebellar connectivity

Seeding the right dentate nucleus and adding a waypoint at the left thalamus results in cross-connectivity. We note that the cerebellum does connect to the contralateral thalamus, but streamlines pass through the thalamus (the physiological endpoint) and continue onto the cortex and cross the corpus callosum into the ipsilateral cortex. This produces false-connections between the cerebellum and the ipsilateral cortex, which could be a factor as to why we saw changes in connectivity in the contralesional hemisphere in chapter 3 (aim 2).
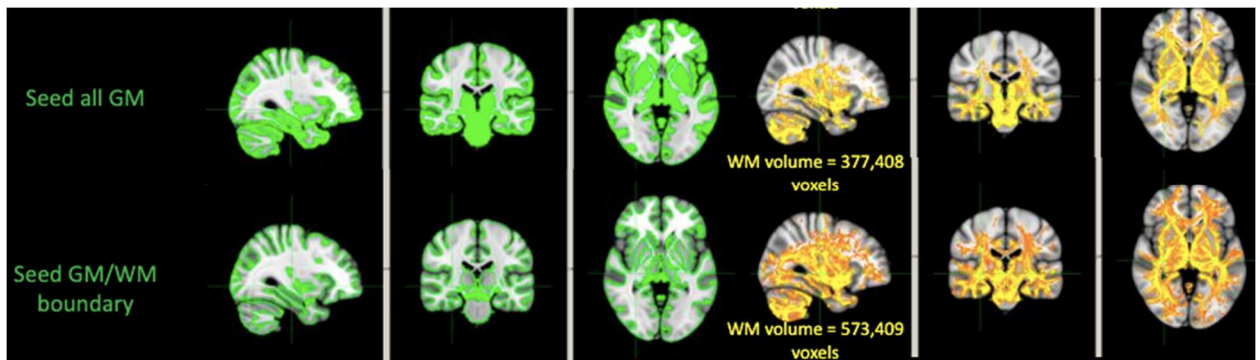
Figure 6-3: Seeding the gray matter vs the gray matter/white matter boundary: future work

Chapter 2 seeded the gray matter volume in order to determine gray-matter connectivity, and chapters 3 and 4 seeded white matter volume in order to determine white matter tracks. Future work would need to assess the level of information obtainable by seeding the GM/WM boundary. Seeding the boundary results in a greater span in connectivity, and determining how the connectome and the probability of connectivity changes would be necessary in order to determine the best approach.
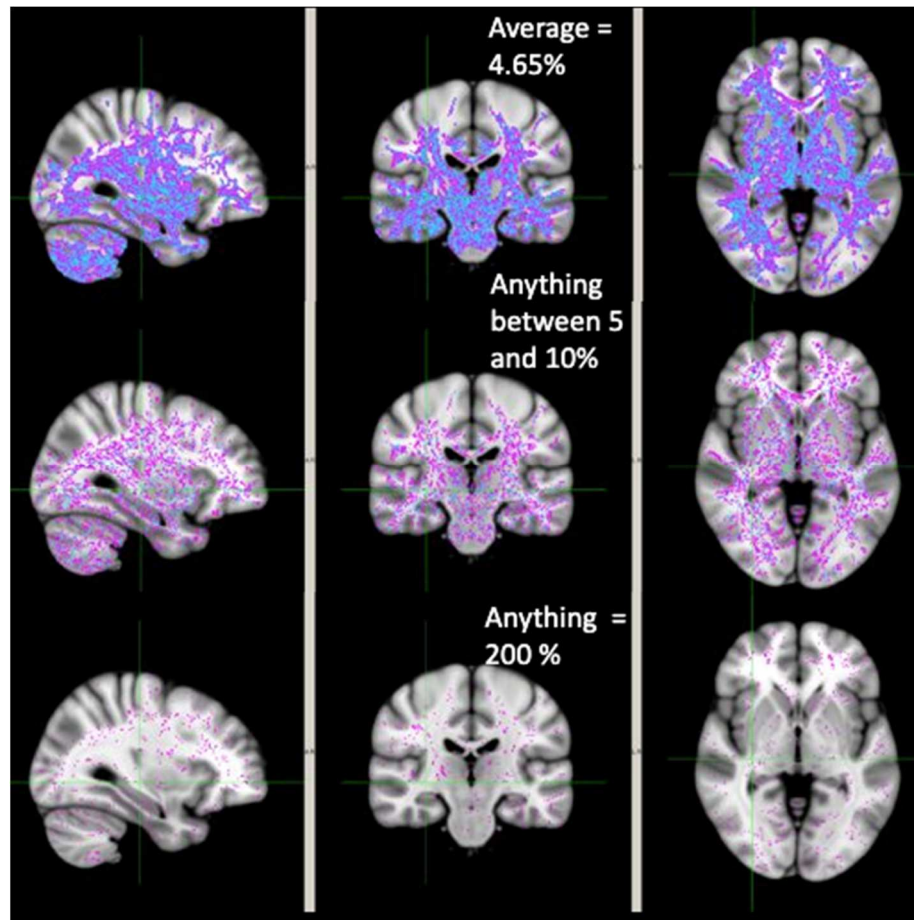
Figure 6-4: Determining the effect of running tractography in parallel

We ran tractography in parallel in all three aims, and before doing that we assessed the difference in connectivity probability at every voxel between running tractography in parallel or not. We seeded every WM voxel at 500 streamlines per voxel and compared the percent difference. Most large white matter tracks and their volumes were within 5%. Edges of large white matter tracks were within 5 and 10%.
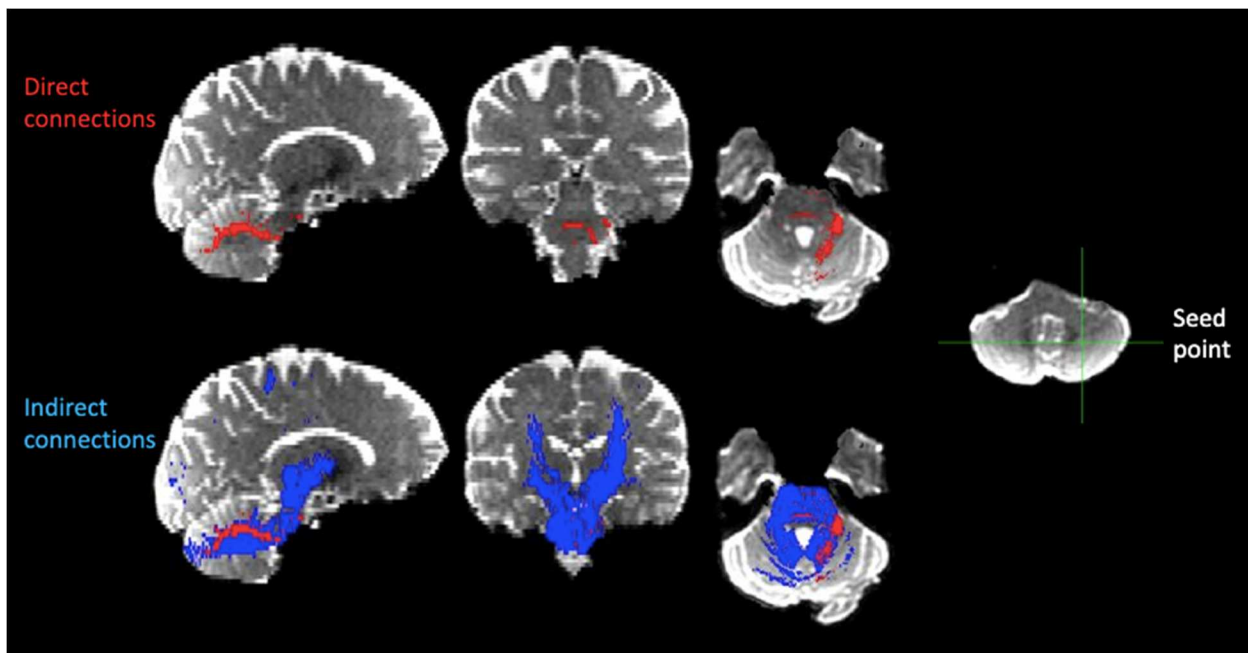
Figure 6-5: Example of direct and indirect connections

Seeding a single voxel in the cerebellum produces direct connections (red) in the cerebellar peduncle, crossing over to the contralateral side (as can be seen in the coronal slice in the top row). Indirect connections (blue) connect that single voxel to other voxels in the cerebellum, expanding the span of connections. Additionally, indirect connections connect the single voxel to bilateral thalamic regions.
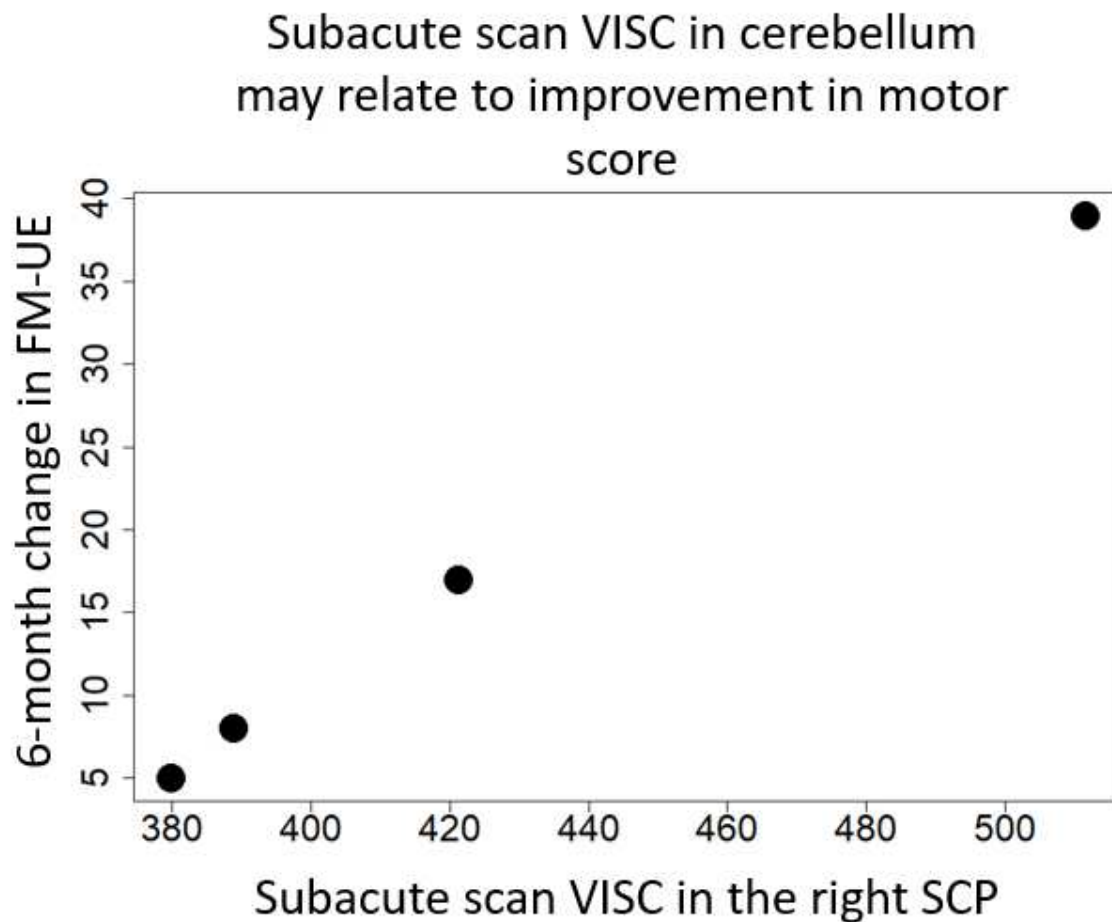
Figure 6-6: Correlation between the change in Fugl-Meyer score at the 6-month follow-up and the subacute scan VISC in the SCP

Pertaining to chapter 4 (aim 3), we correlated the change in Fugl-Meyer score at the 6-month follow-up with the VISC in the right SCP at the subacute scan. We note a high correlation, indicating that participants with high initial connectivity in the contralesional SCP saw more increase in their Fugl-Meyer score (measure of motor impairment).

7   BIBLIOGRAPHY

Allen, G. I., & Tsukahara, N. (1974). Cerebrocerebellar communication systems. *Physiological Reviews*, *54*(4), 957–1006. https://doi.org/10.1152/physrev.1974.54.4.957

Allen, L. M., Hasso, a. N., Handwerker, J., & Farid, H. (2012). Sequence-specific MR Imaging Findings That Are Useful in Dating Ischemic Stroke. *Radiographics*, *32*(5), 1285–1297. https://doi.org/10.1148/rg.325115760

ATS Statement: Guidelines for the Six-Minute Walk Test. (2002). *AMERICAN JOURNAL OF RESPIRATORY AND CRITICAL CARE MEDICINE*, *166*(1), 111–117. https://doi.org/10.1164

Avants, B., Epstein, C., Grossman, M., & Gee, J. (2008). Symmetric diffeomorphic image registration with cross-correlation: Evaluating automated labeling of elderly and neurodegenerative brain. *Medical Image Analysis*, *12*(1), 26–41. https://doi.org/10.1016/j.media.2007.06.004

Baron, C. A. llan, Kate, M., Gioia, L., Butcher, K., Emery, D., Budde, M., & Beaulieu, C. (2015). Reduction of Diffusion-Weighted Imaging Contrast of Acute Ischemic Stroke at Short Diffusion Times. *Stroke; a Journal of Cerebral Circulation*, *46*(8), 2136–2141. https://doi.org/10.1161/STROKEAHA.115.008815

Basser, P. J., Mattiello, J., & LeBihan, D. (1994). MR diffusion tensor spectroscopy and imaging. *Biophysical Journal*, *66*(1), 259–267. https://doi.org/10.1016/S0006-3495(94)80775-1

Behrens, T. E. J., Berg, H. J., Jbabdi, S., Rushworth, M. F. S., & Woolrich, M. W. (2007). Probabilistic diffusion tractography with multiple fibre orientations: What can we gain? *NeuroImage*, *34*(1), 144–155. https://doi.org/10.1016/j.neuroimage.2006.09.018

Behrens, T. E. J., Johansen-Berg, H., Woolrich, M. W., Smith, S. M., Wheeler-Kingshott, C. A. M., Boulby, P. A., … Matthews, P. M. (2003). Non-invasive mapping of connections between human thalamus and cortex using diffusion imaging. *Nature Neuroscience*, *6*(7), 750–757. https://doi.org/10.1038/nn1075

Behrens, T. E. J., Woolrich, M. W., Jenkinson, M., Johansen-Berg, H., Nunes, R. G., Clare, S., … Smith, S. M. (2003). Characterization and propagation of uncertainty in diffusion-weighted MR imaging. *Magnetic Resonance in Medicine*, *50*(5), 1077–1088. https://doi.org/10.1002/mrm.10609

Bhanpuri, N. H., Okamura, A. M., & Bastian, A. J. (2013). Predictive Modeling by the Cerebellum Improves Proprioception. *Journal of Neuroscience*, *33*(36), 14301–

14306. https://doi.org/10.1523/JNEUROSCI.0784-13.2013

Borstad, A. L., Choi, S., Schmalbrock, P., & Nichols-Larsen, D. S. (2016). Frontoparietal white matter integrity predicts haptic performance in chronic stroke. *NeuroImage: Clinical*, *10*, 129–139. https://doi.org/10.1016/j.nicl.2015.11.007

Bosnell, R. A., Kincses, T., Stagg, C. J., Tomassini, V., Kischka, U., Jbabdi, S., … Johansen-Berg, H. (2011). Motor Practice Promotes Increased Activity in Brain Regions Structurally Disconnected After Subcortical Stroke. *Neurorehabilitation and Neural Repair*, *25*(7), 607–616. https://doi.org/10.1177/1545968311405675

Boyd, L. A., & Winstein, C. J. (2004). Cerebellar Stroke Impairs Temporal but not Spatial Accuracy during Implicit Motor Learning. *Neurorehabilitation and Neural Repair*, *18*(3), 134–143. https://doi.org/10.1177/0888439004269072

Buchanan, C. R., Pernet, C. R., Gorgolewski, K. J., Storkey, A. J., & Bastin, M. E. (2014). Test–retest reliability of structural brain networks from diffusion MRI. *NeuroImage*, *86*, 231–243. https://doi.org/10.1016/j.neuroimage.2013.09.054

Buckner, R. L., Krienen, F. M., Castellanos, A., Diaz, J. C., & Yeo, B. T. T. (2011). The organization of the human cerebellum estimated by intrinsic functional connectivity. *Journal of Neurophysiology*, *106*(5), 2322–2345. https://doi.org/10.1152/jn.00339.2011

Budde, M. D., & Annese, J. (2013). Quantification of anisotropy and fiber orientation in human brain histological sections. *Frontiers in Integrative Neuroscience*, *7*(February), 3. https://doi.org/10.3389/fnint.2013.00003

Budde, M. D., & Frank, J. A. (2012). Examining brain microstructure using structure tensor analysis of histological sections. *NeuroImage*, *63*(1), 1–10. https://doi.org/10.1016/j.neuroimage.2012.06.042

C. von Monakow. (1914). Die Lokalisation im Grosshirn und der Abbau der Funktion durch Kortikale Herde. *Journal of the American Medical Association*, *LXIII*(9), 797. https://doi.org/10.1001/jama.1914.02570090083033

Caldwell, D. J., Cronin, J. A., Wu, J., Weaver, K. E., Ko, A. L., Rao, R. P. N., & Ojemann, J. G. (2019). Direct stimulation of somatosensory cortex results in slower reaction times compared to peripheral touch in humans. *Scientific Reports*, *9*(1), 3292. https://doi.org/10.1038/s41598-019-38619-2

Carey, L. M., Matyas, T. A., & Baum, C. (2018). Effects of Somatosensory Impairment on Participation After Stroke. *American Journal of Occupational Therapy*, *72*(3), 7203205100p1. https://doi.org/10.5014/ajot.2018.025114

Carrera, E., & Tononi, G. (2014). Diaschisis: past, present, future. *Brain*, *137*(9), 2408–

2422. https://doi.org/10.1093/brain/awu101

Charles, S. K., Okamura, A. M., & Bastian, A. J. (2013). Does a basic deficit in force control underlie cerebellar ataxia? *Journal of Neurophysiology*, *109*(4), 1107–1116. https://doi.org/10.1152/jn.00152.2012

Chen, F. (2012). Magnetic resonance diffusion-perfusion mismatch in acute ischemic stroke: An update. *World Journal of Radiology*, *4*(3), 63. https://doi.org/10.4329/wjr.v4.i3.63

Chen, H.-M., Chen, C., Hsueh, I.-P., Huang, S., & Hsieh, C. (2009). Test-Retest Reproducibility and Smallest Real Difference of 5 Hand Function Tests in Patients With Stroke. *Neurorehabilitation and Neural Repair*, *23*(17), 435–440. https://doi.org/10.1177/1545968308331146

Cheng, B., Schulz, R., Bönstrup, M., Hummel, F. C., Sedlacik, J., Fiehler, J., … Thomalla, G. (2015). Structural plasticity of remote cortical brain regions is determined by connectivity to the primary lesion in subcortical stroke. *Journal of Cerebral Blood Flow and Metabolism*, *35*, 1507–1514. https://doi.org/10.1038/jcbfm.2015.74

Chi, N. F., Ku, H. L., Chen, D. Y. T., Tseng, Y. C., Chen, C. J., Lin, Y. C., … Hu, C. J. (2018). Cerebral Motor Functional Connectivity at the Acute Stage: An Outcome Predictor of Ischemic Stroke. *Scientific Reports*, *8*(1), 1–11. https://doi.org/10.1038/s41598-018-35192-y

Cramer, S. C., Finklestein, S. P., Schaechter, J. D., Bush, G., & Rosen, B. R. (1999). Activation of Distinct Motor Cortex Regions During Ipsilateral and Contralateral Finger Movements. *Journal of Neurophysiology*. https://doi.org/10.1152/jn.1999.81.1.383

Crofts, J., Higham, D. J., Bosnell, R., Jbabdi, S., Matthews, P. M., Behrens, T. E. J., & Johansen-Berg, H. (2011). Network analysis detects changes in the contralesional hemisphere following stroke. *NeuroImage*, *54*(1), 161–169. https://doi.org/10.1016/j.neuroimage.2010.08.032

Crofts, J. J., & Higham, D. J. (2009). A weighted communicability measure applied to complex brain networks. *Journal of the Royal Society, Interface / the Royal Society*, *6*(33), 411–414. https://doi.org/10.1098/rsif.2008.0484

Cunningham, D. A., Machado, A., Janini, D., Varnerin, N., Bonnett, C., Yue, G., … Plow, E. B. (2015). Assessment of inter-hemispheric imbalance using imaging and noninvasive brain stimulation in patients with chronic stroke. *Archives of Physical Medicine and Rehabilitation*, *96*(4), S94–S103. https://doi.org/10.1016/j.apmr.2014.07.419

Dacosta-Aguayo, R., Graña, M., Fernández-Andújar, M., López-Cancio, E., Cáceres, C., Bargalló, N., … Mataró, M. (2014). Structural integrity of the contralesional hemisphere predicts cognitive impairment in ischemic stroke at three months. *PLoS ONE*, *9*(1), 1–11. https://doi.org/10.1371/journal.pone.0086119

Dang, C., Liu, G., Xing, S., Xie, C., Peng, K., Li, C., … Zeng, J. (2013). Longitudinal cortical volume changes correlate with motor recovery in patients after acute local subcortical infarction. *Stroke*, *44*(10), 2795–2801. https://doi.org/10.1161/STROKEAHA.113.000971

De Bruyn, N., Meyer, S., Kessner, S. S., Essers, B., Cheng, B., Thomalla, G., … Verheyden, G. (2018). Functional network connectivity is altered in patients with upper limb somatosensory impairments in the acute phase post stroke: A cross-sectional study. *PLoS ONE*, *13*(10), 1–18. https://doi.org/10.1371/journal.pone.0205693

DeBoy, C. A., Zhang, J., Dike, S., Shats, I., Jones, M., Reich, D. S., … Calabresi, P. A. (2007). High resolution diffusion tensor imaging of axonal damage in focal inflammatory and demyelinating lesions in rat spinal cord. *Brain*, *130*(8), 2199–2210. https://doi.org/10.1093/brain/awm122

Derrick, B., Toher, D., Russ, B., & White, P. (2017). Test statistics for the comparison of means for two samples that include both paired and independent observations. *Journal of Modern Applied Statistical Methods*, *16*(1), 137–157. https://doi.org/10.22237/jmasm/1493597280

Diedrichsen, J., Balsters, J. H., Flavell, J., Cussans, E., & Ramnani, N. (2009). A probabilistic MR atlas of the human cerebellum. *NeuroImage*, *46*(1), 39–46. https://doi.org/10.1016/j.neuroimage.2009.01.045

Diedrichsen, J., & Bastian, A. J. (2013). Cerebellar Function. *The Cognitive Neurosciences*.

Domercq, M., Sanchez-Gomez, M. V., Sherwin, C., Etxebarria, E., Fern, R., & Matute, C. (2007). System xc- and Glutamate Transporter Inhibition Mediates Microglial Toxicity to Oligodendrocytes. *The Journal of Immunology*, *178*(10), 6549–6556. https://doi.org/10.4049/jimmunol.178.10.6549

Douaud, G., Behrens, T. E., Poupon, C., Cointepas, Y., Jbabdi, S., Gaura, V., … Remy, P. (2009). In vivo evidence for the selective subcortical degeneration in Huntington's disease. *NeuroImage*, *46*(4), 958–966. https://doi.org/10.1016/j.neuroimage.2009.03.044

Douaud, G., Jbabdi, S., Behrens, T. E. J., Menke, R. A., Gass, A., Monsch, A. U., … Smith, S. (2011). NeuroImage DTI measures in crossing- fi bre areas : Increased diffusion anisotropy reveals early white matter alteration in MCI and mild

Alzheimer ' s disease. *NeuroImage*, *55*(3), 880–890. https://doi.org/10.1016/j.neuroimage.2010.12.008

Du, J., Hu, J., Hu, J., Xu, Q., Zhang, Q., Liu, L., … Yang, F. (2018). Aberrances of Cortex Excitability and Connectivity Underlying Motor Deficit in Acute Stroke. *Neural Plasticity*, *2018*, 1–10. https://doi.org/10.1155/2018/1318093

Duering, M., Righart, R., Wollenweber, F. A., Zietemann, V., Gesierich, B., & Dichgans, M. (2015). Acute infarcts cause focal thinning in remote cortex via degeneration of connecting fiber tracts. *Neurology*, *84*(16), 1685–1692. https://doi.org/10.1212/WNL.0000000000001502

Duque, J., Hummel, F., Celnik, P., Murase, N., Mazzocchio, R., & Cohen, L. G. (2005). Transcallosal inhibition in chronic subcortical stroke. *NeuroImage*, *28*(4), 940–946. https://doi.org/10.1016/j.neuroimage.2005.06.033

Ellingson, B. M., Kurpad, S. N., & Schmit, B. D. (2008). Ex vivo diffusion tensor imaging and quantitative tractography of the rat spinal cord during long-term recovery from moderate spinal contusion. *Journal of Magnetic Resonance Imaging*, *28*(5), 1068–1079. https://doi.org/10.1002/jmri.21578

Feeney, D. M., & Baron, J. C. (1986). Diaschisis. *Stroke*, *17*(5), 817–830. https://doi.org/10.1161/01.STR.17.5.817

Ferris, J. K., Edwards, J. D., Ma, J. A., & Boyd, L. A. (2017). Changes to white matter microstructure in transient ischemic attack: A longitudinal diffusion tensor imaging study. *Human Brain Mapping*, *38*(11), 5795–5803. https://doi.org/10.1002/hbm.23768

Fischl, B., Kouwe, A. Van Der, Destrieux, C., Halgren, E., Ségonne, F., Salat, D. H., … Dale, A. M. (2004). Automatically Parcellating the Human Cerebral Cortex. *Cerebral Cortex*, *14*(1), 11–22. https://doi.org/10.1093/cercor/bhg087

Fischl, B., Salat, D. H., Busa, E., Albert, M., Dieterich, M., Haselgrove, C., … Dale, A. M. (2002). Whole Brain Segmentation: Automated Labeling of Neuroanatomical Structures in the Human Brain. *Neuron*, *33*(3), 341–355. https://doi.org/10.1016/S0896-6273(02)00569-X

Fisher, C. M. (1978). Ataxic Hemiparesis: A Pathologic Study. *Archives of Neurology*, *35*(3).

Förster, A., Kerl, H. U., Goerlitz, J., Wenz, H., & Groden, C. (2014). Crossed Cerebellar Diaschisis in Acute Isolated Thalamic Infarction Detected by Dynamic Susceptibility Contrast Perfusion MRI. *PLoS ONE*, *9*(2), e88044. https://doi.org/10.1371/journal.pone.0088044

Frigeri, T., Paglioli, E., de Oliveira, E., & Rhoton, A. L. (2015). Microsurgical anatomy of the central lobe. *Journal of Neurosurgery*, *122*(March), 483–498. https://doi.org/10.3171/2014.11.jns14315

Fugl-Meyer, A. R., Jaasko, L., Leyman, I., Olsson, S., & Steglind, S. (1975). The post-stroke hemiplegic patient. A method for evaluation of physical performance. *Scandinavian Journal of Rehabilitation Medicine*, *7*(1), 13–31.

Ghika-Schmid, F., & Bogousslavsky, J. (2000). The acute behavioral syndrome of anterior thalamic infarction: a prospective study of 12 cases. *Annals of Neurology*, *48*(2), 220–227. Retrieved from http://www.ncbi.nlm.nih.gov/pubmed/10939573

Gold, L., & Lauritzen, M. (2002). Neuronal deactivation explains decreased cerebellar blood flow in response to focal cerebral ischemia or suppressed neocortical function. *Proceedings of the National Academy of Sciences*, *99*(11), 7699–7704. https://doi.org/10.1073/pnas.112012499

Gong, G., Rosa-Neto, P., Carbonell, F., Chen, Z. J., He, Y., & Evans, A. C. (2009). Age- and Gender-Related Differences in the Cortical Anatomical Network. *Journal of Neuroscience*, *29*(50), 15684–15693. https://doi.org/10.1523/JNEUROSCI.2308-09.2009

Gracies, J.-M. (2005). Pathophysiology of spastic paresis. I: Paresis and soft tissue changes. *Muscle & Nerve*, *31*(5), 535–551. https://doi.org/10.1002/mus.20284

Grefkes, C., & Ward, N. S. (2014). Cortical reorganization after stroke: How much and how functional? *Neuroscientist*, *20*(1), 56–70. https://doi.org/10.1177/1073858413491147

Griffis, J. C., Metcalf, N. V, Corbetta, M., & Shulman, G. L. (2019). Increases in structural shortest path lengths provide information about the distal neurophysiological consequences of focal brain lesions. *BioRxiv*, 785576. https://doi.org/10.1101/785576

Groisser, B. N., Copen, W. A., Singhal, A. B., Hirai, K. K., & Schaechter, J. D. (2014). Corticospinal tract diffusion abnormalities early after stroke predict motor outcome. *Neurorehabilitation and Neural Repair*, *28*(8), 751–760. https://doi.org/10.1177/1545968314521896

Gupta, R. K., Saksena, S., Hasan, K. M., Agarwal, A., Haris, M., Pandey, C. M., & Narayana, P. A. (2006). Focal Wallerian degeneration of the corpus callosum in large middle cerebral artery stroke: Serial diffusion tensor imaging. *Journal of Magnetic Resonance Imaging*, *24*(3), 549–555. https://doi.org/10.1002/jmri.20677

Habegger, S., Wiest, R., Weder, B. J., Mordasini, P., Gralla, J., Häni, L., … McKinley, R. (2018). Relating Acute Lesion Loads to Chronic Outcome in Ischemic Stroke–An

Exploratory Comparison of Mismatch Patterns and Predictive Modeling. *Frontiers in Neurology*, *9*(September), 1–11. https://doi.org/10.3389/fneur.2018.00737

Hagmann, P., Jonasson, L., Maeder, P., Thiran, J. P., Wedeen, V. J., & Meuli, R. (2006). Understanding diffusion MR imaging techniques: from scalar diffusion-weighted imaging to diffusion tensor imaging and beyond. *Radiographics*, *26 Suppl 1*, S205-23. https://doi.org/10.1148/rg.26si065510

Hahn, E. L. (1949). An Accurate Nuclear Magnetic Resonance Method for Measuring Spin-Lattice Relaxation Times. *Physical Review*, *76*(1), 145–146. https://doi.org/10.1103/PhysRev.76.145

Haque, M. E., Gabr, R. E., Hasan, K. M., George, S., Arevalo, O. D., Zha, A., … Savitz, S. (2019). Ongoing Secondary Degeneration of the Limbic System in Patients With Ischemic Stroke: A Longitudinal MRI Study. *Frontiers in Neurology*, *10*(March). https://doi.org/10.3389/fneur.2019.00154

Hayward, K. S., Neva, J. L., Mang, C. S., Peters, S., Wadden, K. P., Ferris, J. K., & Boyd, L. A. (2017). Interhemispheric Pathways Are Important for Motor Outcome in Individuals with Chronic and Severe Upper Limb Impairment Post Stroke. *Neural Plasticity*, *2017*. https://doi.org/10.1155/2017/4281532

He, B. J., Snyder, A. Z., Vincent, J. L., Epstein, A., Shulman, G. L., & Corbetta, M. (2007). Breakdown of Functional Connectivity in Frontoparietal Networks Underlies Behavioral Deficits in Spatial Neglect. *Neuron*, *53*(6), 905–918. https://doi.org/10.1016/j.neuron.2007.02.013

Honey, C. J., Sporns, O., Cammoun, L., Gigandet, X., Thiran, J. P., Meuli, R., & Hagmann, P. (2009). Predicting human resting-state functional connectivity from structural connectivity. *Proceedings of the National Academy of Sciences*, *106*(6), 2035–2040. https://doi.org/10.1073/pnas.0811168106

Hua, K., Zhang, J., Wakana, S., Jiang, H., Li, X., Reich, D. S., … Mori, S. (2008). Tract probability maps in stereotaxic spaces: Analyses of white matter anatomy and tract-specific quantification. *NeuroImage*, *39*(1), 336–347. https://doi.org/10.1016/j.neuroimage.2007.07.053

Husain, J., & Juurlink, B. H. J. (1995). Oligodendroglial precursor cell susceptibility to hypoxia is related to poor ability to cope with reactive oxygen species. *Brain Research*, *698*(1–2), 86–94. https://doi.org/10.1016/0006-8993(95)00832-B

Iglesias, J. E., Liu, C. Y., Thompson, P. M., & Tu, Z. (2011). Robust brain extraction across datasets and comparison with publicly available methods. *IEEE Transactions on Medical Imaging*, *30*(9), 1617–1634. https://doi.org/10.1109/TMI.2011.2138152

Itabashi, R., Nishio, Y., Kataoka, Y., Yazawa, Y., Furui, E., Matsuda, M., & Mori, E.

(2016). Damage to the left precentral gyrus is associated with apraxia of speech in acute stroke. *Stroke*, *47*(1), 31–36. https://doi.org/10.1161/STROKEAHA.115.010402

Iturria-Medina, Y., Sotero, R. C., Canales-Rodríguez, E. J., Alemán-Gómez, Y., & Melie-García, L. (2008). Studying the human brain anatomical network via diffusion-weighted MRI and Graph Theory. *NeuroImage*, *40*(3), 1064–1076. https://doi.org/10.1016/j.neuroimage.2007.10.060

Jenkinson, M., Beckmann, C. F., Behrens, T. E. J., Woolrich, M. W., & Smith, S. M. (2012). FSL. *NeuroImage*, *62*(2), 782–790. https://doi.org/10.1016/j.neuroimage.2011.09.015

Jeurissen, B., Leemans, A., Tournier, J.-D., Jones, D. K., & Sijbers, J. (2013). Investigating the prevalence of complex fiber configurations in white matter tissue with diffusion magnetic resonance imaging. *Human Brain Mapping*, *34*(11), 2747–2766. https://doi.org/10.1002/hbm.22099

Jirjis, M. B., Valdez, C., Vedantam, A., Schmit, B. D., & Kurpad, S. N. (2017). Diffusion tensor imaging as a biomarker for assessing neuronal stem cell treatments affecting areas distal to the site of spinal cord injury. *Journal of Neurosurgery: Spine*, *26*(2), 243–251. https://doi.org/10.3171/2016.5.SPINE151319

Jirjis, M. B., Vedantam, A., Budde, M. D., Kalinosky, B., Kurpad, S. N., & Schmit, B. D. (2016). Severity of spinal cord injury influences diffusion tensor imaging of the brain. *Journal of Magnetic Resonance Imaging*, *43*(1), 63–74. https://doi.org/10.1002/jmri.24964

Jones, T. A., & Adkins, D. L. (2015). Motor System Reorganization After Stroke: Stimulating and Training Toward Perfection. *Physiology*, *30*(5), 358–370. https://doi.org/10.1152/physiol.00014.2015

Kalinosky, B. T., Berrios Barillas, R., & Schmit, B. D. (2017). Structurofunctional resting-state networks correlate with motor function in chronic stroke. *NeuroImage: Clinical*, *16*, 610–623. https://doi.org/10.1016/j.nicl.2017.07.002

Kalinosky, B. T., Schindler-Ivens, S., & Schmit, B. D. (2013). White matter structural connectivity is associated with sensorimotor function in stroke survivors. *NeuroImage: Clinical*, *2*, 767–781. https://doi.org/10.1016/j.nicl.2013.05.009

Kalinosky, B. T., Vinehout, K., Sotelo, M. R., Hyngstrom, A. S., & Schmit, B. D. (2019). Tasked-Based Functional Brain Connectivity in Multisensory Control of Wrist Movement After Stroke. *Frontiers in Neurology*, *10*. https://doi.org/10.3389/fneur.2019.00609

Karthikeyan, S., Jeffers, M. S., Carter, A., & Corbett, D. (2019). Characterizing

Spontaneous Motor Recovery Following Cortical and Subcortical Stroke in the Rat. *Neurorehabilitation and Neural Repair*, *33*(1), 27–37. https://doi.org/10.1177/1545968318817823

Koh, C. L., Tang, P. F., Chen, H. I., Hsu, Y. C., Hsieh, C. L., & Tseng, W. Y. I. (2018). Impaired Callosal Motor Fiber Integrity and Upper Extremity Motor Impairment Are Associated With Stroke Lesion Location. *Neurorehabilitation and Neural Repair*, (1). https://doi.org/10.1177/1545968318779730

Koton, S., Schneider, A. L. C., Rosamond, W. D., Shahar, E., Sang, Y., Gottesman, R. F., & Coresh, J. (2014). Stroke Incidence and Mortality Trends in US Communities, 1987 to 2011. *JAMA*, *312*(3), 259. https://doi.org/10.1001/jama.2014.7692

Koyama, T., & Domen, K. (2017). Diffusion Tensor Fractional Anisotropy in the Superior Longitudinal Fasciculus Correlates with Functional Independence Measure Cognition Scores in Patients with Cerebral Infarction. *Journal of Stroke and Cerebrovascular Diseases*, *26*(8), 1704–1711. https://doi.org/10.1016/j.jstrokecerebrovasdis.2017.03.034

Kuceyeski, A., Kamel, H., Navi, B. B., Raj, A., & Iadecola, C. (2014). Predicting future brain tissue loss from white matter connectivity disruption in ischemic stroke. *Stroke*, *45*(3), 717–722. https://doi.org/10.1161/STROKEAHA.113.003645

Kuceyeski, A., Maruta, J., Relkin, N., & Raj, A. (2013). The Network Modification (NeMo) Tool: Elucidating the Effect of White Matter Integrity Changes on Cortical and Subcortical Structural Connectivity. *Brain Connectivity*, *3*(5), 451–463. https://doi.org/10.1089/brain.2013.0147

Kushner, M., Alavi, A., Reivich, M., Dann, R., Burke, A., & Robinson, G. (1984). Contralateral cerebellar hypometabolism following cerebral insult: A positron emission tomographic study. *Annals of Neurology*, *15*(5), 425–434. https://doi.org/10.1002/ana.410150505

Lam, T. K., Binns, M. A., Honjo, K., Dawson, D. R., Ross, B., Stuss, D. T., … Chen, J. L. (2018). Variability in stroke motor outcome is explained by structural and functional integrity of the motor system. *Scientific Reports*, *8*(1), 1–11. https://doi.org/10.1038/s41598-018-27541-8

Lee, J., Grabb, M. C., Zipfel, G. J., & Choi, D. W. (2000). Brain tissue responses to ischemia. *Journal of Clinical Investigation*, *106*(6), 723–731. https://doi.org/10.1172/JCI11003

Lemkaddem, A., Skioldebrand, D., Dal Palu, A., Thiran, J.-P., & Daducci, A. (2014). Global Tractography with Embedded Anatomical Priors for Quantitative Connectivity Analysis. *Frontiers in Neurology*, *5*. https://doi.org/10.3389/fneur.2014.00232

Lewerenz, J., & Maher, P. (2015). Chronic Glutamate Toxicity in Neurodegenerative Diseases—What is the Evidence? *Frontiers in Neuroscience*, *9*(DEC), 1–20. https://doi.org/10.3389/fnins.2015.00469

Li, M., Zhang, Y., Song, L., Huang, R., Ding, J., Fang, Y., … Han, Z. (2017). Structural connectivity subserving verbal fluency revealed by lesion-behavior mapping in stroke patients. *Neuropsychologia*, *101*(May), 85–96. https://doi.org/10.1016/j.neuropsychologia.2017.05.008

Liang, Z., Zeng, J., Zhang, C., Liu, S., Ling, X., Xu, A., … Pei, Z. (2008). Longitudinal Investigations on the Anterograde and Retrograde Degeneration in the Pyramidal Tract following Pontine Infarction with Diffusion Tensor Imaging. *Cerebrovascular Diseases*, *25*(3), 209–216. https://doi.org/10.1159/000113858

Lin, L. Y., Ramsey, L., Metcalf, N. V., Rengachary, J., Shulman, G. L., Shimony, J. S., & Corbetta, M. (2018). Stronger prediction of motor recovery and outcome post-stroke by cortico-spinal tract integrity than functional connectivity. *PLoS ONE*, *13*(8), 1–13. https://doi.org/10.1371/journal.pone.0202504

Liu, G., Dang, C., Chen, X., Xing, S., Dani, K., Xie, C., … Zeng, J. (2015). Structural remodeling of white matter in the contralesional hemisphere is correlated with early motor recovery in patients with subcortical infarction. *Restorative Neurology and Neuroscience*, *33*(3), 309–319. https://doi.org/10.3233/RNN-140442

Liu, J., Qin, W., Zhang, J., Zhang, X., & Yu, C. (2015). Enhanced Interhemispheric Functional Connectivity Compensates for Anatomical Connection Damages in Subcortical Stroke. *Stroke*, *46*(4), 1045–1051. https://doi.org/10.1161/STROKEAHA.114.007044

Lo, E. H., Moskowitz, M. A., & Jacobs, T. P. (2005). Exciting, Radical, Suicidal: how brain cells die after stroke. *Stroke*, *36*(2), 189–192. https://doi.org/10.1161/01.STR.0000153069.96296.fd

Maier-Hein, K. H., Neher, P. F., Houde, J. C., Côté, M. A., Garyfallidis, E., Zhong, J., … Descoteaux, M. (2017). The challenge of mapping the human connectome based on diffusion tractography. *Nature Communications*, *8*(1). https://doi.org/10.1038/s41467-017-01285-x

Mang, C. S., Borich, M. R., Brodie, S. M., Brown, K. E., Snow, N. J., Wadden, K. P., & Boyd, L. A. (2015). Diffusion imaging and transcranial magnetic stimulation assessment of transcallosal pathways in chronic stroke. *Clinical Neurophysiology*, *126*(10), 1959–1971. https://doi.org/10.1016/j.clinph.2014.12.018

Manuweera, T., Yarossi, M., Adamovich, S., & Tunik, E. (2019). Parietal Activation Associated With Target-Directed Right Hand Movement Is Lateralized by Mirror

Feedback to the Ipsilateral Hemisphere. *Frontiers in Human Neuroscience*, *12*(January), 1–11. https://doi.org/10.3389/fnhum.2018.00531

Maraka, S., Jiang, Q., Jafari-Khouzani, K., Li, L., Malik, S., Hamidian, H., … Mitsias, P. D. (2014). Degree of corticospinal tract damage correlates with motor function after stroke. *Annals of Clinical and Translational Neurology*, *1*(11), 891–899. https://doi.org/10.1002/acn3.132

Marchand, W. R., Lee, J. N., Thatcher, J. W., Hsu, E. W., Rashkin, E., Suchy, Y., … Barbera, S. S. (2008). Putamen coactivation during motor task execution. *Neuroreport*, *19*(9), 957–960. https://doi.org/10.1097/WNR.0b013e328302c873

Marek, M., Paus, S., Allert, N., Madler, B., Klockgether, T., Urbach, H., & Coenen, V. A. (2015). Ataxia and tremor due to lesions involving cerebellar projection pathways: A DTI tractographic study in six patients. *Journal of Neurology*, *262*(1), 54–58. https://doi.org/10.1007/s00415-014-7503-8

Meskaldji, D. E., Fischi-Gomez, E., Griffa, A., Hagmann, P., Morgenthaler, S., & Thiran, J.-P. (2013). Comparing connectomes across subjects and populations at different scales. *NeuroImage*, *80*, 416–425. https://doi.org/10.1016/j.neuroimage.2013.04.084

Morecraft, R. J., Ge, J., Stilwell-Morecraft, K. S., Rotella, D. L., Pizzimenti, M. A., & Darling, W. G. (2018). New Corticopontine Connections in the Primate Brain: Contralateral Projections From the Arm/Hand Area of the Precentral Motor Region. *Frontiers in Neuroanatomy*, *12*, 68. https://doi.org/10.3389/fnana.2018.00068

Mori, S., Crain, B. J., Chacko, V. P., & van Zijl, P. C. (1999). Three-dimensional tracking of axonal projections in the brain by magnetic resonance imaging. *Annals of Neurology*, *45*(2), 265–269. https://doi.org/10.1002/1531-8249(199902)45:2<265::aid-ana21>3.0.co;2-3

Motovylyak, A., Skinner, N. P., Schmit, B. D., Wilkins, N., Kurpad, S. N., & Budde, M. D. (2019). Longitudinal In Vivo Diffusion Magnetic Resonance Imaging Remote from the Lesion Site in Rat Spinal Cord Injury. *Journal of Neurotrauma*, *36*(9), 1389–1398. https://doi.org/10.1089/neu.2018.5964

Murase, N., Duque, J., Mazzocchio, R., & Cohen, L. G. (2004). Influence of interhemispheric interactions on motor function in chronic stroke. *Annals of Neurology*, *55*(3), 400–409. https://doi.org/10.1002/ana.10848

Nicholls, J. G., & Paton, J. F. R. (2009). Brainstem: neural networks vital for life. *Philosophical Transactions of the Royal Society of London. Series B, Biological Sciences*, *364*(1529), 2447–2451. https://doi.org/10.1098/rstb.2009.0064

Özcan, A., Wong, K. H., Larson-Prior, L., Cho, Z.-H., & Mun, S. K. (2012). Background and mathematical analysis of diffusion MRI methods. *International Journal of*

Imaging Systems and Technology, *22*(1), 44–52. https://doi.org/10.1002/ima.22001

Park, C., Chang, W. H., Ohn, S. H., Kim, S. T., Bang, O. Y., Pascual-Leone, A., & Kim, Y.-H. (2011). Longitudinal Changes of Resting-State Functional Connectivity During Motor Recovery After Stroke. *Stroke*, *42*(5), 1357–1362. https://doi.org/10.1161/STROKEAHA.110.596155

Podsiadlo, D., & Richardson, S. (1991). The Timed "Up & Go": A Test of Basic Functional Mobility for Frail Elderly Persons. *Journal of the American Geriatrics Society*, *39*(2), 142–148. https://doi.org/10.1111/j.1532-5415.1991.tb01616.x

Puig, J., Blasco, G., Alberich-Bayarri, A., Schlaug, G., Deco, G., Biarnes, C., … Pedraza, S. (2018). Resting-state functional connectivity magnetic resonance imaging and outcome after acute stroke. *Stroke*, *49*(10), 2353–2360. https://doi.org/10.1161/STROKEAHA.118.021319

Puig, J., Blasco, G., Daunis-I-Estadella, J., Thomalla, G., Castellanos, M., Figueras, J., … Pedraza, S. (2013). Decreased Corticospinal Tract Fractional Anisotropy Predicts Long-term Motor Outcome After Stroke. *Stroke*, *44*(7), 2016–2018. https://doi.org/10.1161/STROKEAHA.111.000382

Puig, J., Pedraza, S., Blasco, G., Daunis-i-Estadella, J., Prados, F., Remollo, S., … Serena, J. (2011). Acute damage to the posterior limb of the internal capsule on diffusion tensor tractography as an early imaging predictor of motor outcome after stroke. *American Journal of Neuroradiology*, *32*(5), 857–863. https://doi.org/10.3174/ajnr.A2400

Puig, J., Pedraza, S., Blasco, G., Daunis-i-Estadella, J., Prats, A., Prados, F., … Serena, J. (2010). Wallerian Degeneration in the Corticospinal Tract Evaluated by Diffusion Tensor Imaging Correlates with Motor Deficit 30 Days after Middle Cerebral Artery Ischemic Stroke. *American Journal of Neuroradiology*, *31*(7), 1324–1330. https://doi.org/10.3174/ajnr.A2038

Pustina, D., Coslett, H. B., Turkeltaub, P. E., Tustison, N., Schwartz, M. F., & Avants, B. (2016). Automated segmentation of chronic stroke lesions using LINDA: Lesion identification with neighborhood data analysis. *Human Brain Mapping*, *37*(4), 1405–1421. https://doi.org/10.1002/hbm.23110

Qin, W., Zhang, M., Piao, Y., Guo, D., Zhu, Z., Tian, X., … Yu, C. (2012). Wallerian Degeneration in Central Nervous System: Dynamic Associations between Diffusion Indices and Their Underlying Pathology. *PLoS ONE*, *7*(7), e41441. https://doi.org/10.1371/journal.pone.0041441

Rocha, E. A., Ji, R., Ay, H., Li, Z., Arsava, E. M., Silva, G. S., … Singhal, A. B. (2019). Reduced Ischemic Lesion Growth with Heparin in Acute Ischemic Stroke. *Journal of Stroke and Cerebrovascular Diseases*, *28*(6), 1500–1508.

https://doi.org/10.1016/j.jstrokecerebrovasdis.2019.03.016

Rorden, C., Karnath, H.-O., & Bonilha, L. (2007). Improving Lesion-Symptom Mapping. *Journal of Cognitive Neuroscience*, *19*(7), 1081–1088. https://doi.org/10.1162/jocn.2007.19.7.1081

Rubinov, M., & Sporns, O. (2010). Complex network measures of brain connectivity: Uses and interpretations. *NeuroImage*, *52*(3), 1059–1069. https://doi.org/10.1016/j.neuroimage.2009.10.003

Sakayori, N., Kato, S., Sugawara, M., Setogawa, S., Fukushima, H., Ishikawa, R., … Kobayashi, K. (2019). Motor skills mediated through cerebellothalamic tracts projecting to the central lateral nucleus. *Molecular Brain*, *12*(1), 13. https://doi.org/10.1186/s13041-019-0431-x

Sanford, J., Moreland, J., Swanson, L. R., Stratford, P. W., & Gowland, C. (1993). Reliability of the Fugl-Meyer assessment for testing motor performance in patients following stroke. *Physical Therapy*, *73*(7), 447–454. Retrieved from http://www.ncbi.nlm.nih.gov/pubmed/8316578

Schmahmann, J. D., MacMore, J., & Vangel, M. (2009). Cerebellar stroke without motor deficit: clinical evidence for motor and non-motor domains within the human cerebellum. *Neuroscience*, *162*(3), 852–861. https://doi.org/10.1016/j.neuroscience.2009.06.023

Schmitz-Hubsh, T., Montcel, T. du, Baliko, L., Berciano, J., Boesch, S., Depondt, C., … Kockgether, T. (2006). *Scale for the assessment and rating of ataxia: Development of a new clinical scale*. *66*(11).

Schonewille, W., Tuhrim, S., Singer, M., & Atlas, S. (1999). Diffusion-weighted MRI in Acute Lacunar Syndromes: A clinical-radiological correlation study. *Stroke*, *30*.

Schulz, R., Braass, H., Liuzzi, G., Hoerniss, V., Lechner, P., Gerloff, C., & Hummel, F. C. (2015). White matter integrity of premotor-motor connections is associated with motor output in chronic stroke patients. *NeuroImage: Clinical*, *7*, 82–86. https://doi.org/10.1016/j.nicl.2014.11.006

Schulz, R., Frey, B. M., Koch, P., Zimerman, M., Bönstrup, M., Feldheim, J., … Hummel, F. C. (2015). Cortico-Cerebellar Structural Connectivity Is Related to Residual Motor Output in Chronic Stroke. *Cerebral Cortex*, *27*(January), bhv251. https://doi.org/10.1093/cercor/bhv251

Schulz, R., Park, C.-H., Boudrias, M.-H., Gerloff, C., Hummel, F. C., & Ward, N. S. (2012). Assessing the Integrity of Corticospinal Pathways From Primary and Secondary Cortical Motor Areas After Stroke. *Stroke*, *43*(8), 2248–2251. https://doi.org/10.1161/STROKEAHA.112.662619

Schwamm, L. H., Koroshetz, W. J., Sorensen, A. G., Wang, B., Copen, W. A., Budzik, R., … Gonzalez, R. G. (1998). Time course of lesion development in patients with acute stroke. Serial diffusion- and hemodynamic-weighted magnetic resonance imaging. *Stroke*, *29*(11), 2268–2276. https://doi.org/10.1161/01.STR.29.11.2268

Seidler, R. ., Noll, D. ., & Thiers, G. (2004). Feedforward and feedback processes in motor control. *NeuroImage*, *22*(4), 1775–1783. https://doi.org/10.1016/j.neuroimage.2004.05.003

Small, S. L., Hlustik, P., Noll, D. C., Genovese, C., & Solodkin, A. (2002). Cerebellar hemispheric activation ipsilateral to the paretic hand correlates with functional recovery after stroke. *Brain : A Journal of Neurology*, *125*(Pt 7), 1544–1557. https://doi.org/10.1093/brain/awf148

Smith, R. E., Tournier, J. D., Calamante, F., & Connelly, A. (2012). Anatomically-constrained tractography: Improved diffusion MRI streamlines tractography through effective use of anatomical information. *NeuroImage*, *62*(3), 1924–1938. https://doi.org/10.1016/j.neuroimage.2012.06.005

Smith, S. M., Jenkinson, M., Johansen-Berg, H., Rueckert, D., Nichols, T. E., Mackay, C. E., … Behrens, T. E. J. (2006). Tract-based spatial statistics: Voxelwise analysis of multi-subject diffusion data. *NeuroImage*, *31*(4), 1487–1505. https://doi.org/10.1016/j.neuroimage.2006.02.024

Sommer, W. H., Bollwein, C., Thierfelder, K. M., Baumann, A., Janssen, H., Ertl-Wagner, B., … von Baumgarten, L. (2016). Crossed cerebellar diaschisis in patients with acute middle cerebral artery infarction: Occurrence and perfusion characteristics. *Journal of Cerebral Blood Flow & Metabolism*, *36*(4), 743–754. https://doi.org/10.1177/0271678X15617953

Sporns, O. (2011). The human connectome: A complex network. *Annals of the New York Academy of Sciences*, *1224*(1), 109–125. https://doi.org/10.1111/j.1749-6632.2010.05888.x

Stejskal, E. O., & Tanner, J. E. (1965). Spin Diffusion Measurements: Spin Echoes in the Presence of a Time☐Dependent Field Gradient. *The Journal of Chemical Physics*, *42*(1), 288–292. https://doi.org/10.1063/1.1695690

Suryanarayana, S. M., Hellgren Kotaleski, J., Grillner, S., & Gurney, K. N. (2019). Roles for globus pallidus externa revealed in a computational model of action selection in the basal ganglia. *Neural Networks : The Official Journal of the International Neural Network Society*, *109*, 113–136. https://doi.org/10.1016/j.neunet.2018.10.003

Tamari, M., Umeki, S., Goto, J., & Kawano, Y. (2018). Relationship between white matter fiber damage and revised version of the ability for basic movement scale in patients with stroke: a diffusion tensor tract-based spatial statistic study. *Journal of*

Physical Therapy Science, *30*(6), 809–812. https://doi.org/10.1589/jpts.30.809

Thomalla, G. (2005). Time course of wallerian degeneration after ischaemic stroke revealed by diffusion tensor imaging. *Journal of Neurology, Neurosurgery & Psychiatry*, *76*(2), 266–268. https://doi.org/10.1136/jnnp.2004.046375

Thomalla, Götz, Glauche, V., Koch, M. A., Beaulieu, C., Weiller, C., & Röther, J. (2004). Diffusion tensor imaging detects early Wallerian degeneration of the pyramidal tract after ischemic stroke. *NeuroImage*, *22*(4), 1767–1774. https://doi.org/10.1016/j.neuroimage.2004.03.041

Torrey, H. C. (1956). Bloch Equations with Diffusion Terms. *Physical Review*, *104*(3), 563–565. https://doi.org/10.1103/PhysRev.104.563

Tournier, J. D., Calamante, F., & Connelly, A. (2007). Robust determination of the fibre orientation distribution in diffusion MRI: Non-negativity constrained super-resolved spherical deconvolution. *NeuroImage*, *35*(4), 1459–1472. https://doi.org/10.1016/j.neuroimage.2007.02.016

Tuladhar, A. M., Snaphaan, L., Shumskaya, E., Rijpkema, M., Fernandez, G., Norris, D. G., & de Leeuw, F.-E. (2013). Default Mode Network Connectivity in Stroke Patients. *PLoS ONE*, *8*(6), e66556. https://doi.org/10.1371/journal.pone.0066556

Tustison, N. J., Avants, B. B., Cook, P. A., Yuanjie Zheng, Egan, A., Yushkevich, P. A., & Gee, J. C. (2010). N4ITK: Improved N3 Bias Correction. *IEEE Transactions on Medical Imaging*, *29*(6), 1310–1320. https://doi.org/10.1109/TMI.2010.2046908

van Baarsen, K. M., Kleinnijenhuis, M., Jbabdi, S., Sotiropoulos, S. N., Grotenhuis, J. A., & van Cappellen van Walsum, A. M. (2016). A probabilistic atlas of the cerebellar white matter. *NeuroImage*, *124*, 724–732. https://doi.org/10.1016/j.neuroimage.2015.09.014

van der Knaap, L. J., & van der Ham, I. J. M. (2011). How does the corpus callosum mediate interhemispheric transfer? A review. *Behavioural Brain Research*, *223*(1), 211–221. https://doi.org/10.1016/j.bbr.2011.04.018

van Meer, M. P. A., Otte, W. M., van der Marel, K., Nijboer, C. H., Kavelaars, A., van der Sprenkel, J. W. B., … Dijkhuizen, R. M. (2012). Extent of bilateral neuronal network reorganization and functional recovery in relation to stroke severity. *The Journal of Neuroscience : The Official Journal of the Society for Neuroscience*, *32*(13), 4495–4507. https://doi.org/10.1523/JNEUROSCI.3662-11.2012

van Wijk, B. C. M., Stam, C. J., & Daffertshofer, A. (2010). Comparing brain networks of different size and connectivity density using graph theory. *PLoS ONE*, *5*(10). https://doi.org/10.1371/journal.pone.0013701

Vedantam, A., Jirjis, M. B., Schmit, B. D., Wang, M. C., Ulmer, J. L., & Kurpad, S. N. (2014). Diffusion Tensor Imaging of the Spinal Cord: Insights from Animal and Human Studies. *Neurosurgery*, *74*(1), 1–8. https://doi.org/10.1227/NEU.0000000000000171

Vinehout, K., Schmit, B. D., & Schindler-Ivens, S. (2019). Lower Limb Task-Based Functional Connectivity Is Altered in Stroke. *Brain Connectivity*, *9*(4), 365–377. https://doi.org/10.1089/brain.2018.0640

Wakana, S., Caprihan, A., Panzenboeck, M. M., Fallon, J. H., Perry, M., Gollub, R. L., … Mori, S. (2007). Reproducibility of quantitative tractography methods applied to cerebral white matter. *NeuroImage*, *36*(3), 630–644. https://doi.org/10.1016/j.neuroimage.2007.02.049

Wang, L. E., Tittgemeyer, M., Imperati, D., Diekhoff, S., Ameli, M., Fink, G. R., & Grefkes, C. (2012). Degeneration of corpus callosum and recovery of motor function after stroke: A multimodal magnetic resonance imaging study. *Human Brain Mapping*, *33*(12), 2941–2956. https://doi.org/10.1002/hbm.21417

Welton, T., Kent, D. A., Auer, D. P., & Dineen, R. A. (2015). Reproducibility of Graph-Theoretic Brain Network Metrics: A Systematic Review. *Brain Connectivity*, *5*(4), 193–202. https://doi.org/10.1089/brain.2014.0313

Wen, H., Alshikho, M. J., Wang, Y., Luo, X., Zafonte, R., Herbert, M. R., & Wang, Q. M. (2016). Correlation of Fractional Anisotropy With Motor Recovery in Patients With Stroke After Postacute Rehabilitation. *Archives of Physical Medicine and Rehabilitation*, *97*(9), 1487–1495. https://doi.org/10.1016/j.apmr.2016.04.010

Wheeler-Kingshott, C. A. M., & Cercignani, M. (2009). About "axial" and "radial" diffusivities. *Magnetic Resonance in Medicine*, *61*(5), 1255–1260. https://doi.org/10.1002/mrm.21965

Woodbury, M., Velozo, C. A., Thompson, P. A., Light, K., Uswatte, G., Taub, E., … Wolf, S. L. (2010). Measurement Structure of the Wolf Motor Function Test: Implications for Motor Control Theory. *Neurorehabilitation and Neural Repair*, *24*(9), 791–801. https://doi.org/10.1177/1545968310370749

Yang, Y., Chen, Y., Chen, K., Wei, D., Li, P., Zeng, W., … Zhang, Z. (2019). Increased intrinsic connectivity for structural atrophy and functional maintenance after acute ischaemic stroke. *European Journal of Neurology*, *26*(6), 935–942. https://doi.org/10.1111/ene.13913

Yassi, N., Malpas, C. B., Campbell, B. C. V., Moffat, B., Steward, C., Parsons, M. W., … Bivard, A. (2015). Contralesional thalamic surface atrophy and functional disconnection 3 months after ischemic stroke. *Cerebrovascular Diseases*, *39*(3–4), 232–241. https://doi.org/10.1159/000381105

Yu, C., Zhu, C., Zhang, Y., Chen, H., Qin, W., Wang, M., & Li, K. (2009). A longitudinal diffusion tensor imaging study on Wallerian degeneration of corticospinal tract after motor pathway stroke. *NeuroImage*, *47*(2), 451–458. https://doi.org/10.1016/j.neuroimage.2009.04.066

Yu, X., Jiaerken, Y., Xu, X., Jackson, A., Huang, P., Yang, L., … Zhang, M. (2018). Abnormal corpus callosum induced by diabetes impairs sensorimotor connectivity in patients after acute stroke. *European Radiology*, *55*(3), 400–409. https://doi.org/10.1007/s00330-018-5576-y

Yung, A., Mattucci, S., Bohnet, B., Liu, J., Fournier, C., Tetzlaff, W., … Oxland, T. (2019). Diffusion tensor imaging shows mechanism-specific differences in injury pattern and progression in rat models of acute spinal cord injury. *NeuroImage*, *186*, 43–55. https://doi.org/10.1016/j.neuroimage.2018.10.067

Yushkevich, P. A., Piven, J., Hazlett, H. C., Smith, R. G., Ho, S., Gee, J. C., & Gerig, G. (2006). User-guided 3D active contour segmentation of anatomical structures: Significantly improved efficiency and reliability. *NeuroImage*, *31*(3), 1116–1128. https://doi.org/10.1016/j.neuroimage.2006.01.015

Zalesky, A., Fornito, A., Harding, I. H., Cocchi, L., Yücel, M., Pantelis, C., & Bullmore, E. T. (2010). Whole-brain anatomical networks: Does the choice of nodes matter? *NeuroImage*, *50*(3), 970–983. https://doi.org/10.1016/j.neuroimage.2009.12.027

Zou, K. H., Warfield, S. K., Bharatha, A., Tempany, C. M. C., Kaus, M. R., Haker, S. J., … Kikinis, R. (2004). Statistical validation of image segmentation quality based on a spatial overlap index1. *Academic Radiology*, *11*(2), 178–189. https://doi.org/10.1016/S1076-6332(03)00671-8